Site U1340[1]

Expedition 323 Scientists[2]

Chapter contents

Background and objectives

The primary objective of drilling at Integrated Ocean Drilling Program (IODP) Site U1340 (proposed Site BOW-12B; Takahashi et al., 2009) was to study high-resolution Pliocene and Pleistocene paleoceanography in the southernmost part of the Bering Sea at a topographic high on Bowers Ridge (Fig. F1), where relatively good calcium carbonate preservation is expected. Bowers Ridge is well situated to study the past extent of water mass exchange with the Pacific Ocean through adjacent Aleutian passes such as Amukta, Amchitka, and Buldir. In particular, its location allows for an examination of the influence of the warm Alaskan Stream water mass entry into this region, which influenced the distribution of past sea ice coverage (Katsuki and Takahashi, 2005). Although productivity in the Bering Sea in general is very high with respect to other parts of the global oceans, it was expected to be lower at this site than at the Bering slope sites, which are substantially more influenced by the nearby Bering shelf, which was partially exposed during glacial lowstands. The relatively shallow water depth of this site should allow us to study physical and chemical changes in upper water mass conditions such as the low dissolved oxygen concentration conditions that caused the formation of laminated sediments at a site on the Bering shelf at a similar water depth (Cook et al., 2005). The vertical structure of past water masses can be determined by comparing results at this site with those at other drilling sites on Bowers Ridge (IODP Site U1341, water depth = 2177 m, and IODP Site U1342, water depth = 837 m) (Fig. F1).

Site U1340 on Bowers Ridge can also be used to study the impact of subseafloor microbes on biogeochemical fluxes in the highest surface-ocean productivity areas of the drill sites in the Bering Sea. Samples used to study organic-fueled subseafloor respiration and its impact on biogeochemistry at the highly productive region of IODP Site U1339 and other Bering slope sites can be compared to analyses at the Bowers Ridge sites, including Site U1340; however, the high-resolution sampling that occurred at the Bering slope sites was not performed at Site U1340. Sediments drilled at Bowers Ridge were used to determine subseafloor cell abundances and to investigate the link between the mass and characteristics of subseafloor microbes and the extent of export productivity from the surface ocean.

[1] Expedition 323 Scientists, 2011. Site U1340. *In* Takahashi, K., Ravelo, A.C., Alvarez Zarikian, C.A., and the Expedition 323 Scientists, *Proc. IODP,* 323: Tokyo (Integrated Ocean Drilling Program Management International, Inc.). doi:10.2204/iodp.proc.323.104.2011
[2] **Expedition 323 Scientists' addresses.**

doi:10.2204/iodp.proc.323.104.2011

Site U1340 is located on the eastern flank of the southern part of Bowers Ridge (Fig. F1) at 1295 m water depth in a basin ~10 km east of the ridge crest (Fig. F2). Close-ups of the seismic images in the basin (Figs. F3, F4, F5) indicate that strata dip to the east (Fig. F4). Some shallow sections do not have continuous parallel strata, but most of the rest of the section appears to have continuous features in the seismic images (Figs. F4, F5). The ages of basement and the deeper sediments are unknown, but sediments as old as upper Miocene were found at Deep Sea Drilling Project (DSDP) Site 188 on the western flank of Bowers Ridge (Scholl and Creager, 1973). Specifically, Scholl and Creager (1973) found recent to upper Miocene diatom ooze interbedded with silt-rich diatom ooze and diatomaceous silt. They also found calcareous nannofossils in the uppermost 120 m and planktonic foraminifers in the uppermost 300–400 m. In the interval between 580 and 638 meters below seafloor (mbsf), they encountered mudstone. They reported sedimentation rates of ~100 m/m.y. A piston core study from the same general region provided sedimentation rates of 80 m/m.y. (Takahashi, 2005). Thus, before drilling we expected to recover sections ranging from the entire Pleistocene to the Pliocene and possibly Miocene.

Operations

We arrived at Site U1340 on 22 July 2009 after a 1.5 day, 344 nmi transit from Site U1339. One relatively deep and three relatively shallow holes were drilled and cored with the advanced piston corer (APC) and extended core barrel (XCB) coring systems at a water depth of 1294.7 m on Bowers Ridge (Table T1). A complete set of site-specific tide tables was provided by the science party for Site U1340 and used to make adjustments relative to initial mudline core and for each successive core in each hole. The third-generation advanced piston corer temperature tool (APCT-3) was deployed four times, and three out of four data points fell on a linear curve describing a temperature gradient of +4.34°C per 100 m of depth. Overall core recovery for Site U1340 using the APC and XCB coring systems was 91.0%.

Hole U1340A

Hole U1340A was spudded at 0520 h on 23 July (all times are ship local time, Universal Time Coordinated [UTC] – 11 h). Hole U1340A was cored to 604.6 m drilling depth below seafloor (DSF) using both the APC and XCB coring systems. APC core recovery was 105%, whereas XCB core recovery averaged 61% (Table T1). APC coring using the nonmagnetic coring assemblies with the FlexIt orientation tool installed continued through Core 323-U1340A-17H to 1461.9 m drilling depth below rig floor (DRF). Standard steel coring assemblies were used from Cores 323-U1340A-18H through 42H. APC coring was terminated after Core 323-U1340A-42H after two successive short, incomplete strokes of the core barrel. The XCB coring system was then deployed for Core 323-U1340A-43X, and coring continued with the XCB system through Core 323-U1340A-62X. The APC coring system was redeployed after three straight zero-recovery runs. APC coring through Core 323-U1340A-67H was successful in recovering ~25 m of very sandy sediment. At this point, the XCB system was redeployed. The hole was terminated after Core 323-U1340A-71X when the XCB cutting shoe spacer sub failed, leaving a portion of the sub and the XCB cutting shoe at the bottom of the hole. The drill string was pulled back to the seafloor at 2103 h on 25 July, officially ending the hole. Shear pressures were consistent throughout the coring process at 2800 psi. Core recovery for Hole U1340A using the APC coring system was 105.0% with 398.8 m recovered. Core recovery for Hole U1340A using the XCB coring system was 61.0% with 136.7 m recovered. Combined core recovery for Hole U1340A using both the APC and XCB coring systems was 88.7% (Table T1).

Hole U1340B

Hole U1340B officially began when the bit cleared the seafloor at 2103 h on 25 July, ending Hole U1340A. The vessel was offset 350 m east of Hole U1340A. The top drive was picked up and the drill string was spaced out, placing the bit at 1305.4 m DRF, or 5 m above the corrected precision depth recorder (PDR) depth of 1310.4 m DRF. The first APC barrel was pressured up and fired, and the barrel recovered 6.4 m of core, establishing an official seafloor depth at 1308.5 m DRF. Hole U1340B was spudded at 2340 h on 25 July. The nonmagnetic coring assemblies and the FlexIt core orientation system were used through Core 323-U1340B-6H. Hole U1340B ended at 0400 h on 26 July when the bit cleared the seafloor. Shear pressures were consistent throughout the coring process at 2800 psi. Average core recovery for the APC was 103.0% (Table T1). The total depth of Hole U1340B was 1362.4 m DRF (53.9 mbsf).

Hole U1340C

Hole U1340C officially began when the drill string cleared the seafloor at 0400 h on 26 July. The ship was offset 300 m south of Hole U1340A. A new PDR depth was established, and the bit was placed at 1313 m DRF to optimize the core breaks between

Holes U1340A and U1340B. The APC was deployed, and Hole U1339C was spudded at 0620 h on 26 July. Unfortunately, a mistake in the corrected PDR depth resulted in the first core being taken well below the mudline, and the 9.5 m of core recovered in Core 323-U1340C-1H failed to establish the seafloor depth. APC coring continued through Core 323-U1340C-3H to 1341.5 m DRF using the FlexIt core orientation system and the nonmagnetic coring assemblies. With the exception of the first core, shear pressures were consistent throughout the coring process at 2800 psi. Overall core recovery for the APC was 105.3% (Table T1). The drill string was pulled clear of the seafloor at 0835 h on 26 July, officially ending Hole U1340C.

Hole U1340D

Hole U1340D officially began when the drill string cleared the seafloor at 0835 h on 26 July. The ship was offset 20 m from Hole U1340C at 180°. Hole U1340D was spudded at 0905 h on 26 July, and the 7.3 m recovered in Core 323-U1339D-1H established the seafloor depth at 1304.7 m DRF. Three APC cores were shot to 26.3 mbsf. APC coring through Core 323-U1340D-3H used the nonmagnetic coring assemblies with the FlexIt orientation tool attached. Shear pressures were consistent throughout the coring process at 2800 psi. APC core recovery was 103.5% (Table T1). The drill string was then pulled and secured for transit. Once the drill collars were racked back and the rig floor was secured for transit, control was transferred from dynamic positioning to the bridge. The ship was placed in cruise mode at 1534 h on 26 July for the scheduled 6 h, 65 nmi transit to Site U1341.

Official APC coring for Site U1340 totaled 83 cores, 713.2 m penetrated, and 648.7 m recovered, for 91.0% core recovery.

Lithostratigraphy

Four holes were drilled at Site U1340, with the deepest (Hole U1340A) reaching 604.5 mbsf (608.7 m core composite depth below seafloor [CCSF-A]). The sediments recovered at Site U1340 are a mix of biogenic (mainly diatom frustules with minor amounts of calcareous nannofossils, foraminifers, silicoflagellates, sponge spicules, and radiolarians), volcaniclastic (fine to coarse ash), and siliciclastic (mainly silt-sized and minor pebble-sized clasts) sediments. Authigenic carbonates occur frequently below 230 mbsf. In general, the color of the sediment reflects its lithologic characteristics: sediment composed of siliciclastic sediment or mixed lithologies (clay, silt, or diatom silt) tends to be very dark greenish gray to dark gray, whereas diatom ooze tends to be olive-gray to olive or dark gray. Volcaniclastic ash layers are dark gray to black or shades of light gray to white and, rarely, weak red. Many are mixed with biogenic and siliciclastic sediment through bioturbation. Intervals showing soft-sediment deformation were observed intermittently above 1.40 mbsf. Three lithologic units were defined at Site U1340 (Figs. F6, F7, F8, F9). The Unit I/II boundary was defined as a major lithologic change from sediments dominated by diatom ooze (Unit II) and sediments that alternate between diatom ooze and diatom silt (Unit I). This boundary is early Pleistocene in age. The Unit II/III boundary was defined as the contact between a sponge spicule–bearing sand (Subunit IIIA) and Unit II. Subunit IIIB is a sponge spicule–bearing diatom ooze.

Description of units

Sedimentary features common to all units at Site U1340 include thin to thick laminations and bedding that are often distinguished by variations in sediment color. Transitions between alternating beds can be sharp or gradational (and sometimes obviously bioturbated). Alternating laminae and beds vary in thickness from submillimeter to decimeter scale and occur throughout the hole, although the interval from 0 to 200 mbsf contains the greatest number of laminated intervals. Smear slide observations indicate that adjacent laminae are commonly characterized by the same lithology (mainly diatom ooze). However, individual laminae composed almost exclusively of fine or coarse ash, silicoflagellates, sponge spicules, or a single diatom species (*Lioloma pacificum*) (Fig. F10) were also observed (see "Site U1340 smear slides" in "Core descriptions").

Distinct volcaniclastic layers ranging in thickness from a few millimeters to 3 cm occur throughout (Figs. F6, F7, F8, F9). Most have sharp parallel or undulating contacts with the underlying sediment, whereas the top boundary is often gradational, with the volcaniclastic material mixed with the overlying diatom ooze, most likely from bioturbation. Most volcaniclastic layers are graded (fining upward; Fig. F11). Volcaniclastic ash layers are black to light gray, and distinctive weak-red beds as thick as 2 cm were found in all holes. Volcaniclastic sediment was also found in black patches and pods that likely resulted from the bioturbation of thin ash beds and laminae. Volcanic ash is a common secondary or trace lithologic component in most of the recovered sediment.

X-ray diffraction (XRD) (see XRD in "Supplementary material") shows that opal-A, as well as the more mature silica phases cristobalite and tridymite, occurs together at all depths at Site U1340, regardless

of lithology (Fig. F12). Thin tabular to acicular crystals found in some sediment were interpreted as zeolite minerals, which usually form during transformation phases of amorphous silica (both volcanic glass and biogenic opal).

Bioturbation varies from slight to strong in all holes and is typically characterized by mottling defined by color changes. Individual burrows are not often well preserved and hence bioturbation cannot be related to specific ichnofacies types in most cases. Where visible, bioturbation was mostly assigned to the *Chondrites* ichnofacies with minor *Skolithos* and *Planolites*.

Unit I

Intervals: Sections 323-U1340A-1H-1, 0 cm, through 32H-2, 57 cm; 323-U1340B-1H-1, 0 cm, through 6H-CC, 28 cm; 323-U1340C-1H-1, 0 cm, through 3H-CC, 25 cm; and 323-U1340D-1H-1, 0 cm, through 3H-CC, 24 cm

Depths: Hole U1340A, 0–274.5 mbsf; Hole U1340B, 0–54.3 mbsf; Hole U1340C, 0–29.1 mbsf; and Hole U1340D, 0–26.8 mbsf

Age: Pliocene through Pleistocene

Unit I is composed of alternating beds of olive (5Y 4/2) to dark gray (5Y 4/1) diatom ooze and dark gray (5Y 4/1) to dark greenish gray (10Y 3/1) diatom silt (Fig. F13). The diatom ooze is predominantly composed of both centric and pennate diatoms. The preservation of diatom frustules is generally good. Diatom frustules hosting pyrite framboids were observed. Additionally, minor (<20%) amounts of other biogenic components, including nannofossils, foraminifers, and trace (<5%) amounts of silicoflagellates and sponge spicules, occur mainly in thin laminae mixed with variable amounts (<5%–40%) of silt-sized volcaniclastic and siliciclastic material, including quartz, feldspar, and clay minerals and trace amounts of mica, ferromagnesian, and zeolite minerals. The diatom silt contains subequal proportions of siliciclastic (silt-sized quartz, feldspar, and rock fragments and/or clay) and biogenic (mainly diatoms and secondarily nannofossils, foraminifers, silicoflagellates, and sponge spicules) components with a minor volcaniclastic component (see **"Site U1340 smear slides"** in "Core descriptions"). Variable amounts of dispersed vitric ash and isolated pebbles occur throughout, as do distinct ash layers, bioturbated ash/diatom ooze layers, and laminated intervals. Light-colored sediments (olive) tend to contain predominantly biogenic components, whereas dark-colored sediments (gray) tend to contain subequal proportions of siliciclastic and biogenic components. The volcanic ash layers are typically black (5Y 2.5/1), light gray (10Y 7/1 and 10YR 7/2), and, rarely, weak red (2.5YR 5/2).

Solitary pebbles occur mainly in two intervals in Unit I: from Cores 323-U1340A-1H through 8H (0–67.3 mbsf) and from Cores 323-U1340A-17H through 30H (153.2–258.9 mbsf) (Figs. F6, F7, F8, F9; black diamonds). The petrology of most pebbles was not described; however, some pebbles are composed of basalt and pumice or scoria, indicating a volcanic source.

The most prominent sedimentary structure in Unit I at Site U1340 is soft-sediment deformation of laminated and bedded diatom ooze and diatom silt (Fig. F14). Intervals with soft-sediment deformation extend from Core 323-U1340A-3H through Section 323-U1340A-8H-2 and throughout Cores 323-U1340A-11H, 12H, 14H, and 15H. In Hole U1340B, soft-sediment deformation is present in Cores 323-U1340B-3H through 6H. In Hole U1340C, soft-sediment deformation is present in Cores 323-U1340C-2H and 3H, and, in Hole U1340D, deformation is present in all cores (Figs. F6, F7, F8, F9). Folded and tilted bed boundaries are clearly visible in these cores, suggesting the occurrence of synsedimentary slumps as a potential mechanism for deformation.

Unit II

Interval: Sections 323-U1340A-32H-2, 57 cm, through 64H-4, 22 cm

Depth: Hole U1340A, 274.5–547.6 mbsf

Age: Pliocene

Unit II is composed of diatom ooze with minor amounts of diatom silt and volcaniclastic sediment. This unit differs from Unit I in having significantly more diatom ooze, less interbedded diatom silt, and fewer laminated intervals. The main lithology is therefore an olive-gray (5/Y 4/2 and 5Y 5/2) to olive (5Y 4/4, 5Y 5/4, and 5/Y 5/3) to dark olive-gray (5Y 3/2) diatom ooze with variable amounts of dispersed vitric ash, isolated pebbles, and distinct ash layers, as well as bioturbated ash/diatom ooze layers and laminated intervals. Bioturbation varies from slight to strong.

A layer of gravel was recovered at 380 mbsf in Hole U1340A. This layer is in the lower portion of an interval between 326.8 and 384.1 mbsf that contains numerous pebbles isolated within diatom ooze and diatom silt (Figs. F6, F7, F8, F9; black triangles).

Rare semi-indurated to indurated layers of authigenic carbonates were found between 275 and 435 mbsf in Hole U1340A. Semilithified or lithified yellowish layers are 5–10 cm thick. Additionally, authigenic carbonate microcrystals were found scattered

throughout the sediment. Several of these intervals were examined using XRD and were determined to be dolomite (Fig. F15).

Unit III

Interval: Sections 323-U1340A-64H, 22 cm, through 71X-CC, 10 cm
Depth: Hole U1340A, 547.6 mbsf to bottom of hole
Age: Pliocene

Unit III is distinguished from the other units by the predominance of ash and siliciclastic sediments and the abundance of sponge spicules (>5%). Unit III is composed of diatom-bearing, sponge spicule–rich ashy sand; sponge spicule–rich diatom ooze; diatom ooze; and minor amounts of volcaniclastic and siliciclastic sediment.

Subunit IIIA

Interval: Sections 323-U1340A-64H-4, 22 cm, through 64H-CC, 22 cm
Depth: Hole U1340A, 547.6–555.7 mbsf
Age: Pliocene

Subunit IIIA is composed of black (5Y 2.5/1), massive diatom-bearing sponge spicule–rich coarse-ashy sand. Although the coring device was advanced only 4 m, 8 m of sediments was recovered in this subunit from flow-in; therefore, the true subunit thickness could not be determined.

Significant coring disturbances occurred during the recovery of Core 323-U1340A-64H. Because Cores 323-U1340A-60X through 62X retrieved no sediments using XCB coring, APC coring was resumed for Core 323-U1340A-63H. It is possible that Cores 323-U1340A-60X through 62X were empty because coring occurred in an unconsolidated sandy layer with low cohesion. The rotation of the XCB core barrel and washing decreased cohesion even more by adding water to the sandy layer and possibly washing away silt- and clay-sized particles. The sandy sediments could not be retrieved without suction. Once APC coring resumed, the first core (323-U1340A-63H) penetrated through the sandy fill and retrieved diatom ooze, and the force of the piston compacted the sandy layer. The next core (323-U1340A-64H) retrieved the recompacted sandy layer.

Subunit IIIA has sharp upper contact with a thin (2 cm), light-colored ash bed of Unit II (Fig. F16). The sand extends to the bottom of the core catcher of Core 323-U1340A-64H and is absent from Core 323-U1340A-65H, where Subunit IIIB begins.

The coarse-ashy sand consists of 40%–50% siliciclastic grains composed mainly of plagioclase and amphibole with minor biotite, 25%–30% plagioclase-phyric vitric clasts, and 25%–30% biogenic grains, including 17%–20% sponge spicules and 8%–10% diatoms (Fig. F17; see also "Site U1340 thin sections" in "Core descriptions"). Sand grains are angular and moderately well sorted. The finer components of this bed may have been washed away during XCB coring; however, it is likely that low sand cohesion led to the drilling problems, so sand may have been present in high amounts in the layer.

The upper sand bed contains a 6 cm long, light-colored clast of diatom-rich fine ash. The ash has sharp contacts with the surrounding sand. Because of drilling disturbance, it is unclear whether this clast is isolated or is a disturbed ash bed within Unit III. There were no gravel-sized clasts in this subunit.

Core disturbance was observed in all sections collected in Subunit IIIA. The sediment was described as a slurry with water-rich areas at the core surface and along the liners.

Subunit IIIB

Interval: Sections 323-U1340A-64H-CC, 22 cm, through 71X-CC, 10 cm
Depth: Hole U1340A, 555.7 mbsf to bottom of hole
Age: Pliocene

The sponge spicule–rich diatom ooze is olive (5Y 4/3) or olive-gray (5Y 4/2) to dark olive-gray (5Y 3/2) and contains 60%–70% diatom frustules, 10%–30% sponge spicules, minor siliciclastic grains, and glass shards (Fig. F18; see also "Site U1340 smear slides" in "Core descriptions"). The diatom ooze is similar to that found in Units I and II. There are several intervals of lithified diatom ooze with authigenic carbonate. Bioturbation varies from absent to moderate.

Discussion

The estimated ages of the three units at Site U1340 are similar to the three units identified at Site U1341. In addition, the depositional history of the terrigenous sediments at this site has some similarities to that at Site U1341. See "Lithostratigraphy" in the "Site U1341" chapter.

Five intervals of high terrigenous content were noted at Site U1340:

1. Poorly sorted gravel to clay in Core 323-U1340A-44X (380 mbsf; ~2.5 Ma), indicating the presence of a gravel deposit of unknown thickness;
2. Isolated pebbles above 384.1 mbsf (~2.6 Ma);
3. Diatom silt to clay and clayey silt in Cores 323-U1340A-47X through 56X (~2.5 Ma);

4. Mixed and siliciclastic lithologies in Unit I (the base of which is dated to ~1.78 Ma); and
5. Subunit IIIA.

Potential mechanisms of siliciclastic sediment transport include density or gravity flows, bottom currents, and sea ice or glacial ice rafting. Potential sources of siliciclastic sediments include the Alaskan continent, the Aleutian Islands, or Bowers Ridge, if it was exposed at this time. The occurrence of isolated clasts overlaps the onset of increased siliciclastic components and is coeval with a subtle increase in gamma ray attenuation (GRA) bulk density (Figs. **F6, F7, F8, F9**). Many of these isolated clasts are well rounded, suggesting that their source was a coastal environment. They are matrix supported, which favors a hypothesis that they were picked up, transported, and deposited as a consequence of either sea ice or glacial ice rafting. Additionally, the extensively laminated mixed sediments deposited at ~2.5 Ma correlate with an interval of laminated mixed sediments at Site U1341 (Cores 323-U1341B-37X through 46X) (see **"Lithostratigraphy"** in the "Site U1341" chapter).

If the interpretation of isolated matrix-supported pebbles as dropstones is correct, their deposition, along with the deposition of laminated mixed sediments, may reflect increased mechanical weathering of the continents by terrestrial ice and greater exposure of the continental shelf during low sea level stands due to the onset of large glacial–interglacial cycles as well as the onset of large glaciations, known as Northern Hemisphere glaciation (NHG), at 2.6 Ma (Lisiecki and Raymo, 2005). Additionally, at ~260 mbsf (~1.78 Ma) (see **"Biostratigraphy"**), magnetic susceptibility values increase (Figs. **F6, F7, F8, F9**), possibly reflecting the more magnetic nature of grains in the siliciclastic component, such as ferromagnesian minerals and rock fragments. The composition and combination of siliciclastic grains (quartz, feldspar, and polycrystalline quartz aggregates) suggest both volcanic and sedimentary/metamorphic provenances and therefore favors elevated areas of the Alaskan continent as the source of the detritus (VanLaningham et al., 2009).

Unit I, on the other hand, consists of a relatively large amount of silt- to clay-sized siliciclastic grains. At this point, it is not possible to interpret the transport mechanism for these grains; however, note that sea ice may selectively entrain silt- to clay-sized particles in regions where ice formation occurs (Reimnitz et al., 1998).

The occurrence of extensive intervals with soft-sediment deformation related to slumping is somewhat unexpected because the slope of Bowers Ridge is only slightly inclined at the drill sites. The trigger for movement of sediment downslope could have been seismogenic activity related to the magmatic arc of Bowers Ridge or the nearby Aleutian arc. Sediment instability could also be due to water loss during mineral phase changes in deeper sediment, resulting in less cohesive sediment packages prone to deformation.

The combination of grading, sharp bases, and bioturbated tops is typical of air fall ash deposited in deep marine settings. Alternately, the ash may have been delivered to the site by sediment gravity-flow mechanisms. The source of the darker colored, more mafic ash is likely to be proximal, whereas lighter colored, more felsic ash (which tends to be more explosive and thus be spread farther from the source) could be from proximal or distal sources.

The primarily biogenic component of Unit II and Subunit IIIB may reflect warmer, highly productive Pliocene conditions or a higher sea level and little exposure of the continental shelf. High productivity prior to 1.9 Ma (~300 mbsf) is also corroborated by a change in foraminifer occurrences and preservation at Site U1340. Benthic foraminiferal assemblages changed from species building an agglutinated test in Unit II to species producing a carbonate test in Unit I, whereas planktonic foraminifers were only observed in Unit I (see **"Biostratigraphy"**).

There are at least two interpretations for Subunit IIIA, a coarse-ashy sand. As stated above, significant drilling disturbances, particularly flow-in and fill, prevent us from knowing the thickness of the layer or its original composition because finer grained components may have been removed. Nevertheless, a sand-rich layer is present near 550 mbsf. If the sharp upper contact, moderately well sorted sand-sized grains, and massive to subtly coarsening-upward structure are primary structures, then this subunit may have been deposited by a submarine grain flow. Grain sorting may have occurred on a beach adjacent to an active andesitic volcano. Alternatively, sorting and possibly grading may have occurred during drilling. The angular and compositionally immature nature of the particles suggests they were rapidly redistributed to water depths below wave base after initial sorting. Biostratigraphic marker species (see **"Biostratigraphy"**) and the lack of dropstones in this subunit compared to Units I and II also indicate rapid sedimentation and favor deposition by mass movement. This sand unit is correlative to Subunit IIIA at Site U1341, which is composed of authigenic carbonate–rich clay, suggesting an increase in terrigenous deposition on both sides of Bowers Ridge.

Unit III was defined as being particularly rich in sponge spicules when compared to other units. Al-

though we cannot point to a reason for such high accumulation of sponge spicules, this may also reflect high productivity or ecological change during the early Pliocene.

Biostratigraphy

Core catcher samples from Site U1340 are dominated by diatom microfossil assemblages with high diversity. Samples also contain assemblages of radiolarian, calcareous nannofossil, foraminiferal, and organic-walled microfossils with medium to high diversity. The preservation of different microfossil groups ranges from very good to moderate. Biostratigraphic datums are derived from diatom, radiolarian, dinoflagellate, ebridian, and silicoflagellate bioevents and show that Site U1340 contains Pliocene to recent sediments. In total, 17 bioevents were identified in Hole U1340A (Fig. **F19;** Table **T2**). Age estimation below 2 Ma (~300 mbsf) is difficult because few well-confirmed biostratigraphic datums were identified. Our strategy to establish a preliminary age framework was based on percent *Neodenticula* species patterns (diatoms) compared with those at Site U1341 and tied with paleomagnetic datums (Fig. **F20;** see **"Diatoms"**). Samples 323-U1340A-1H-CC through 30H-CC (~1.8 Ma) exhibit a broadly linear sedimentation rate of ~15 cm/k.y. and rapidly increase to ~28 cm/k.y. between Samples 323-U1340A-30H-CC and 63H-CC. The sedimentation rate below Sample 323-U1340-63H-CC is apparently very low (~4 cm/k.y.) according to this preliminary age model. Siliceous microfossils occur consistently throughout the section and are mainly composed of high-latitude pelagic species that indicate changes in surface water productivity. Calcareous microfossils are mostly confined to the top of the section (approximately Samples 323-U1340A-23H-CC and above for nannofossils and 31H-CC and above for foraminifers). Below this level, only sporadic occurrences of calcareous cemented agglutinated foraminifers were detected. Benthic foraminifers are largely characteristic of those found within or near the oxygen minimum zone (OMZ) in high-latitude regions. Dinoflagellates consistently occur throughout the section, indicating changes to the productivity and sea ice cover of the surface waters.

Calcareous nannofossils

The existence, abundance, and preservation of calcareous nannofossils in the sedimentary sequences recovered at Site U1340 were determined by examining all core catcher samples from Holes U1340A–U1340D. Additional analyses of the composition of calcareous nannofossil assemblages and the abundance of individual taxa were performed simultaneously. The recorded data are shown in Table **T3** (see **"Biostratigraphy"** in the "Methods" chapter for a definition of the codes used).

Calcareous nannofossils are present in the upper third of the sediment record of Site U1340 (Samples 323-U1340A-1H-CC through 23H-CC and Holes U1340B–U1340D), but their presence is not continuous and some samples are barren. The remaining samples recovered from Hole U1340A are devoid of calcareous nannofossils, with the exception of Samples 323-U1340A-42H-CC and 43X-CC, which yielded few specimens. Preservation of the observed specimens ranges from good to moderate in Hole U1340A and from good to moderate-good in Holes U1340B–U1340D. In all holes, assemblages are mainly dominated by *Coccolithus pelagicus,* although small gephyrocapsids are more abundant in Samples 323-U1340B-3H-CC and 6H-CC, Hole U1340C, and Sample 323-U1340D-3H-CC. In Holes U1340C and U1340D, the total abundance of small gephyrocapsids exceeds 50 specimens per field of view (FOV). Reworked specimens, mostly of Miocene and Paleogene ages, were found in some samples.

A chronology based on calcareous nannofossil datums was not achieved at Site U1340 because of discontinuous records that prevented the full allocation of datums to specific samples. *Emiliania huxleyi* was identified in Samples 323-U1340B-1H-CC and 4H-CC, 323-U1340C-2H-CC, and 323-U1340D-1H-CC and 3H-CC. In these three holes, the first occurrence (FO) datum of *E. huxleyi* (0.29 Ma), which marks the base of nannofossil Zone NN21 (Martini, 1971), could not be reasonably constrained because the holes were terminated before the end of this zone. All samples from Holes U1340B–U1340D were assumed to occur within Zone NN21. Specimens of *Pseudoemiliania lacunosa* were observed in Samples 323-U1340A-7H-CC, 15H-CC, 17H-CC, 19H-CC, and 23H-CC, but only Sample 323-U1340A-7H-CC was considered to occur in Zone NN19. This zone is defined at its top by the last occurrence (LO) datum of *P. lacunosa* at 0.44 Ma and at its bottom by the LO of *Discoaster brouweri* at 2.06 Ma. Because no specimens of *D. brouweri* were found in Hole U1340A, the bottom of Zone NN19 could not be constrained and the location of Samples 323-U1340A-8H-CC through 23H-CC could not be determined. All extant taxa present at Site U1340 are characteristic of the subarctic and transitional coccolithophore zones in the Pacific (Okada and Honjo, 1973).

Planktonic foraminifers

Eighty-three core catcher samples from the >125 µm fraction from Holes U1340A–U1340D were analyzed

for planktonic foraminifers (Table T4). In addition, the >63 µm fraction of the mudline sample from the top of Core 323-U1340A-1H was analyzed. Most core catcher samples and the mudline sample are dominated by diatoms and siliciclastics. Sponge spicules are also present in the samples. However, core catcher samples from Cores 323-U1340A-1H, 9H, and 10H; Cores 323-U1340B-2H and 6H; and Core 323-U1340C-3H are dominated by planktonic foraminifers with low abundances of diatoms and siliciclastics. Planktonic foraminifers disappear downcore from Core 323-U1340A-24H only to reappear in Cores 323-U1340A-31H, 42H, and 43H. The fauna does not change significantly throughout the Pleistocene (above 200 mbsf) and is dominated by *Neogloboquadrina pachyderma* (sinistral), a subpolar–polar species (Bé and Tolderlund, 1971). This species is also the dominating species in the water column of the Bering Sea today (Asahi and Takahashi, 2007). The faunal assemblages also include the subpolar species *Globigerina bulloides, Globigerina umbilicata,* and *Neogloboquadrina pachyderma* (dextral). For the duration of the scattered reappearances of the planktonic fauna in the early Pleistocene–late Pliocene (below 200 mbsf), only these subpolar species are present. The distribution of *N. pachyderma* (dextral) is controlled by temperature (Bé and Tolderlund, 1971). *Globigerina bulloides* and *G. umbilicata* are controlled both by temperature and food availability (Reynolds and Thunell, 1985), but studies in the Bering Sea indicate that these species are also mostly controlled by temperature in this region (Asahi and Takahashi, 2007).

Benthic foraminifers

More than 40 species of benthic foraminifers were recovered in 83 samples (>63 µm fraction) from Holes U1340A–U1340D (Tables T5, T6, T7, T8). The majority of core catcher samples down to Sample 31H-CC (Assemblage I) in all holes contain abundant calcareous foraminifers. Calcareous foraminifers from this assemblage resemble species from OMZs on Umnak Plateau and in the Sea of Okhotsk (Bubenshchikova et al., 2008), as well as more common deepwater Pacific Ocean species (Butt, 1980). Abundance and diversity fall markedly below Sample 323-U1340A-32H-CC (282.17 mbsf), below which samples are either barren or consist of a monospecific agglutinated assemblage.

Assemblage I (*Islandiella norcrossi–Uvigerina* aff. *peregrina*)

Assemblage I is varyingly dominated by *Bulimina* aff. *exilis, Brizalina earlandi, Epistominella pulchella, Globobulimina pacifica, Uvigerina* aff. *peregrina,* and *Islandiella norcrossi* in Samples 1H-CC to 31H-CC in all holes. Many other species occur only occasionally, with diversity generally ranging from 5 to 15 species per sample. Variation in species dominance is likely controlled by oxygen and nutrient flux to the seafloor and may be linked to glacial–interglacial cycles, although further high-resolution work is required.

Assemblage II (depauperate)

The major characteristic of Assemblage II is the high number of barren samples between Samples 32H-CC and 55H-CC in all holes. Occasional occurrences of *Eggerella bradyi, Globocassidulina* sp., and *Gyroidinoides soldanii* are present. This interval may have been affected by dissolution because other calcareous microfossil groups are largely absent.

Assemblage III (*Martinottiella communis*)

This low-abundance assemblage is characterized by the more or less continuous and singular occurrence of *Martinottiella communis* in Samples 56H-CC through 71H-CC in all holes. This species is cosmopolitan in the modern ocean and dominant in the low-oxygen intermediate water (300–700 m) along the Pacific coast of Japan (Kaiho and Hasegawa, 1986). This interval may have suffered from some dissolution, but *M. communis* has calcareous cement, and preservation of this species is fair to good.

Ostracodes

Core catcher samples were examined for the presence of ostracodes, but no specimens were found.

Diatoms

Diatom biostratigraphy is based on analysis of core catcher samples from Hole U1340A. Depth positions and age estimates of biostratigraphic marker events are shown in Table T9. Diatoms are the dominant microfossil in all holes and show good preservation throughout. At lower depths, gaps exist in the record because of poor core retrieval during XCB coring.

Biostratigraphic zonation was constructed as far back as the early Pliocene for Hole U1340A. The LOs of *Proboscia curvirostris, Thalassiosira jouseae,* and *Proboscia barboi* were identified in Sample 323-U1340A-5H-CC (42.35 mbsf), giving a composite estimated age of 0.3 Ma. The LOs of *P. curvirostris* and *T. jouseae* were set at 0.26 and 0.31 Ma, respectively, based on a piston core recovered from the northernmost Emperor seamount (K. Katsuki and K. Takahashi, unpubl. data). However, their datums are defined as 0.3 Ma in this report because both datums co-occur in Core 323-U1340A-5H and have also been recorded at other IODP Expedition 323 sites. This age estimation

is the same as previous results from the northern subarctic Pacific and around Japan (Barron and Gladenkov, 1995; Yanagisawa and Akiba, 1998). Hence, estimated diatom datums are essentially valid for age determination at this site, although minor datum revisions at the 0.01 m.y.-scale resolution are needed in the near future. Cores above Sample 323-U1340A-5H-CC were assigned to the *Neodenticula seminae* Zone of 0.3 Ma and younger.

An age of 0.9 Ma was assigned to Sample 323-U1340A-18H-CC (165.89 mbsf) by the LO of *Actinocyclus oculatus,* which is followed by the first common occurrence (FCO) of *P. curvirostris* at 1.7–2.0 Ma in Sample 323-U1340A-23H-CC. The last common occurrence (LCO) of *Neodenticula koizumii* was found in Sample 323-U1340A-25H-CC (215.65 mbsf), giving an age of 2.1 ± 0.1 Ma. The FCO of *N. koizumii* was found in Sample 323-U1340A-59X-CC (515.1 mbsf), and the LCO of *Neodenticula kamtschatica* was found in Sample 323-U1340A-57X-CC (2.7 Ma; Barron and Gladenkov, 1995; Yanagisawa and Akiba, 1998). The interval between Samples 323-U1340A-57X-CC and 59X-CC possibly corresponds to North Pacific Diatom (NPD) Zone 8 of ~2.7–3.9 Ma. Although *N. kamtschatica* occurs earlier, beginning in Sample 323-U1340A-46X-CC, specimens are sporadic and become consistent only in Sample 56X-CC. Indeed, the LCO of *N. kamtschatica* was used to define this zone.

The FCO of *N. seminae* was initially determined in Sample 323-U1340A-38H-CC, giving an age of 2.7 ± 0.1 Ma (Barron and Gladenkov, 1995). The distinction between *N. seminae* and *N. koizumii* in the light microscope is problematic and is discussed in greater depth by Yanagisawa and Akiba (1998). The distinguishing feature between *N. seminae* and the intermediary species *Neodenticula* sp. A (which is now defined as *N. koizumii:* Yanagisawa and Akiba, 1998) under a light microscope is the presence of a closed versus an open copula. Therefore, samples were revised to verify the occurrence of *N. koizumii* and *N. seminae* by counting the presence of closed and open copulas (see **"Biostratigraphy"** in the "Methods" chapter for further discussion). The datums and subsequent age model were further confirmed by comparison of the relative abundance of *N. seminae* and *N. kamtschatica* in Holes U1340A and U1341B (Fig. **F20**). This correlation technique using tie points to match similar events in the two records was applied to confirm and support the age models at Sites U1340 and U1341 following the difficulties encountered with the identification of the FO and LO of *N. seminae* and *N. kamtschatica*. It is evident in Hole U1341B that *N. seminae* appears sporadically in older sediments but reveals a rapid increase (RI) that is mirrored in Hole U1340A. A similar correlation occurs for *N. kamtschatica* at both Sites U1340 and U1341, whereby an abrupt decrease in abundance (or rapid decrease [RD]) in Hole U1340A is matched in Hole U1341B.

The newly termed RI of *N. seminae* abundance cooccurs with the top of a paleomagnetic datum—the Olduvai section—giving a date of 1.778 Ma to Sample 323-U1341B-22H-CC. This event was matched in Hole U1340A, and the same datum was extrapolated for Hole U1341B (see **"Biostratigraphy"** in the "Site U1341" chapter for further discussion). The RD of *N. kamtschatica* was also matched to Hole U1340A, where the abrupt decrease coincides with the paleomagnetic Gauss Event, giving a subsequent datum of 2.581 Ma (see **"Biostratigraphy"** in the "Site U1341" chapter for further details).

The FCO of *N. koizumii* and the dominance of *N. kamtschatica* above Sample 323-U1340A-56X-CC define this zone as Subzone NPD7Bb with an age of 3.9 Ma. The absence of *Rouxia californica* and second-order species *Cosmiodiscus insignis, Thalassiosira praeoestrupii,* and *Thalassiosira temperei* signify that the bottom of Hole U1340A does not enter Subzone NPD7Ba (5.5 ± 0.1 Ma). The continued presence of *Thalassiosira latimarginata* s.l. until Sample 323-U1340A-71X-CC also eliminates the possibility that these species are absent because of low abundances or as a consequence of limited sample volume for slide preparation.

Diatom assemblages are mainly composed of pelagic species *N. seminae, Actinocyclus curvatulus* group, and *Thalassiosira* spp. (*Thalassiosira antarctica* spores, *T. latimarginata* group, and *T. oestrupii*) throughout the Pleistocene and upper Pliocene. The assemblage shifts during the late Pliocene (around Sample 323-U1340A-39H-CC) to an assemblage dominated by *Stephanopyxis horridus* and *N. koizumii*. Several significant abundance peaks of *Thalassiothrix longissima,* a high-productivity indicator, occur throughout the upper and lower Pliocene. In general, few freshwater diatoms or coastal water diatoms, including *Chaetoceros* spores, were observed below the upper Pleistocene, which may be attributed to this site's distal location to continental influence. At this site there is a clear shift from a lower diversity, heavily silicified assemblage (e.g., *Coscinodiscus marginatus, Stephanopyxis* spp., and *T. longissima*) to a more diverse species composition at ~260 mbsf, before the LCO of *N. koizumii*.

Silicoflagellates and ebridians

In general, silicoflagellate and ebridian abundances at this site are lower than those at Site U1339 (Table

T10). This is most likely because (1) their main habitats are in coastal waters rather than pelagic waters and (2) they are diluted by mass diatom occurrences. Therefore, the slide preparation procedure used for Site U1339 was changed for Site U1340, as described in "Biostratigraphy" in the "Methods" chapter.

Silicoflagellate and ebridian counting at this site was conducted on samples from Hole U1340A. Based on the silicoflagellate and ebridian zonation established by Ling (1973, 1992), the following datum events were located: the LO of silicoflagellate *Dictyocha subarctios* and the LO of ebridian *Ebriopsis antiqua antiqua*. The youngest datum, LO of silicoflagellate *Distephanus octonarius,* was not defined because its LO in Sample 323-U1340A-2H-CC is too young. The LO of *Dictyocha subarctios* was estimated to occur between Samples 323-U1340A-12H-CC and 13H-CC (108.78–118.63 mbsf). The Brunhes/Matuyama Chron boundary in this hole was found in Section 323-U1340A-16H-3 (134.9–136.4 mbsf). The LO of *Dc. subarctios* was estimated at 0.74 Ma based on a previous study in the Sea of Japan (Ling, 1992). In this hole, the LO of *Dc. subarctios* may be revised to 0.60–0.65 Ma if the linear sedimentation rate is applied from the top to the depth of the Brunhes/Matuyama boundary. The LO of *E. antiqua antiqua* (2.47–2.48 Ma) was found between Samples 323-U1340A-34H-CC and 35H-CC (300.36–310.59 mbsf). Although this taxon was observed in Sample 323-U1340A-12H-CC, it is considered reworked. The bottom of this hole reaches ~4.0 Ma based on micropaleontological and paleomagnetic results. However, characteristic species and their datum events were not defined for sediments older than 2.5 Ma.

Because of limited datum points, silicoflagellate and ebridian zonation is undefined for most of the cored interval in this hole. Sample 323-U1340A-12H-CC and the above interval are assigned to the *Distephanus octangulatus* Zone or the *Ds. octonarius* Zone. Zonation from Samples 323-U1340A-13H-CC to 34H-CC is undefined, but this interval may be correlated to the *Dc. subarctios* Zone and the *Ammodochium rectangulare* Zone. The interval from Sample 323-U1340A-35H-CC to the bottom of the hole is also undefined because the characteristic species *Distephanus jimlingii* needed for the zone definition is absent except for one specimen in Sample 323-U1340A-36H-CC. This undefined zone may be correlated to the *E. antiqua antiqua* Zone and the *Ds. jimlingii* Zone based on the age-depth profile of this hole.

Radiolarians

Radiolarian biostratigraphy is based on analysis of core catcher samples from Hole U1340A. Radiolarian stratigraphy at Site U1340 includes the *Botryostrobus aquilonaris* Zone (upper Quaternary) to the *Dictyophimus bullatus* Zone (middle Pliocene) in the subarctic Pacific (Kamikuri et al., 2007). However, the *Stylatractus universus* Zone (between 0.4 and 0.9 Ma) is missing because of the absence of *S. universus,* which may be attributed to very low species occurrence or a sedimentary hiatus. In addition, review of the *Cyladophora sakaii* Zone in the Bering Sea may be necessary because the occurrence of typical *C. sakaii* in Hole U1340A is very rare. Eleven radiolarian datums derived in the subarctic Pacific were identified at this site (Table T11). These radiolarian datums indicate unusual deposition, with extremely high sedimentation rates below ~500 mbsf that are not consistent with other datums. The LO of *D. bullatus* (3.8–4.0 Ma) was identified between Samples 323-U1340A-58H-CC and 59H-CC. However, its form is not typical and is similar to the *Dictyophimus* sp. B of Motoyama (1996). *Thecosphaera akitaensis* (FO: 3.8–4.0 Ma), *Ceratospyris borealis* (FO: 4.7–5.2 Ma), and *Spongurus pylomaticus* (FO: 5.2–5.5 Ma) were found in Sample 323-U1340A-71X-CC. Although the datum of *T. akitaensis* is not widely confirmed in the subarctic Pacific, we can safely say that the core bottom is younger than 5 Ma. Further investigations for the datums of the FO of *T. akitaensis* and LO of *D. bullatus* are necessary. Radiolarian abundances and preservation are consistent (Table T12), with abundant to common abundances and good to moderate preservation in the upper interval (above ~200 mbsf) and few abundances with moderate to poor preservation in the lower interval (below ~200 mbsf).

Palynology: dinoflagellate cysts, pollen, and other palynomorphs

Palynological assemblages were examined in core catcher samples from Hole U1340A (Table T13). Heavy liquid separation was systematically used because of abundant diatoms and siliciclastic debris. Although this method resulted in relatively clean residues for palynological analysis, it may have biased abundance estimates.

All samples contain poorly to well-preserved palynomorphs. The concentration of terrestrial palynomorphs is low to moderate in most samples (Table T13). Pollen grains and spores are present throughout the sequence and are composed mainly of *Picea, Pinus,* and *Sphagnum*. Their concentration is usually <200 grains/cm^3, suggesting minor input through atmospheric or ocean circulation. However, reworked pre-Neogene palynomorphs, including pollen, spores, and dinocysts, are relatively abundant in most samples (Table T13), with concentrations reaching >1000 grains/cm^3 at 100–156 mbsf and at 400 mbsf. They are generally accompanied by high

numbers of wood microfragments. The abundance of reworked palynomorphs indicates detrital inputs originating from older sediments. Freshwater palynomorphs (*Pediastrum, Botryococcus,* and tintinnids) occur only in the upper part of the sequence from 42 to 186 mbsf. Organic linings of benthic foraminifers are common in most samples, suggesting low to moderate carbonate dissolution.

Dinoflagellate cysts occur in all samples, with concentrations ranging between 55 and 22,000 cysts/cm^3. They are very abundant only in the uppermost 200 m of the sequence (Table **T13**). The assemblages are mainly dominated by the protoperidinial heterotrophic *Brigantedinium* spp., which can be associated with high productivity and upwelling. The gonyaulacale *Operculodinium centrocarpum* co-dominates the assemblage with *Brigantedinium* spp. in Sample 323-U1340A-1H-CC. *Operculodinium centrocarpum* is one of the most ubiquitous species in the Northern Hemisphere, but its distribution in surface sediments of the Bering Sea is closely related to seasonal sea ice cover (Radi et al., 2001). All accompanying taxa except the extinct species *Filisphaera filifera* are known to be abundant in polar and circumpolar regions.

The presence of *F. filifera* in Sample 323-U1340A-25H-CC indicates an age of 1.7 Ma (LO) at 215.6 mbsf. The stratigraphic range of this species (Miocene to lower Pleistocene; LO at ~1.7 Ma) was established by Matsuoka (1983) in the Niigata Basin (Japan) and by Bujak (1984) in the Bering Sea (DSDP Site 185). However, in the eastern North Atlantic the LO of *F. filifera* was established at ~1.41 Ma at DSDP Site 610 (De Schepper, 2006) and 1.4 Ma in the Norwegian-Greenland Sea (M. Smelror et al., unpubl. data).

Discussion

Quantitative and semiquantitative data were collected for each microfossil group at Site U1340 (Fig. **F21**). Diatoms are by far the most common microfossils present and show that older sediments below ~500 m CCSF-A (~2.75 Ma) contain no sea ice species. Heavily silicified valves below ~250 m CCSF-A suggest that nutrient availability may have been higher in the past, allowing valves to become more heavily silicified. The open water species *Neodenticula* spp. is also more prevalent at this time. Although its ecological preference is not well constrained, the presence of benthic foraminifer species *M. communis* above ~500 m CCSF-A (~2.75 Ma) suggests that a different bottom water nutrient regime was in place because this species is not found in younger Bering Sea sediments. Today, *M. communis* is found dominating the low-oxygen zone along the Pacific coast of Japan (Kaiho and Hasegawa, 1986). Calcareous microfossil preservation is poor below ~250 m CCSF-A, suggesting dissolution as the primary cause.

Above ~250 m CCSF-A, sea ice diatoms increase, and the absence of heavily silicified diatoms indicates that nutrients may have become less available after this time, perhaps via enhanced stratification from sea ice. Temperature does not appear to be the limiting factor because the heavily silicified *C. marginatus* valves persist in Pleistocene sediments at the gateway sites (IODP Sites U1343, U1344, and U1345). The general co-occurrence of intermediate water–dwelling radiolarian species and sea ice diatoms provides evidence for elevated intermediate water production at this time. Benthic foraminifers above ~250 m CCSF-A are indicative of low-oxygen environments, suggesting that bottom waters were affected by high organic carbon export production and/or low bottom water ventilation. The absence of warmer water planktonic foraminifers above ~200 m CCSF-A indicates that surface water cooling occurred above this interval.

Paleomagnetism

The archive halves of all APC cores recovered at Site U1340 were measured on the three-axis cryogenic magnetometer at 2.5 cm intervals, except for Section 323-U1340A-34H-4 through Core 323-U1340A-42H, which were measured at 5 cm intervals; cores below Core 323-U1340A-42H were measured at 20 cm intervals. Natural remanent magnetization (NRM) was measured before (NRM step) and/or after (demagnetization step) stepwise alternating-field (AF) demagnetization in peak fields up to 20 mT. Cores 323-U1340A-1H through 6H were measured at 10 and 20 mT demagnetization steps, and Core 323-U1340A-7H through Section 18H-4 were measured at NRM and 20 mT demagnetization steps. Other cores from Hole U1340A were measured only at 20 mT demagnetization step to keep up with core flow.

Inclination, declination, and NRM intensity after 20 mT AF demagnetization from Hole U1340A are plotted in Figure **F22,** and inclination and intensity from Holes U1340B–U1340D are plotted in Figure **F23.** The inclinations average nearly 70° over the entire depth range of the cores. The site axial dipole inclination is ~72°. The inclinations show several distinct intervals of reversed inclinations that we interpret to be polarity epochs. The declinations, after correction with the FlexIt tool to orient the declination data with north, suggest that there are multiple polarity intervals in the uppermost 17 cores from Hole

U1340A, but the FlexIt corrections are too poor to be of much detailed use in assigning polarity boundaries. The inclinations were averaged by core and section to provide an initial guide to polarity zonation in Hole U1340A (Fig. F24). The Brunhes, Jaramillo, Olduvai, and Gauss normal polarity chrons could be discerned. The age of each chron as well as preliminary defined depths are shown in Table T14. Looking more closely at directional data by core to better estimate actual polarity boundaries and comparing polarity boundaries with paleontological age estimates (see "Biostratigraphy") indicate that these two data sets are largely consistent.

NRM intensity largely remains at the same level throughout most of Hole U1340A. The presence of pyrite downcore clearly indicates that the sediments are undergoing sulfate reduction, which may be causing some limited magnetic mineral dissolution but has not caused any significant NRM intensity loss in Hole U1340A. NRM and magnetic susceptibility intensities vary more than an order of magnitude on a meter scale, probably due mostly to variable flux of detrital sediment versus biogenic sediment (mostly diatoms at this site). The large changes in NRM intensity also appear to be associated with notable detrital (and presumably magnetic) grain size changes. Both of these variations make the relative paleointensity estimates (Fig. F25), which were determined by normalizing the cleaned NRM (20 mT) by magnetic susceptibility, questionable in interpretation. The relative paleointensity variability is quite large, but most of it is strongly correlated with NRM and magnetic susceptibility variability and is probably not due mostly to geomagnetic field variability.

As at Site U1339, there is no notable evidence for the presence of magnetic field excursions in any of the cores. Sedimentation rates are sufficient that excursions would be obvious if they existed at this site, although enhanced bioturbation may have masked them. There is no evidence for secular variation that is replicable in Holes U1340A–U1340D in the uppermost ~30 m. Therefore, field variability of some type is preserved in the sediments.

Geochemistry and microbiology

Interstitial water chemistry

Nine interstitial water samples were extracted by the whole-round squeezing technique from Hole U1340B at 2.9, 5.9, 9.3, 12.3, 15.3, 24.8, 34.3, 42.3, and 53.3 mbsf. Aliquot samples were processed for routine shipboard analyses (see "Geochemistry" in the "Methods" chapter) and collected for shore-based analyses of sulfur and oxygen isotopes of sulfate and hydrogen sulfide, trace metals, dissolved organic carbon (DOC), and fatty acids. Samples for hydrocarbon and solid-phase analyses were taken down to 600 mbsf in Hole U1340A.

Chlorinity, salinity, alkalinity, dissolved inorganic carbon, and pH

Interstitial water chloride concentrations vary between 528 and 570 mM in Hole U1340B (Fig. F26G), whereas downhole salinity remains constant at 36 (Fig. F26H).

Alkalinity increases from 4.2 mM at 2.9 mbsf to 9.3 mM at 24.8 mbsf. Below this depth, alkalinity increases subtly, with a maximum concentration of 10 mM at 53.3 mbsf (Fig. F26C). Dissolved inorganic carbon (DIC) shows a similar trend as alkalinity, with a maximum concentration of 10 mM at 42.3 mbsf (Fig. F26A). pH is constant throughout all cores from Hole U1340B, averaging 7.7 (±0.05) (Fig. F26B).

Dissolved sulfate and hydrogen sulfide

The dissolved sulfate concentrations in Hole U1340B decrease from 28.2 mM at 2.9 mbsf to 23.1 mM at 53.3 mbsf (Fig. F26E). Hydrogen sulfide was detected at low concentrations, averaging 4.4 µM (Fig. F26D).

Dissolved ammonium, phosphate, and silica

Ammonium concentrations increase with depth from 0.25 mM at 2.9 mbsf to 0.93 mM at 53.3 mbsf (Fig. F26J). Phosphate concentrations gradually increase throughout the uppermost ~12 m from 2.9 to 23.3 µM, followed by a gradual decrease to 12.8 µM at 53 mbsf (Fig. F26I). Dissolved silica measured by inductively coupled plasma–atomic emission spectrometry (ICP-AES) varies between 120 and 200 µM (Fig. F27I).

Dissolved calcium, magnesium, sodium, and potassium

Major cations were analyzed using ion chromatography. Calcium concentrations decrease slightly from 10.6 to 9.0 mM (Fig. F27D). Potassium, magnesium, and sodium concentrations are 12.1–11.5, 55.1–52.6, and 501–482 mM, respectively, throughout the profile (Fig. F27A–F27C).

Dissolved minor elements

In this low-resolution sampling of the uppermost 53.3 m, all minor elements are scattered without a distinctive trend with depth (Fig. F27E–F27I). Iron is below detection limit.

Volatile hydrocarbons

Sixty headspace samples from Hole U1340A with a sample resolution of one sample per core were analyzed. Eight headspace samples from Hole U1340B were also analyzed. Methane was the only hydrocarbon gas detected at Site U1340. The concentration of methane in Holes U1340A and U1340B is <1 µM (Fig. F26F). Ethane and other volatile hydrocarbons are below detection limit in Holes U1340A and U1340B.

Sedimentary bulk geochemistry

Fourteen core catcher samples from Hole U1340A were used for the preliminary analysis of solid-phase total carbon (TC), total nitrogen (TN), total sulfur (TS), and total inorganic carbon (TIC). From these analyses, total organic carbon (TOC) and calcium carbonate ($CaCO_3$) concentrations were calculated (see "Geochemistry" in the "Methods" chapter). $CaCO_3$ concentrations in Hole U1340A range from 0 to 12.4 wt% (average = 2.2 wt%) (Fig. F28A). The increase in $CaCO_3$ content between 300 and 400 mbsf corresponds to an interval where authigenic dolomite and calcite were observed in the sediment (see "Lithostratigraphy"). TOC and TN contents range from 0.27 to 0.99 wt% (average = 0.61 wt%) and from 0.05 to 0.11 wt% (average = 0.08 wt%), respectively, in sediment from Hole U1340A (Fig. F28B, F28C). TOC concentrations decrease below ~300 mbsf. TS contents range from 0.17 to 1.19 wt% (average = 0.54 wt%) (Fig. F28D). Splits of squeeze cakes were also collected and treated for shore-based analyses of bulk elemental composition, iron mineral phases, and iron-monosulfide and pyrite content and sulfur isotope composition.

Microbiology

Samples for total prokaryotic cell abundance were collected adjacent to interstitial water whole rounds at the same resolution. Samples were fixed according to the methods described in "Microbiology" in the "Methods" chapter.

Conclusion

Undetectable methane, deep sulfate penetration, and low values of DIC, alkalinity, ammonium, and phosphate suggest low microbial activity at Site U1340 compared to Site U1339, despite similar TOC content and water depth. These data also suggest that microbial carbon turnover is driven by organoclastic sulfate reduction, whereas sulfate reduction coupled to the anaerobic oxidation of methane is absent in the uppermost 60 m at present.

Physical properties

Holes U1340A–U1340C were spudded at ~1297 m water depth in a sediment-filled structural depression on the upper eastern flank of Bowers Ridge. Core sections brought into the core laboratory from all holes were placed on the Special Task Multisensor Logger (STMSL) "fast track" and scanned for magnetic susceptibility and GRA bulk density. Core sediment was not gassy, as it was at Site U1339 on Umnak Plateau, and sections were allowed to warm to ambient laboratory temperature before being placed on the Whole-Round Multisensor Logger (WRMSL) for GRA, magnetic susceptibility, and *P*-wave scanning. Because of noisy data, noncontact resistivity values were not recorded. *P*-wave velocity and sediment shear strength measurements were not determined on working-half sections.

Magnetic susceptibility

Magnetic susceptibility values spike irregularly downhole in the uppermost 250 m of Hole U1340A, which was drilled to ~604 mbsf. The readings range from 500 to 1300 SI units. Excursions to higher values are thought to track layers richer in siliciclastic debris, in particular within the diatom silt of lithologic Unit I, which extends from the seafloor to ~275 mbsf (see "Lithostratigraphy"). Swings to high values are uncommon below ~250 mbsf, but at 525 mbsf, readings increase sharply to >1000 SI units, possibly registering a thick tephra unit. Magnetic susceptibility data are described in greater detail in "Lithostratigraphy" and "Stratigraphic correlation."

GRA wet bulk density

Bulk density determinations recorded by the WRMSL GRA sensor reveal high excursions and an apparent rhythmic pattern of higher values alternating with lower ones. The average reading in the tephra-bearing diatom silt of Unit I (surface to ~274.5 mbsf) is ~1.4 g/cm^3. Within Unit I, bulk density decreases with depth to ~1.38 g/cm^3 at ~360 mbsf. Below ~384 mbsf and a shift to XCB coring, values further decrease to ~1.32 g/cm^3. In this section of diatom ooze, which defines lithologic Unit II, bulk density increases downhole from a low of ~1.32 g/cm^3 to ~1.4 g/cm^3 at the bottom of Hole U1340A at ~604 mbsf. GRA data are shown, more fully discussed, and com-

pared with downhole changes in lithologic character in "Lithostratigraphy" and "Stratigraphic correlation." See also the below discussion in "MAD (discrete sample) wet bulk density."

Natural gamma radiation

In Hole U1340A, natural gamma radiation (NGR), which principally reflects clay mineral abundance, decreases with depth from near-surface readings averaging ~20 counts/s to ~10 counts/s at ~380 mbsf (Fig. F29). Below this depth, average NGR remains low, but significant excursions occur at levels of 30–40 counts/s and higher. A downhole oscillation from generally low to high values is discernible with a wavelength of ~80–120 m. The downhole decrease in NGR reflects the increasing relative abundance of siliceous microfossils of lithologic Unit II.

P-wave velocity

WRMSL *P*-wave velocity was measured on all core sections recovered at Site U1340. The recorded velocity profile for Hole U1340A, which reached the greatest subsurface depth (~604 mbsf) at Site U1340, is presented in Figure F30. Scattered values from ~1.45 to ~1.7 km/s increase overall from a near-surface velocity of ~1.52 km/s to ~1.55 km/s at ~280 mbsf. This section corresponds to lithologic Unit I (see "Lithostratigraphy"). The modest downsection increase in *P*-wave velocity presumably reflects slight compaction of the tephra-bearing diatomaceous silt of Unit I. In the underlying Unit II, particularly below the transition from APC to XCB coring at ~384 mbsf, average *P*-wave readings subtly increase from ~1.55 km/s to ~1.56 km/s at the bottom of Hole U1340A at ~604 mbsf. The diatomaceous ooze section and tephra beds of Unit II are likely mechanically stronger and less yielding to compaction than the overlying diatomaceous silt beds of lithologic Unit I. In general, the strength of diatomaceous deposits was also recorded in earlier DSDP holes drilled in the Bering Sea.

MAD (discrete sample) wet bulk density

Moisture and density (MAD) properties were measured on discrete samples (~10 cm^3) of sediment taken from the working halves of core sections.

The depth distribution of MAD wet bulk density is closely similar to that traced by the WRMSL GRA sensor. MAD and GRA downhole profiles are shown and compared in Figure F31. The MAD profile documents a slight downhole trend of decreasing density from ~1.44 g/cm^3 near the seafloor to ~1.38 g/cm^3 at ~360 mbsf. Below this depth, which marks a switch to XCB drilling and a ~25 m thick section of poor core recovery (~360–384 mbsf), a low average density of ~1.32 g/cm^3 was recorded. However, bulk density increases downhole to ~1.4 g/cm^3 at the bottom of Hole U1340A at ~604 mbsf (Fig. F31). A water-rich and partially load bearing section signaled by the recovery of gravelly and sandy beds in the upper part of lithologic Unit II may separate the upper decreasing and lower increasing trends in bulk density. This conjecture is also suggested by the downhole break to higher sediment porosity discussed below in "MAD porosity and water content."

MAD porosity and water content

Figure F32 displays porosity and water content with depth for sediments recovered from Hole U1340A. The two curves are closely similar, following three separate shifts in trend downhole. For porosity, the upper trend from the seafloor to ~350 mbsf displays an average value near 74% that remains virtually constant with depth. The middle trend, which begins below the transition from APC to XCB drilling at ~384 mbsf and the zone of poor recovery from ~360 to 384 mbsf, documents a shift to a higher average porosity value near 80%, below which the average decreases progressively to ~66% at ~550 mbsf. Porosity then increases to ~75% at the bottom of Hole U1340A at ~604 mbsf (Fig. F32). Hydraulically, the middle porosity sections appear to be separated from the upper section by a permeability barrier in the zone of poor core recovery between ~360 and 384 mbsf. This surmised barrier occurs at a gravel-bearing sequence within the diatom ooze section of lithologic unit II (see "Lithostratigraphy"). The isolation of the middle trend from the basal one is coincident with lithologic Subunit IIIA, a coarse-ashy layer overlying the sponge spicule–rich diatom ooze of Subunit IIIB.

Grain density

Average grain density decreases downsection from near-surface values of ~2.6 g/cm^3 to ~2.3 g/cm^3 at the bottom of Hole U1340A at ~604 mbsf (Fig. F33; Table T15). Wide excursions, some of which are so low (<1.5 g/cm^3) or high (>2.9 g/cm^3) that measuring error is suspected, occur about the mean (~2.45 g/cm^3). The downsection decreasing values appear to reflect an increase in biogenic silica, chiefly diatom frustules, with respect to terrigenous mineral debris and tephra.

Thermal conductivity

Thermal conductivity was measured on one section, typically Section 1, of each core collected from Holes U1340A–U1340D; for some cores, thermal conduc-

tivity was also recorded on a second section. Thermal conductivity decreases downhole from 0.88 W/(m·K) near the surface to ~0.77 W/(m·K) at ~580 mbsf, just above the bottom of Hole U1340A (Fig. F34). Excursions to high readings between 1.07 and 1.08 W/(m·K) occur above ~275 mbsf. These excursions are not obviously linked to the occurrence of ash layers revealed by magnetic susceptibility measurements (see "Lithostratigraphy"). A similar downhole trend in decreasing thermal conductivity readings was observed at Site U1339 on Umnak Plateau. The downsection decrease in thermal conductivity presumably reflects increasing content of siliceous biogenic components with respect to terrigenous material and, particularly in Hole U1340A, sediment older than ~2.5 Ma, roughly the onset of NHG.

Stratigraphic correlation

The composite depth scale and splice at Site U1340 is complete from 0.0 to 59.14 m CCSF-A (as defined in "Stratigraphic correlation" in the "Methods" chapter). This splice is tentative because of some evidence for soft-sediment deformation in some of the cores, including features that do not appear to correlate between holes and, in some cases, appear to be repeated within a single hole. Some of the depth transfers implied by the affine table cannot be explained with plausible amounts of heave and likely represent real thickness variations of strata on a small spatial scale. We emphasize that this splice should be checked with more detailed shore-based data, and, because we adjusted depths for all intervals regardless of whether deformation was observed, the composite depths do not represent an estimate of depths in an undeformed sediment column and cannot easily be converted back to drilling depths. The splice ranges from the top of Core 323-U1340D-1H to the bottom of Section 323-U1340B-6H-7 (Tables T16, T17). Cores below the splice are not continuous but are appended with a constant depth adjustment. Correlations were accomplished using IODP Correlator software (version 1.655) linked with the image display software Correlyzer (version 1.3.2).

The composite (CCSF-A) and splice (CCSF-D) depth scales are based primarily on the stratigraphic correlation of WRMSL GRA bulk density and magnetic susceptibility data collected at 5 cm intervals (Figs. F35, F36). These primary correlations were assisted and verified throughout the cored interval with split-core color reflectance parameter b* (Fig. F37). We further improved the ties between holes by visual inspection of the cores and digital line-scan images (Fig. F38), which revealed marker beds such as a distinctive pink ash layers (Fig. F38C).

The CCSF-A and CCSF-D scales were constructed by assuming that the uppermost sediment (the mudline) in Core 323-U1340D-1H was the sediment/water interface; this is the longest of three mudline cores collected (also Cores 323-U1340A-1H and 323-U1340B-1H), and these three cores confirmed the fidelity of the top of the recovered section (Fig. F39). Note that in the CCSF-A scale, the tops of Cores 323-U1340A-1H and 323-U1340B-1H have negative depths at the mudline because their depths were adjusted upward to improve their correlation to Core 323-U1340D-1H, which was selected as the anchor in the composite depth scale because it is longer than the others. Core 323-U1340D-1H is the only core with depths that are the same on the mbsf and CCSF-A scales. From this anchor we worked downhole, correlating the stratigraphy on a core-by-core basis using Correlator; however, we also considered digital line-scan images, especially in complex intervals with nonhorizontal beds or where we suspected that intervals may have been repeated between nonconformable surfaces (Fig. F38).

The match between Cores 323-U1340D-1H and 323-U1340A-2H is not well constrained because of minimal overlap between these two cores (Fig. F39). The match between Cores 323-U1340B-3H and 323-U1340A-3H appears convincing (based on WRMSL GRA bulk density data), but at equivalent drilling depths this interval appears to be missing from Holes U1340C and U1340D. We infer that the same pink ash is present in Cores 323-U1340A-5H, 323-U1340B-4H, and 323-U1340D-3H (Fig. F39). The presence of similar pink ash was observed three times in Hole U1340C (twice in Core 323-U1340C-2H and once in Core 3H) in structures that appear similar in their pattern of magnetic susceptibility variations (Fig. F39). We infer that these are repeated sections caused by soft-sediment deformation. This is consistent with other evidence for tilted beds and nonconformable surfaces (see "Lithostratigraphy"). It is likely that deformation of the sediment column has produced thickened and noncorrelative intervals in the depth interval from ~20 to ~45 m CCSF-A in Holes U1340B and U1340C and perhaps also in Holes U1340A and U1340D. The full sedimentary sequence may not be represented in the composite splice for these intervals. Cores 323-U1340B-3H, 323-U1340A-4H, and 323-U1340B-4H are tentatively spliced and include the least disturbed intervals through the interval of inferred deformation (Figs. F39, F40).

The cumulative offset between the mbsf and CCSF-A depth scales is not straightforward (Fig. F41), in part because of the possibility of slumped and repeated sections and also because Hole U1340C was started 10.13 m below the mudline. Affine growth factors (a

measure of the fractional stretching of the composite section relative to the drilled interval; see **"Stratigraphic correlation"** in the "Methods" chapter) in the spliced interval are 1.14 in Hole U1340A and 1.18 in Hole U1340B. These values are within the normal range typical of many drill sites. Affine growth factors for Holes U1340C and U1340D are not calculated given the apparent dominance of slumping at these locations.

The remaining cores in Hole U1340A (Cores 323-U1340A-7H through 71X) are not tied to the splice but are appended to the bottom of the splice with a constant affine value of 7.31 m.

Downhole measurements

Because of uncertain hole conditions in Hole U1340A and the potentially higher yield of logs for cruise objectives at Site U1341, the logging program was deferred until Site U1341 was drilled. The only downhole measurements made at Site U1340 were APCT-3 in situ temperature measurements.

Temperature measurements

The downhole temperature measurements at Site U1340 included four APCT-3 deployments in Hole U1340A (Table **T18**). During its deployment in Core 323-U1340A-3H, the APCT-3 failed to couple properly with the formation and the recorded data could not be used. The measured temperatures range from 5.67°C at 70.4 m DSF to 9.79°C at 165.4 m DSF and closely fit a linear geothermal gradient of 43.4°C/km (Fig. **F42**). The temperature at the seafloor was 2.8°C based on the average of the measurements at the mudline during all APCT-3 deployments. A simple estimate of the heat flow can be obtained from the product of the geothermal gradient by the average thermal conductivity (0.851 W/[m·K]; see **"Physical properties"**), which gives a value of 36.9 mW/m², within the range of previous measurement in the area (the global heat flow database of the International Heat Flow Commission can be found at **www.heatflow.und.edu/index.html**).

Considering the variations in thermal conductivity with depth, a more accurate measure of the heat flow in a conductive regime can be given by a "Bullard plot." The thermal resistance of an interval is calculated by integrating the inverse of thermal conductivity over depth. If the thermal regime is purely conductive, the heat flow will be the slope of the temperature versus thermal resistance profiles (Bullard, 1939). Thermal resistance calculated over the intervals overlying the APCT-3 measurements is shown in Table **T18,** and the resulting linear fit of the temperature gives a slightly higher heat flow value of 37.8 mW/m².

References

Asahi, H., and Takahashi, K., 2007. A 9-year time-series of planktonic foraminifer fluxes and environmental change in the Bering Sea and the central subarctic Pacific Ocean, 1990–1999. *Prog. Oceanogr.,* 72(4):343–363. **doi:10.1016/j.pocean.2006.03.021**

Barron, J.A., and Gladenkov, A.Y., 1995. Early Miocene to Pleistocene diatom stratigraphy of Leg 145. *In* Rea, D.K., Basov, I.A., Scholl, D.W., and Allan, J.F. (Eds.), *Proc. ODP, Sci. Results,* 145: College Station, TX (Ocean Drilling Program), 3–19. **doi:10.2973/odp.proc.sr.145.101.1995**

Bé, A.W.H., and Tolderlund, D.S., 1971. Distribution and ecology of living planktonic foraminifera in surface waters of the Atlantic and Indian Oceans. *In* Funnel, B.M., and Riedel, W.R. (Eds.), *The Micropaleontology of Oceans:* Cambridge (Cambridge Univ. Press), 105–149.

Bubenshchikova, N., Nürnberg, D., Lembke-Jene, L., and Pavlova, G., 2008. Living benthic foraminifera of the Okhotsk Sea: faunal composition, standing stocks and microhabitats. *Mar. Micropaleontol.,* 69(3–4):314–333. **doi:10.1016/j.marmicro.2008.09.002**

Bujak, J.P., 1984. Cenozoic dinoflagellate cysts and acritarchs from the Bering Sea and northern North Pacific, DSDP Leg 19. *Micropaleontology,* 30(2):180–212. **doi:10.2307/1485717**

Bullard, E.C., 1939. Heat flow in South Africa. *Proc. R. Soc. London, Ser. A,* 173:474–502.

Butt, A., 1980. Biostratigraphic and paleoenvironmental analyses of the sediments at the Emperor Seamounts, DSDP Leg 55, Northwestern Pacific: Cenozoic foraminifers. *In* Jackson, E.D., Koizumi, I., et al., *Init. Repts. DSDP,* 55: Washington, DC (U.S. Govt. Printing Office), 289–325. **doi:10.2973/dsdp.proc.55.108.1980**

Cook, M.S., Keigwin, L.D., and Sancetta, C.A., 2005. The deglacial history of surface and intermediate water of the Bering Sea. *Deep-Sea Res., Part II,* 52(16–18):2163–2173. **doi:10.1016/j.dsr2.2005.07.004**

De Schepper, S., 2006. Plio-Pleistocene dinoflagellate cyst biostratigraphy and palaeoecology from the eastern North Atlantic and southern North Sea Basin [Ph.D. thesis]. Univ. Cambridge, Cambridge.

Kaiho, K., and Hasegawa, S., 1986. Bathymetric distribution of benthic foraminifera in bottom sediments off Onahama, Fukushima Prefecture, northeast Japan. *In* Matoba, Y., and Kato, M. (Eds.), *Studies on Cenozoic Benthic Foraminifera:* Akita (Akita Univ.), 43–52. (in Japanese)

Kamikuri, S., Nishi, H., and Motoyama, I., 2007. Effects of late Neogene climatic cooling on North Pacific radiolarian assemblages and oceanographic conditions. *Palaeogeogr., Palaeoclimatol., Palaeoecol.,* 249(3–4):370–392. **doi:10.1016/j.palaeo.2007.02.008**

Katsuki, K., and Takahashi, K., 2005. Diatoms as paleoenvironmental proxies for seasonal productivity, sea-ice and

surface circulation in the Bering Sea during the late Quaternary. *Deep-Sea Res., Part II,* 52(16–18):2110–2130. **doi:10.1016/j.dsr2.2005.07.001**

Ling, H.Y., 1973. Silicoflagellates and ebridians from Leg 19. *In* Creager, J.S., Scholl, D.W., et al., *Init. Repts.* DSDP, 19: Washington (U.S. Govt. Printing Office), 751–775. **doi:10.2973/dsdp.proc.19.127.1973**

Ling, H.Y., 1992. Late Neogene silicoflagellates and ebridians from Leg 128, Sea of Japan. *In* Pisciotto, K.A., Ingle, J.C., Jr., von Breymann, M.T., and Barron, J., et al. (Eds.), *Proc. ODP, Sci. Results,* 127/128, Pt. 1: College Station, TX (Ocean Drilling Program), 237–248. **doi:10.2973/odp.proc.sr.127128-1.126.1992**

Lisiecki, L.E., and Raymo, M.E., 2005. A Pliocene–Pleistocene stack of 57 globally distributed benthic $\delta^{18}O$ records. *Paleoceanography,* 20(1):PA1003. **doi:10.1029/2004PA001071**

Martini, E., 1971. Standard Tertiary and Quaternary calcareous nannoplankton zonation. *In* Farinacci, A. (Ed.), *Proc. Int. Conf. Planktonic Microfossils Roma:* Rome (Ed. Tecnosci.), 2:739–785.

Matsuoka, K., 1983. Late Cenozoic dinoflagellates and acritarchs in the Niigata District, central Japan. *Palaeontogr. Abt. B Palaeophytol.,* 187(1–3):89–154.

Motoyama, I., 1996. Late Neogene radiolarian biostratigraphy in the subarctic Northwest Pacific. *Micropaleontology,* 42(3):221–262. **doi:10.2307/1485874**

Okada, H., and Honjo, S., 1973. The distribution of oceanic coccolithophorids in the Pacific. *Deep-Sea Res., Part A,* 20(4):355–374.

Radi, T., de Vernal, A., and Peyron, O., 2001. Relationships between dinoflagellate cyst assemblages in surface sediment and hydrographic conditions in the Bering and Chukchi seas. *J. Quat. Sci.,* 16(7):667–680. **doi:10.1002/jqs.652**

Reimnitz, E., McCormick, M., Bischof, J., and Darby, D.A., 1998. Comparing sea-ice sediment load with Beaufort Sea shelf deposits: is entrainment selective? *J. Sediment. Res.,* 68(5):777–787. **http://jsedres.sepmonline.org/cgi/reprint/68/5/777**

Reynolds, L., and Thunell, R.C., 1985. Seasonal succession of planktonic foraminifera in the subpolar North Pacific. *J. Foraminiferal Res.,* 15(4):282–301. **doi:10.2113/gsjfr.15.4.282**

Scholl, D.W., and Creager, J.S., 1973. Geologic synthesis of Leg 19 (DSDP) results; far North Pacific, and Aleutian Ridge, and Bering Sea. *In* Creager, J.S., Scholl, D.W., et al., *Init. Repts. DSDP,* 19: Washington, DC (U.S. Govt. Printing Office), 897–913. **doi:10.2973/dsdp.proc.19.137.1973**

Takahashi, K., 2005. The Bering Sea and paleoceanography. *Deep-Sea Res., Part II,* 52(16–18):2080–2091. **doi:10.1016/j.dsr2.2005.08.003**

Takahashi, K., Ravelo, A.C., and Alvarez Zarikian, C.A., 2009. Pliocene–Pleistocene paleoceanography and climate history of the Bering Sea. *IODP Sci. Prosp.,* 323. **doi:10.2204/iodp.sp.323.2009**

VanLaningham, S., Pisias, N.G., Duncan, R.A., and Clift, P.D., 2009. Glacial–interglacial sediment transport to the Meiji Drift, northwest Pacific Ocean: evidence for timing of Beringian outwashing. *Earth Planet. Sci. Lett.,* 277(1–2):64–72. **doi:10.1016/j.epsl.2008.09.033**

Yanagisawa, Y., and Akiba, F., 1998. Refined Neogene diatom biostratigraphy for the northwest Pacific around Japan, with an introduction of code numbers for selected diatom biohorizons. *Chishitsugaku Zasshi,* 104:395–414.

Publication: 15 March 2011
MS 323-104

Figure F1. Location map for Site U1340 on Bowers Ridge.

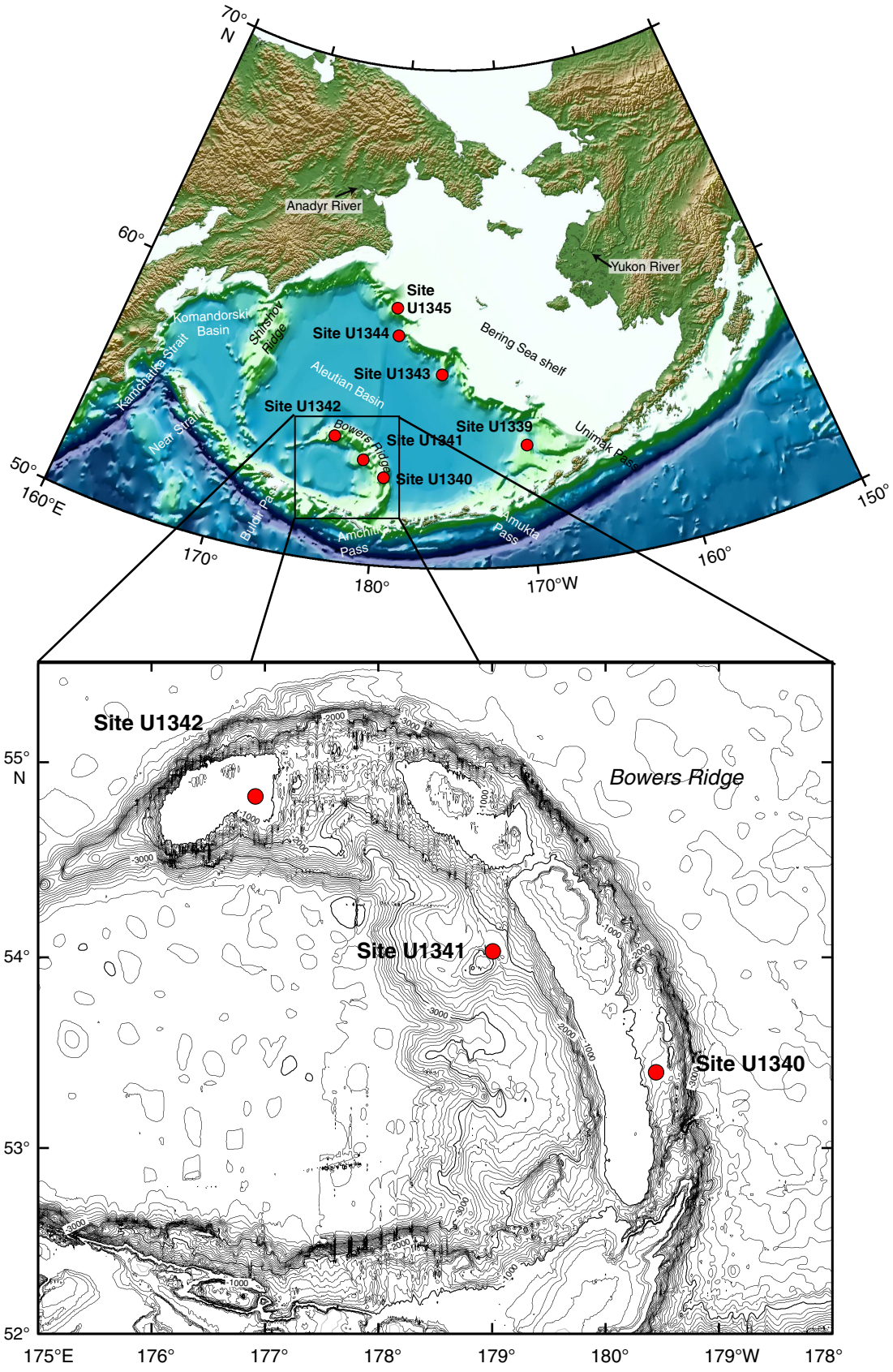

Figure F2. Seismic profile of *Hakuhou-Maru* Cruise KH99-3 Line Stk6-1 (west–east) near Site U1340.

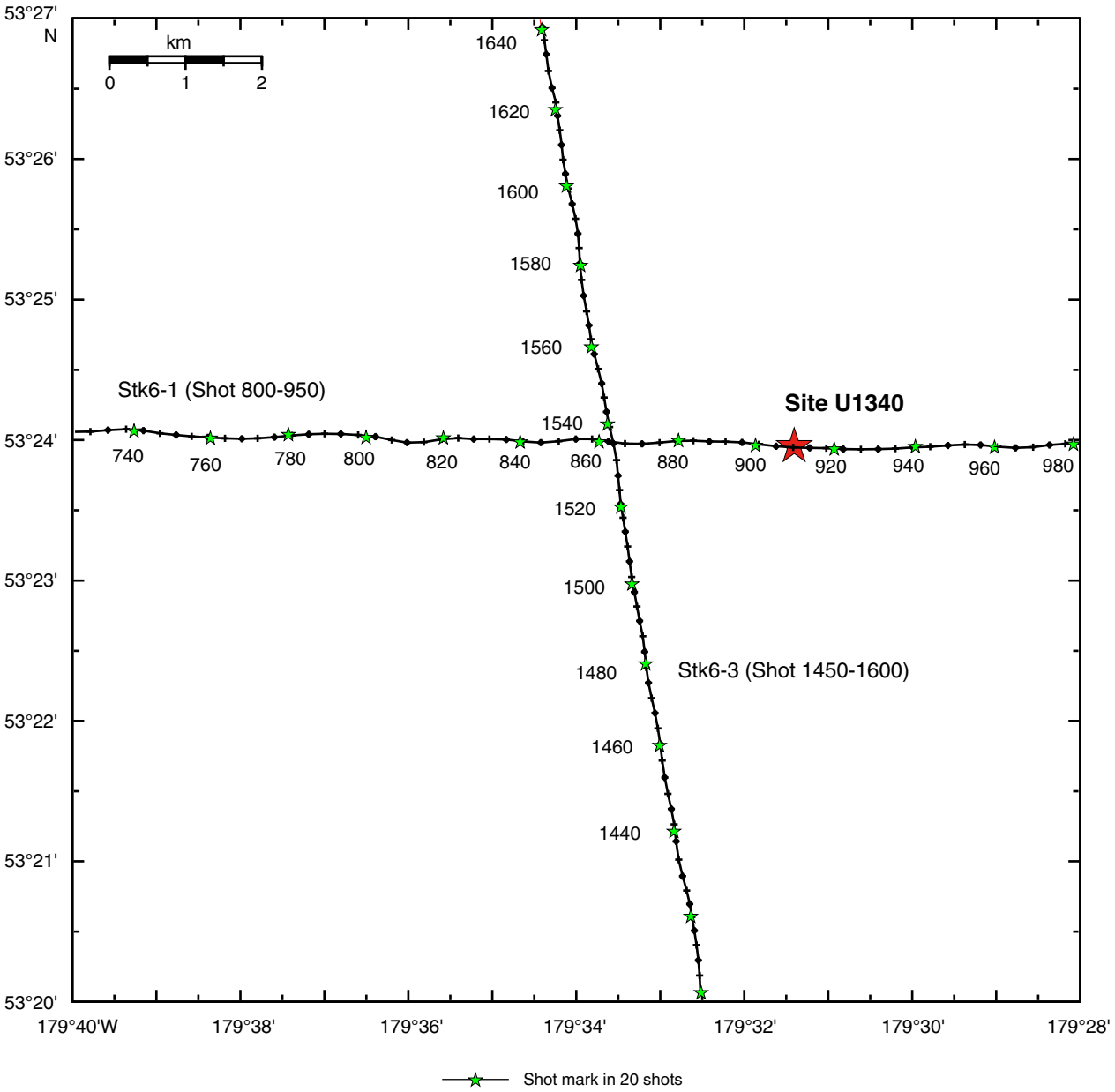

Figure F3. Navigation map of *Hakuhou-Maru* Cruise KH99-3 around Site U1340 for close-up seismic profiles shown in Figures F4 and F5.

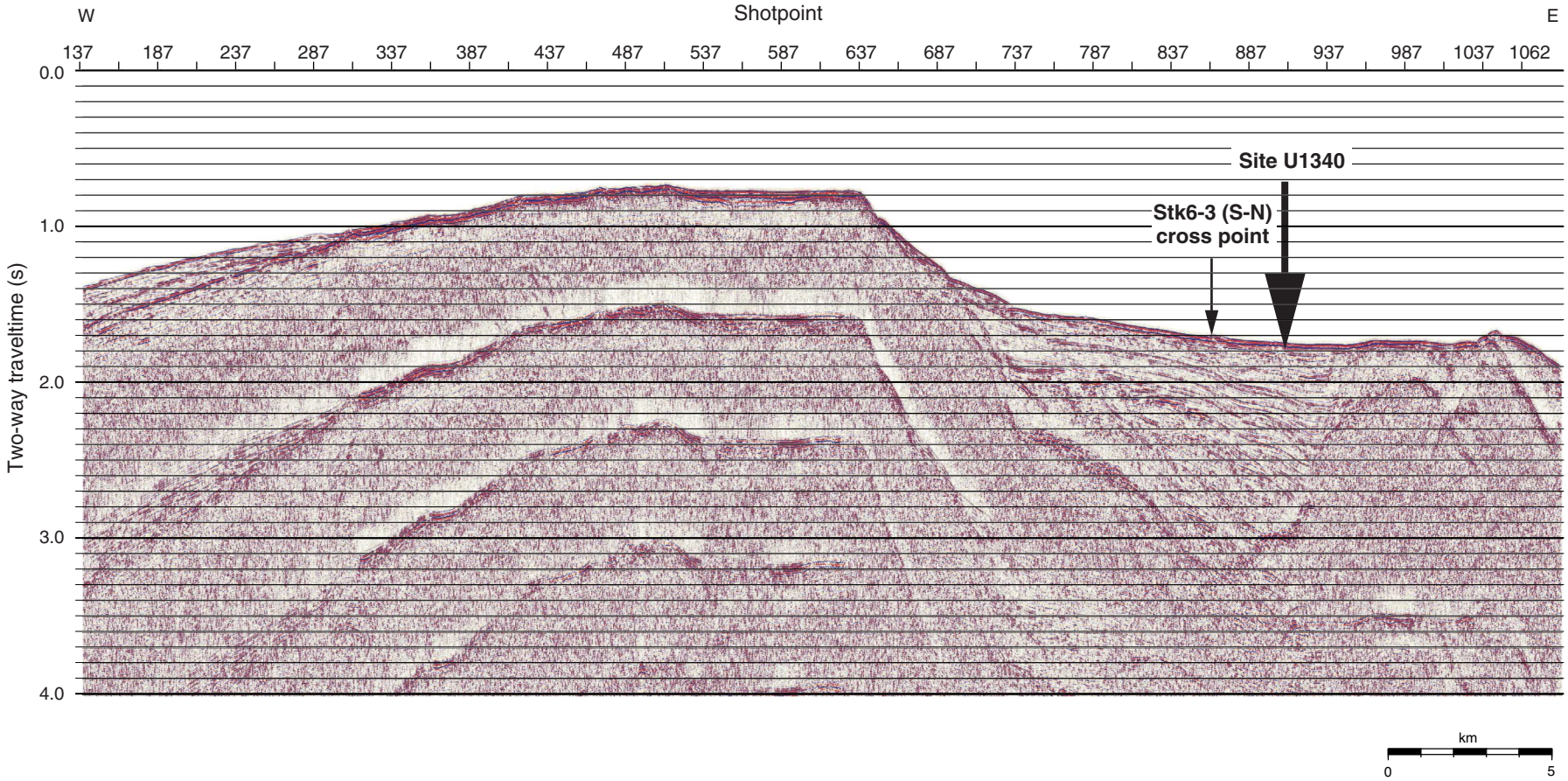

Figure F4. A. Close-up seismic profile of *Hakuhou-Maru* Cruise KH99-3 Line Stk6-1 (west–east) near Site U1340. Cross point with Line Stk6-3 (south–north) is at Shotpoint 863. **B.** Time-depth curve estimated from results of velocity analyses on Lines Stk6-1 and Stk6-3 around Site U1340.

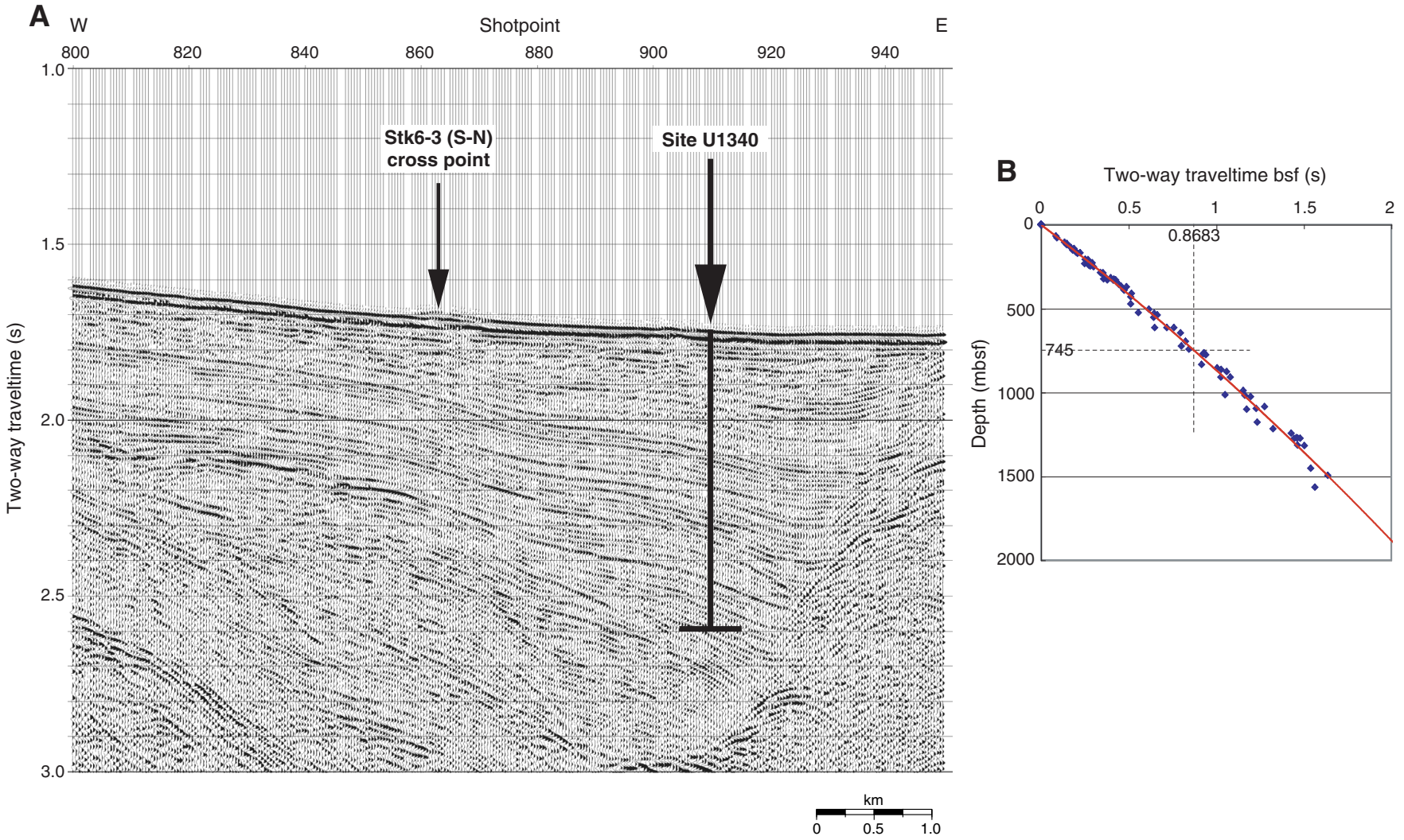

Figure F5. A. Close-up seismic profile of *Hakuhou-Maru* Cruise KH99-3 Line Stk6-3 (south–north) near Site U1340. Penetration depth of this site is projected from the east on the cross point (Fig. F4). **B.** Time-depth curve estimated from results of velocity analyses on Lines Stk6-1 and Stk6-3 around Site U1340.

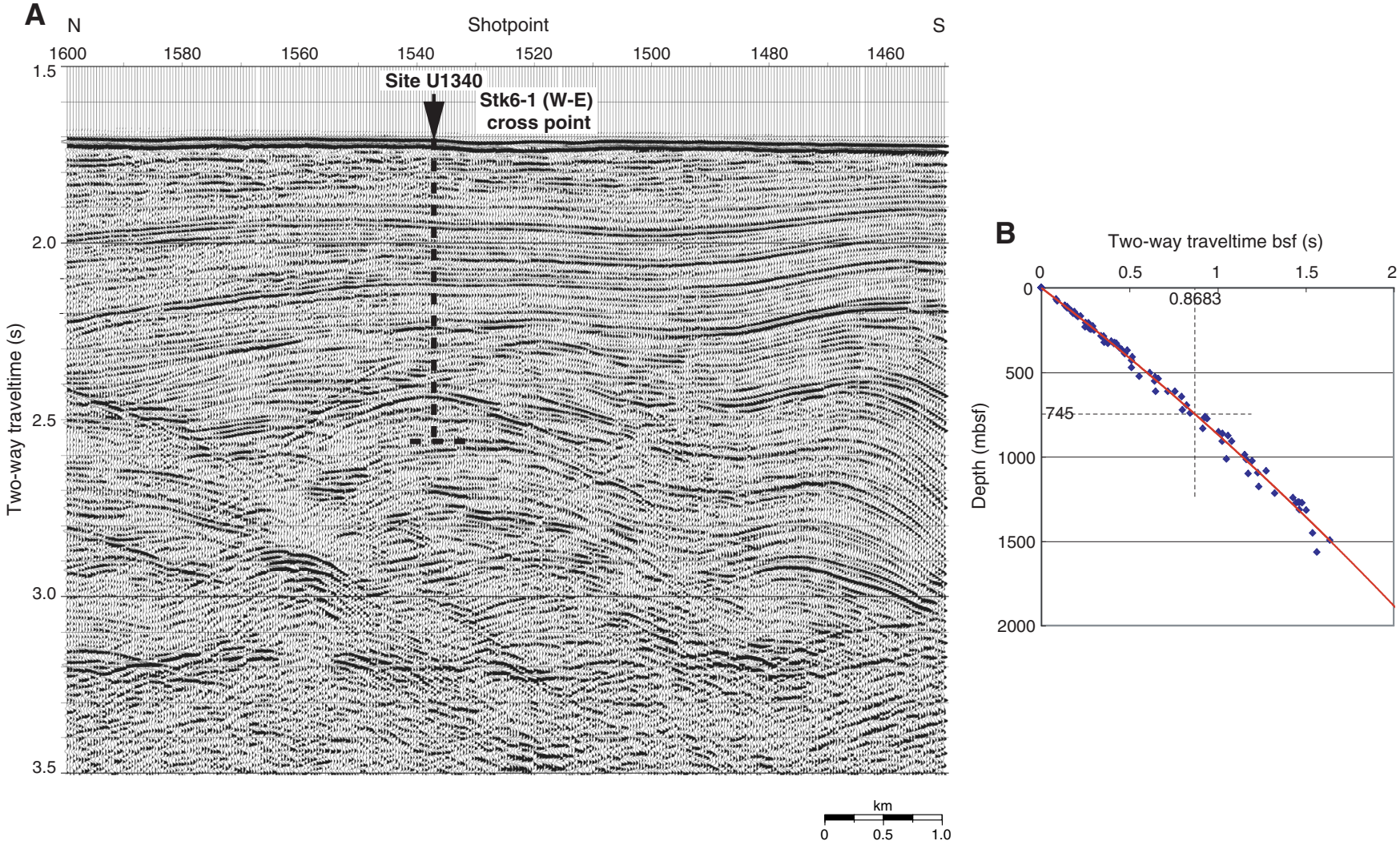

Figure F6. Summary of lithology, structures, accessories, microfossils, and physical properties, Hole U1340A. See legend in Figure F6 in the "Methods" chapter. Soft-sed = soft-sediment, auth = authigenic, calc = calcareous, NGR = natural gamma radiation, GRA = gamma ray attenuation, sed rate = sedimentation rate. **A.** 0–250 mbsf. (**Continued on next two pages.**)

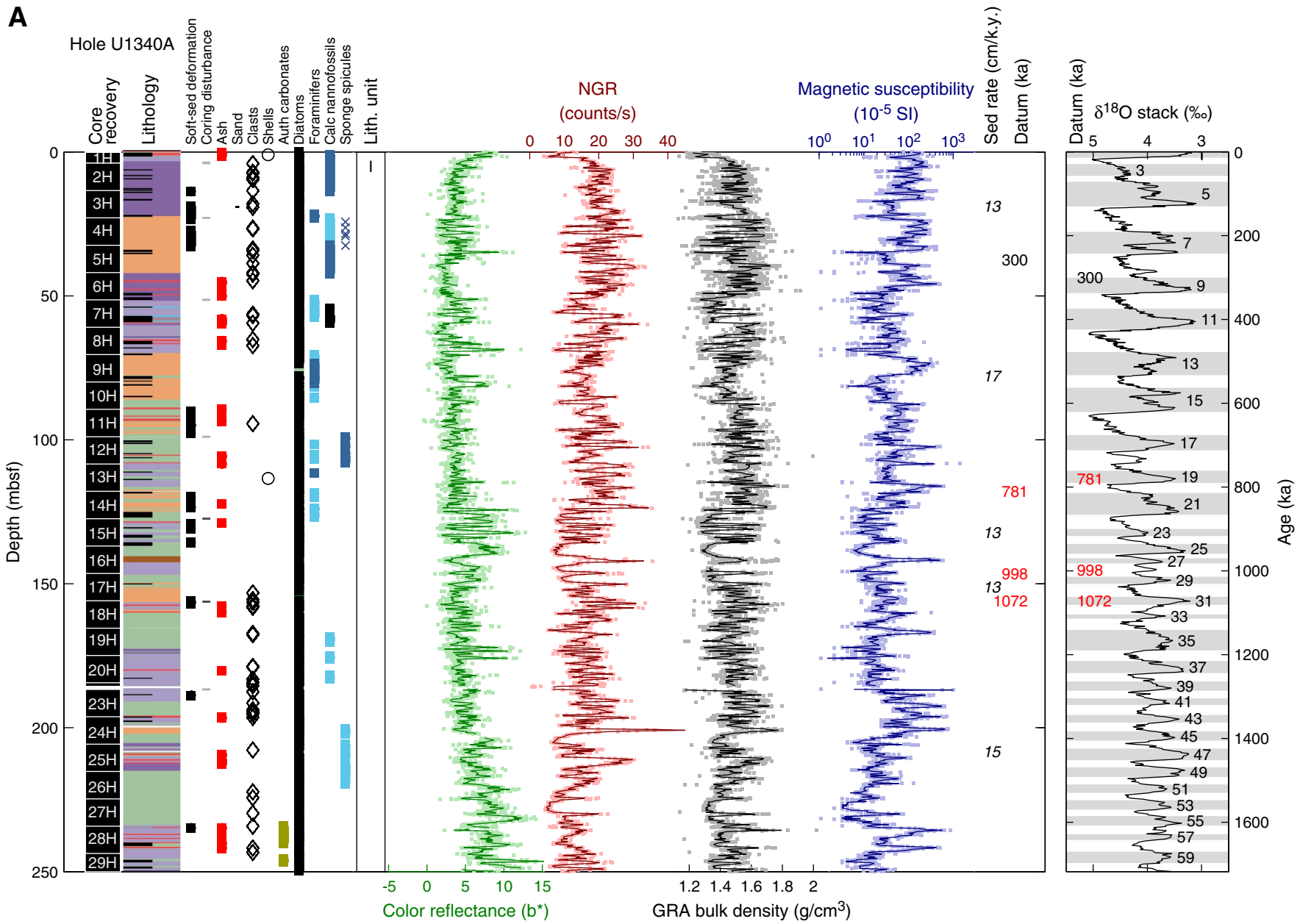

Figure F6 (continued). B. 250–500 mbsf. (Continued on next page.)

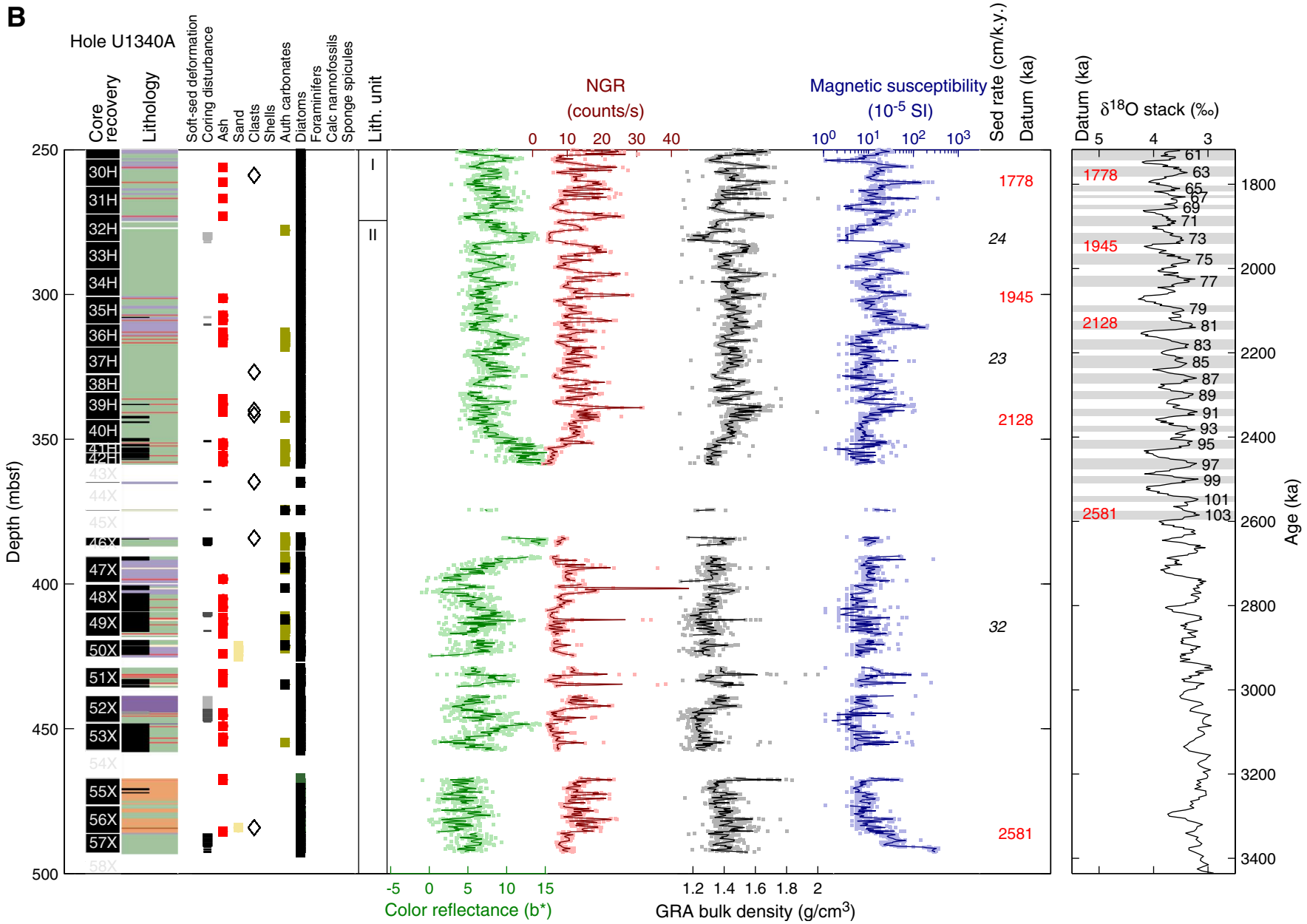

Figure F6 (continued). C. 500–750 mbsf.

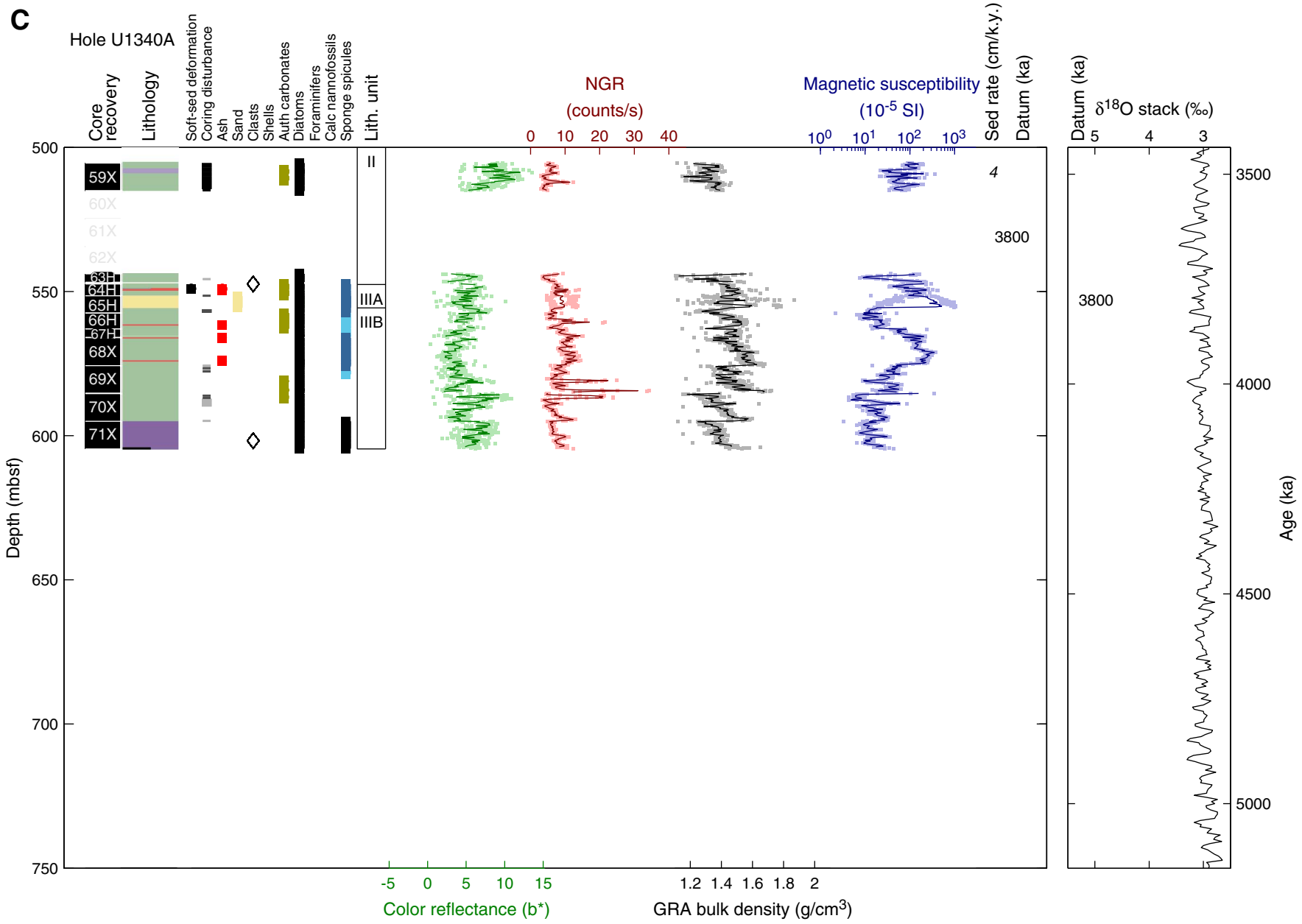

Figure F7. Summary of lithology, structures, accessories, microfossils, and physical properties, Hole U1340B. See legend in Figure F6 in the "Methods" chapter. Soft-sed = soft-sediment, auth = authigenic, calc = calcareous, NGR = natural gamma radiation, GRA = gamma ray attenuation, sed rate = sedimentation rate.

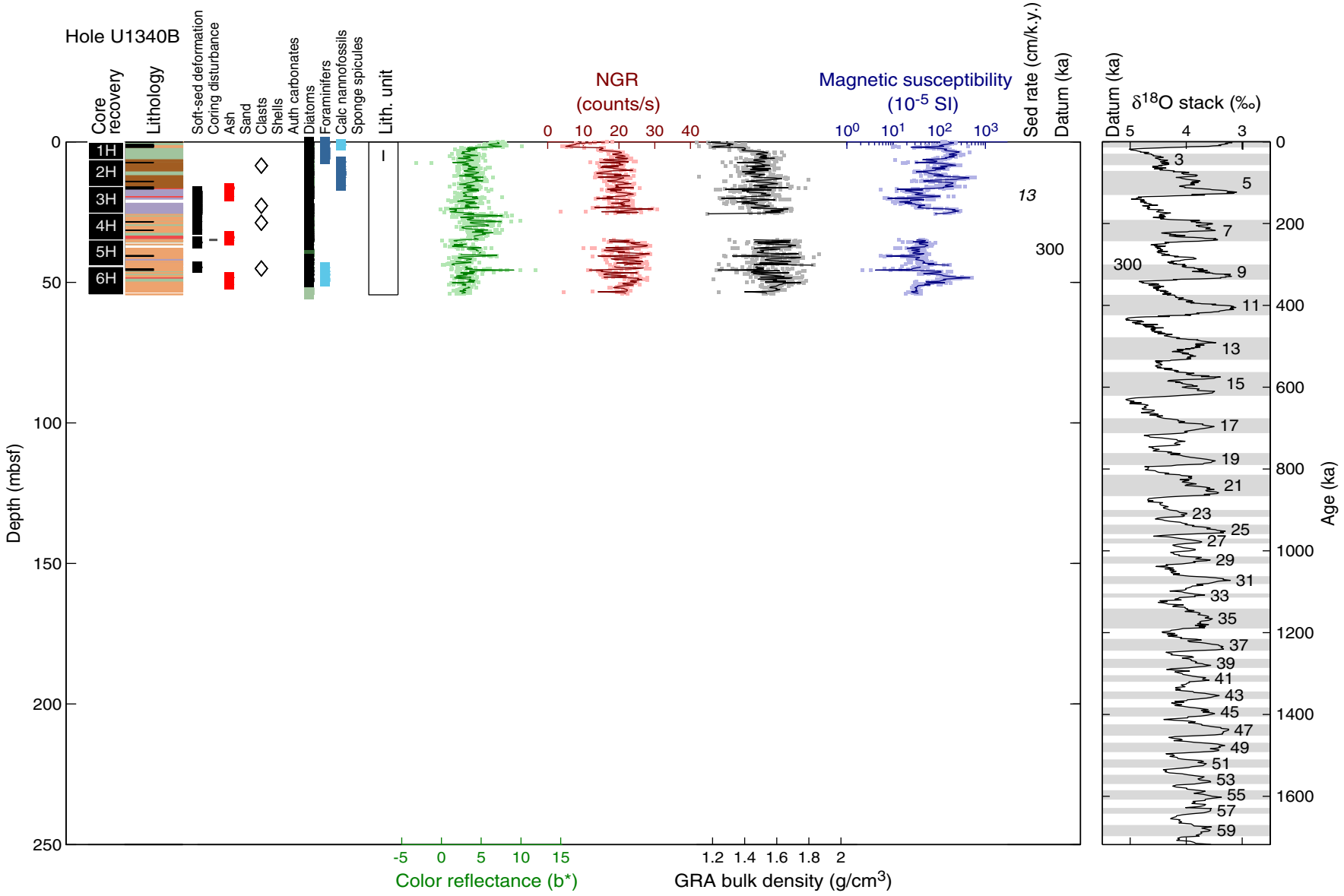

Figure F8. Summary of lithology, structures, accessories, microfossils, and physical properties, Hole U1340C. See legend in Figure F6 in the "Methods" chapter. Soft-sed = soft-sediment, auth = authigenic, calc = calcareous, NGR = natural gamma radiation, GRA = gamma ray attenuation, sed rate = sedimentation rate.

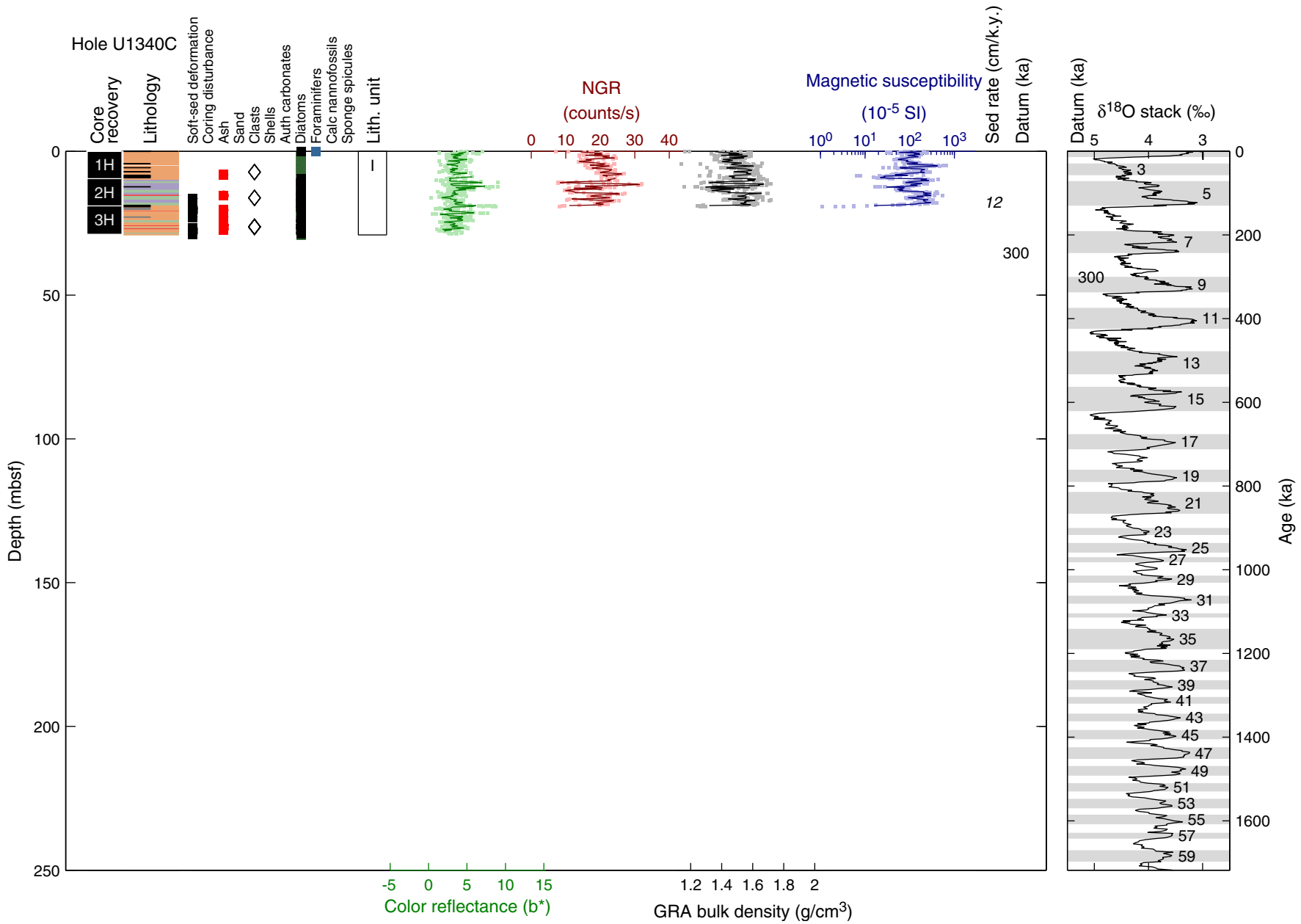

Figure F9. Summary of lithology, structures, accessories, microfossils, and physical properties, Hole U1340D. See legend in Figure F6 in the "Methods" chapter. Soft-sed = soft-sediment, auth = authigenic, calc = calcareous, NGR = natural gamma radiation, GRA = gamma ray attenuation, sed rate = sedimentation rate.

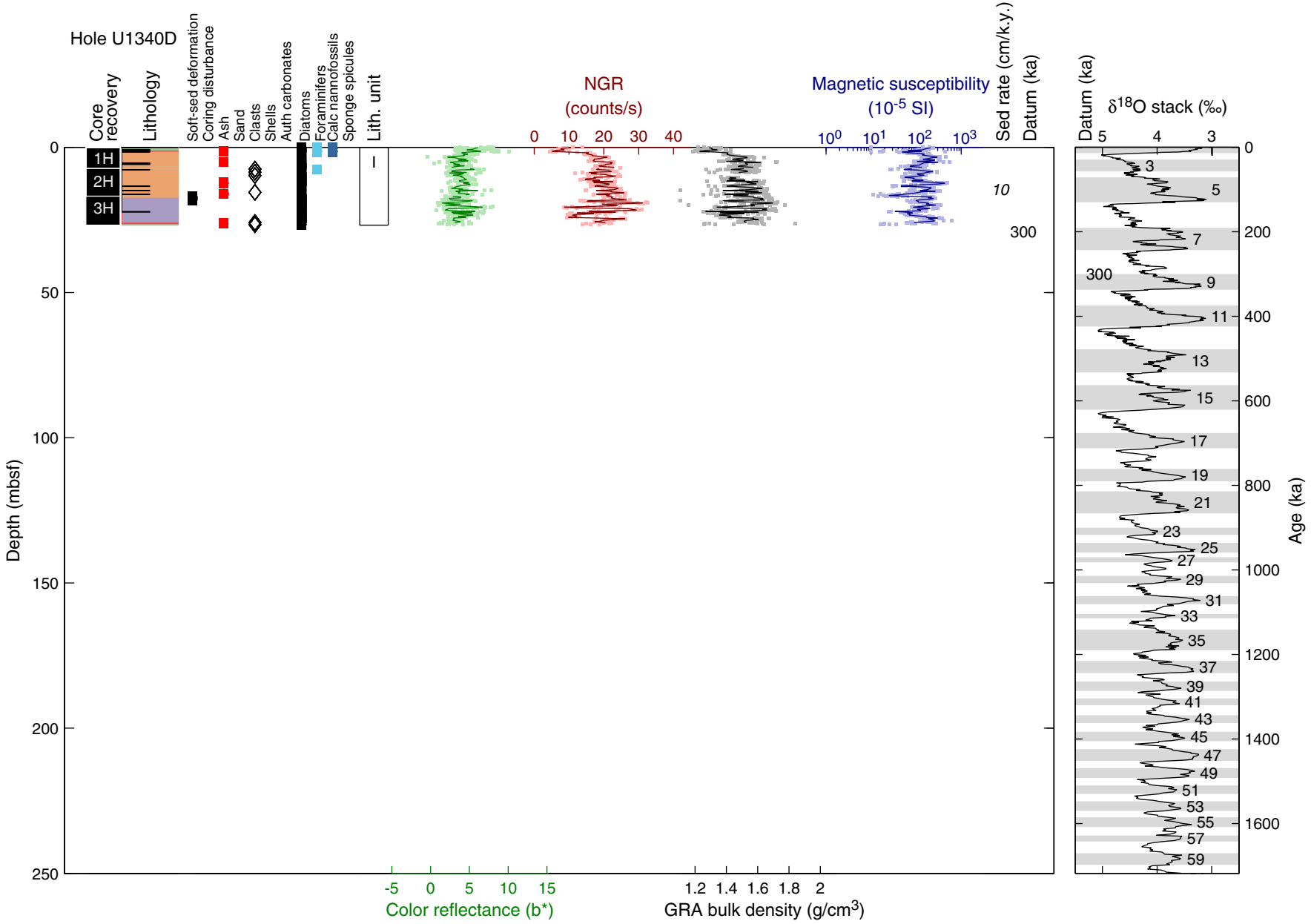

Figure F10. Core photographs and photomicrographs of smear slides of laminations. **A.** Nearly monospecific diatom ooze lamina with *Lioloma pacificum* from interval 323-U1340A-52H-5, 115–150 cm. **B.** Silicoflagellate-rich lamina from interval 323-U1340A-6H-7, 40–55 cm. Boxes indicate the approximate position of smear slide sample locations.

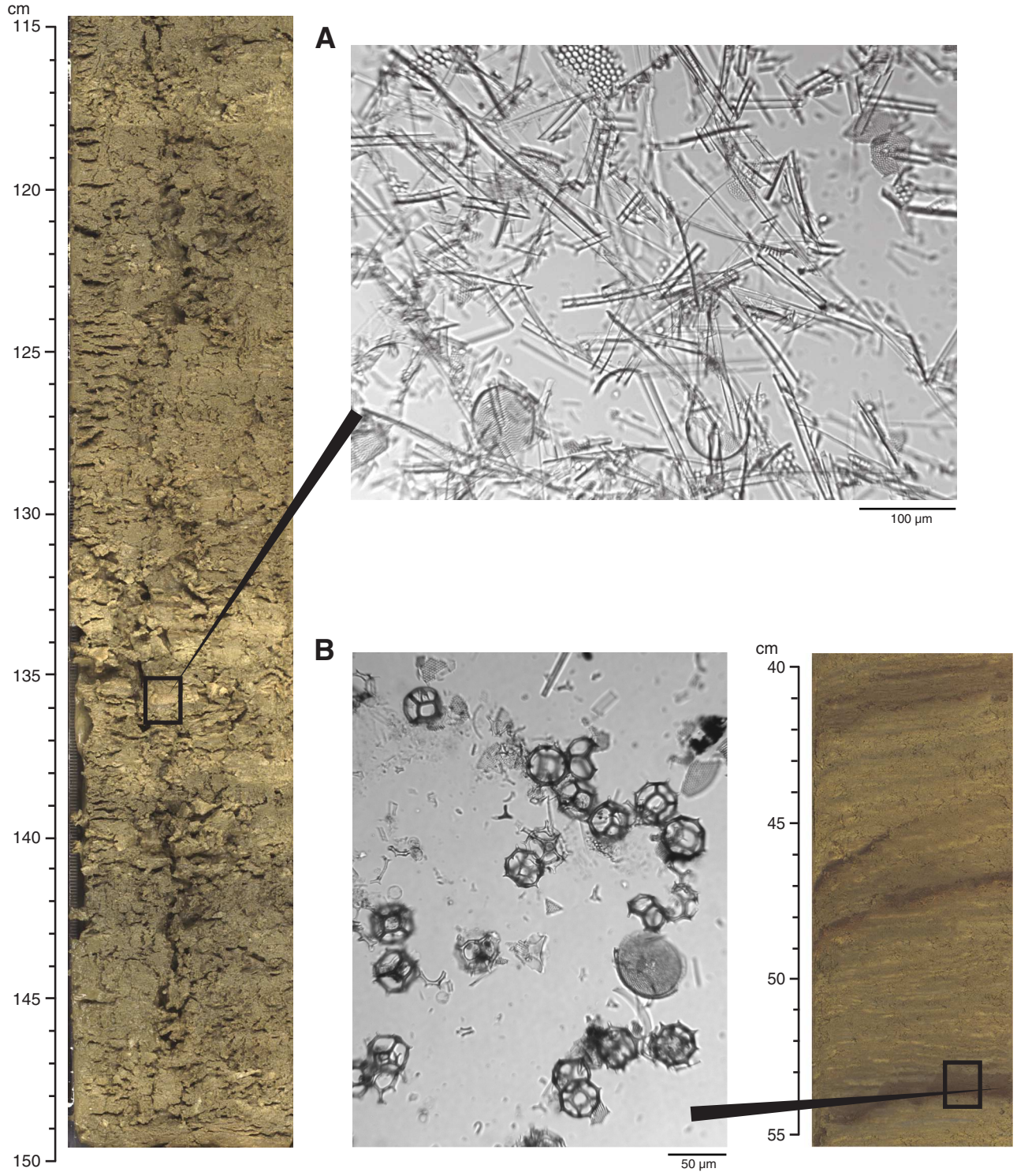

Figure F11. Core photograph of interval 323-U1340A-38H-2, 83–94 cm, showing a graded black ash layer with a sharp base and bioturbated top.

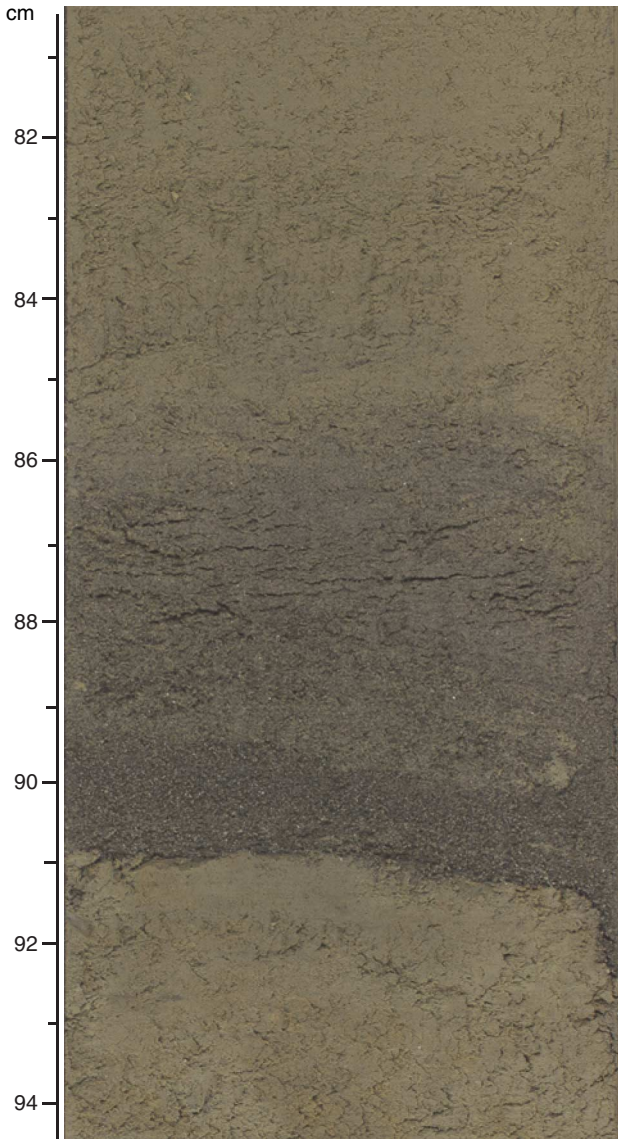

Figure F12. Silica diagenesis summary showing four representative X-ray diffractograms, core recovery, core image, lithologic units, and lithology, Hole U1340A. X-ray diffraction peaks are labeled with the abbreviation of the mineral they represent. Cr = cristobalite, T = tridymite, O-A = opal-A, Q = quartz, C = calcite, H = halite, Fsp = feldspar, Py = pyrite.

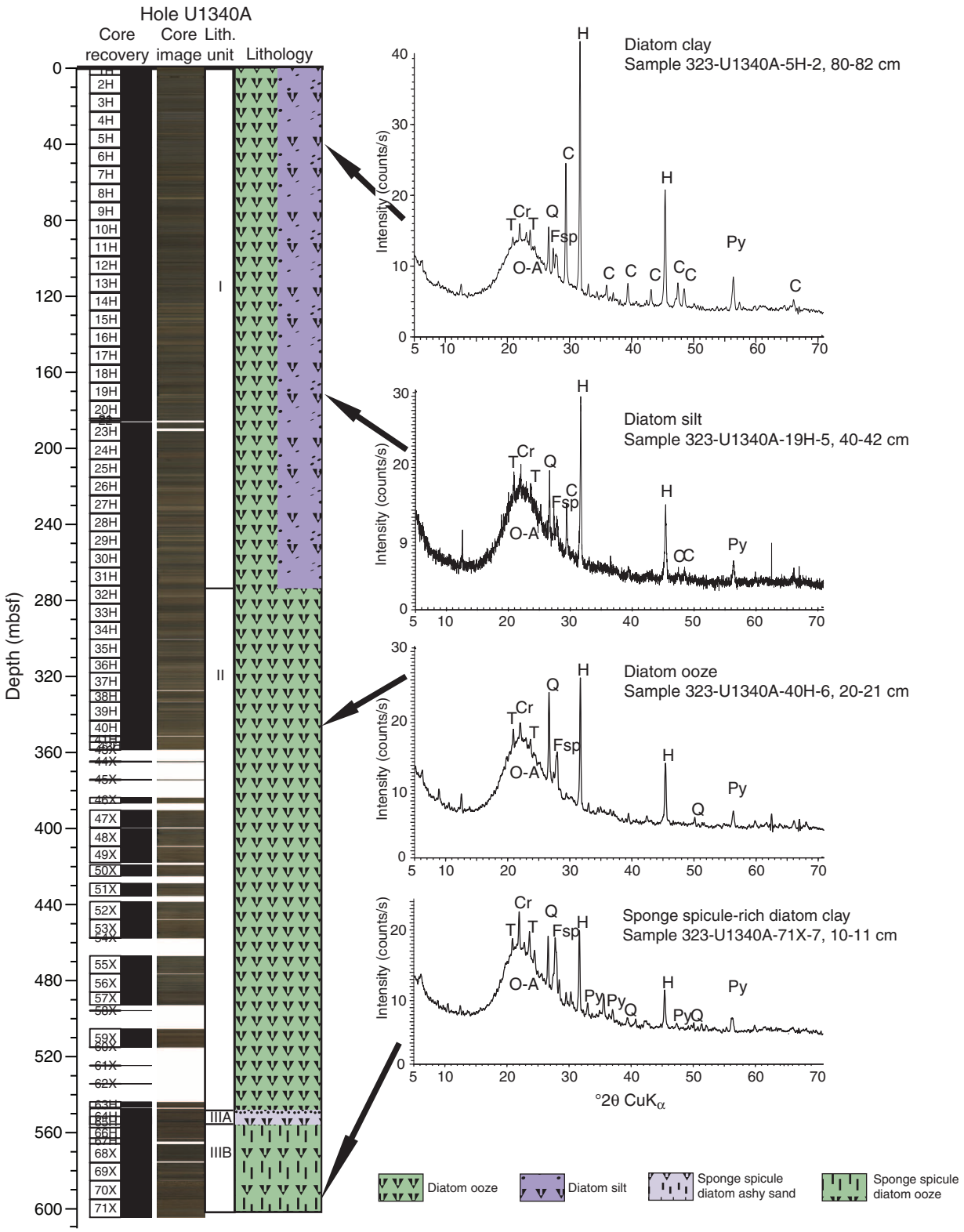

Figure F13. Photomicrographs of lithologies in lithologic Units I and II. **A.** Diatom ooze. **B.** Diatom silt (plane-polarized light). **C.** Diatom silt (cross-polarized light).

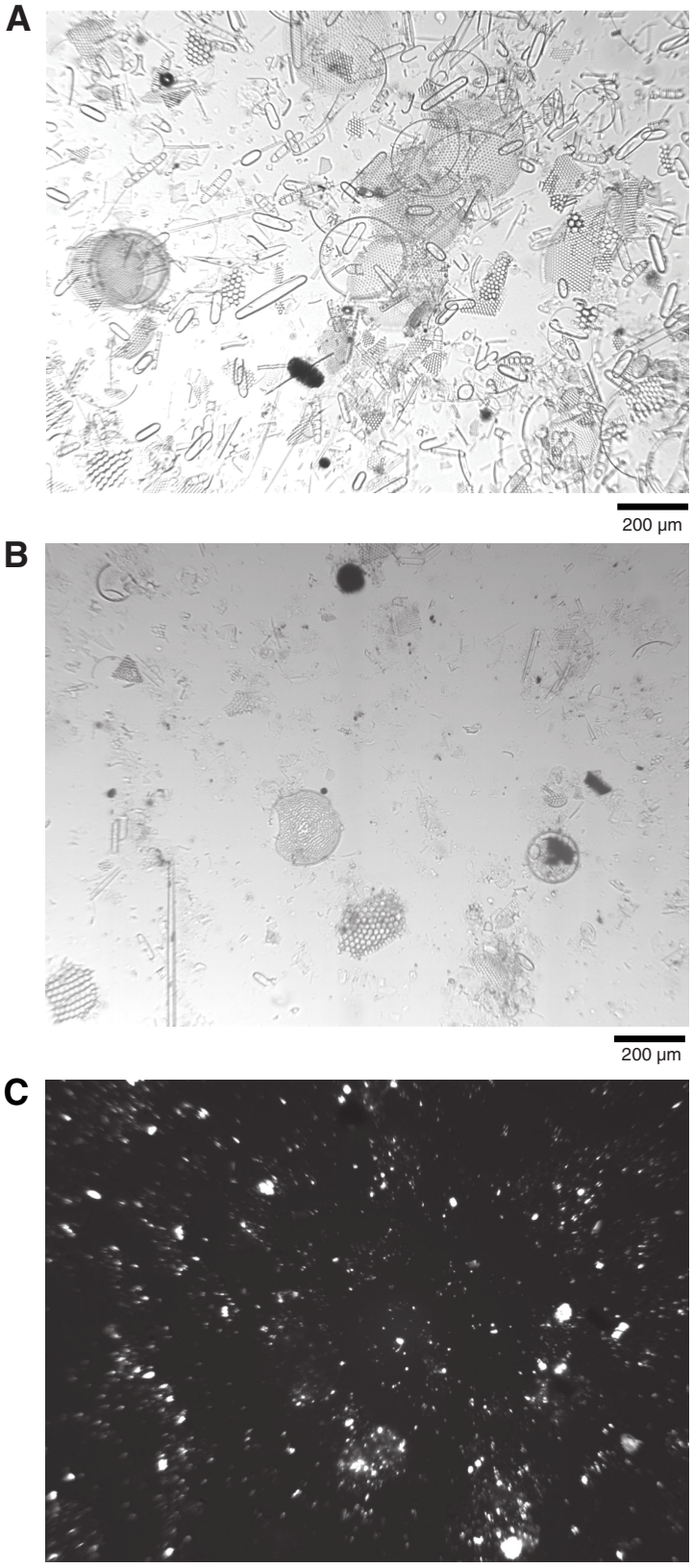

Figure F14. Core photographs showing examples of soft-sediment deformation. **A.** Interval 323-U1340A-3H-7, 5–40 cm. **B.** Interval 323-U1340A-7H-6, 118–140 cm. **C.** Interval 323-U1340B-1H-2, 40–50 cm. Note the truncated laminations.

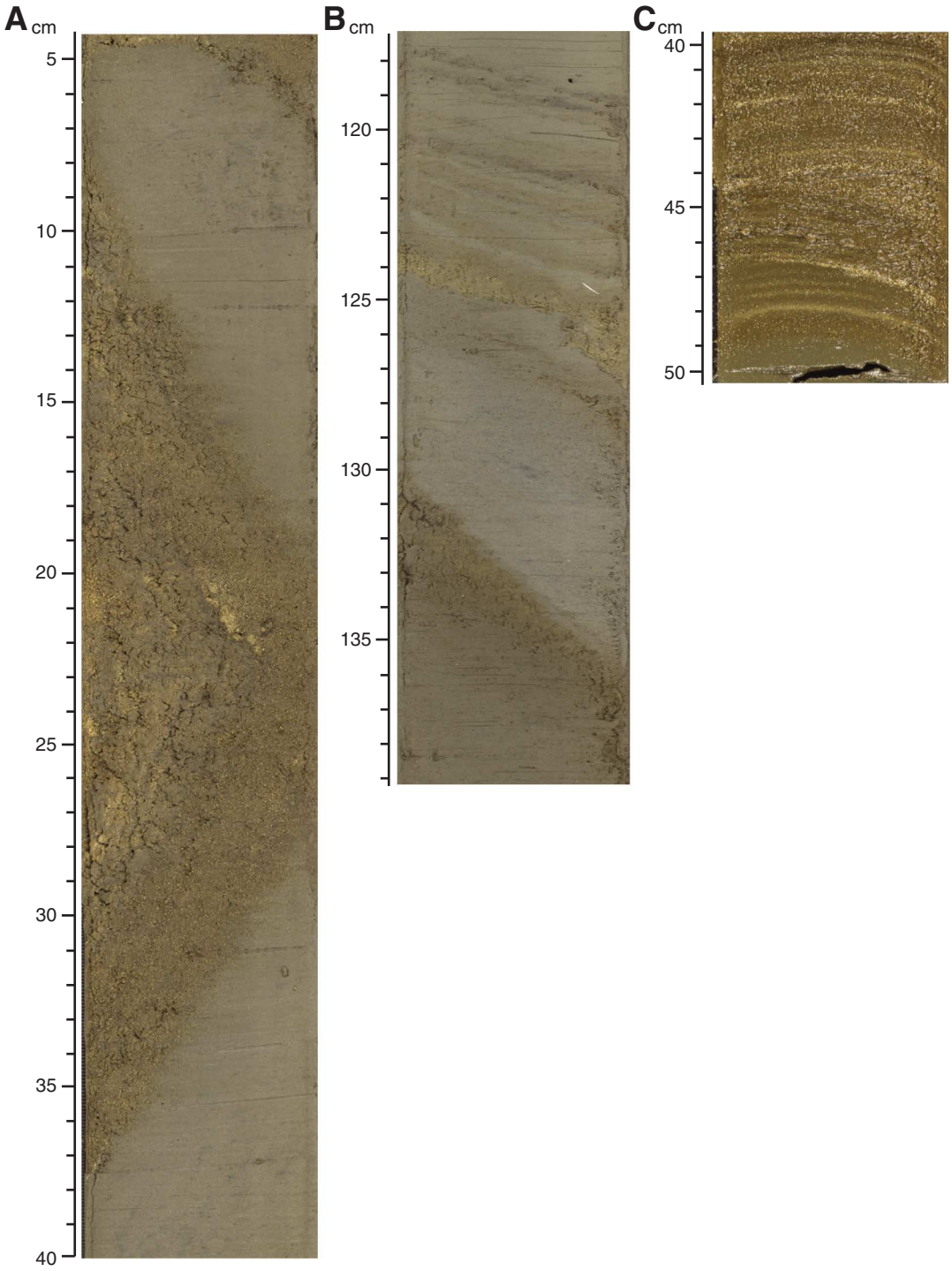

Figure F15. A. Core photograph of indurated dolomite layer at 21–25 cm in interval 323-U1340A-45X-1, 16–28 cm. **B.** Associated X-ray diffraction analysis. FeD = Fe-rich dolomite, Q = quartz, O-A = opal-A, Fsp = feldspar.

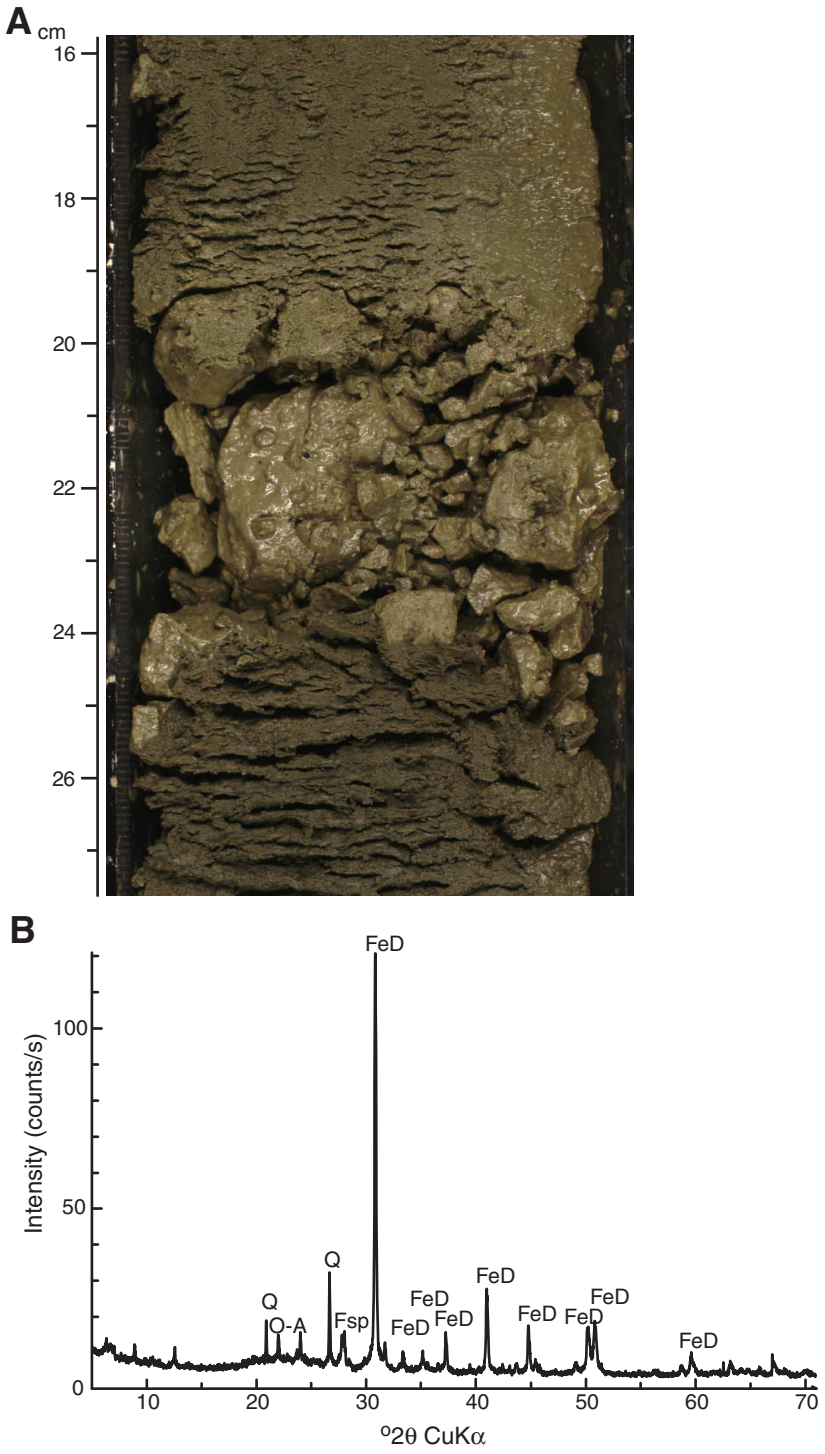

Figure F16. Core photograph showing contact of Subunit IIIB with the ash layer above at 21 cm in interval 323-U1340A-64H-4, 12–38 cm.

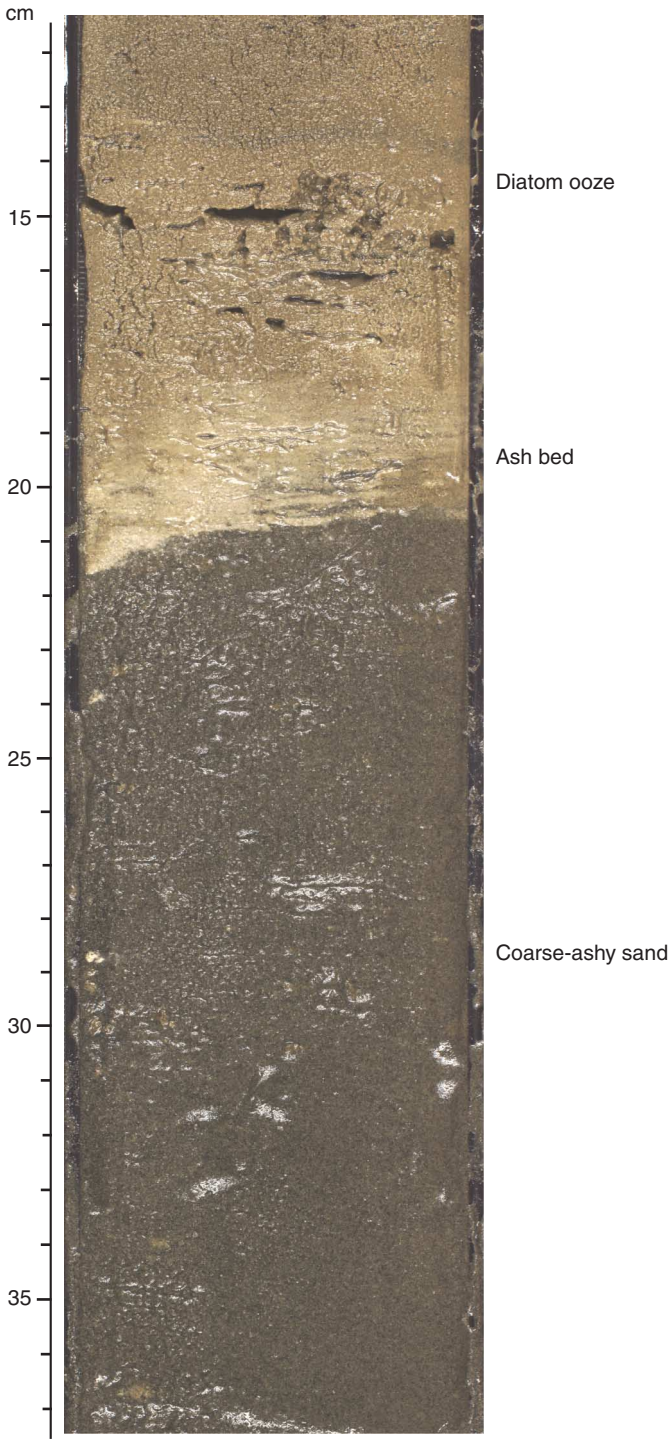

Figure F17. Photomicrographs of a grain mount and smear slide from Subunit IIIA (diatom-bearing sponge spicule–rich coarse-ashy sand), Core 323-U1340A-64H.

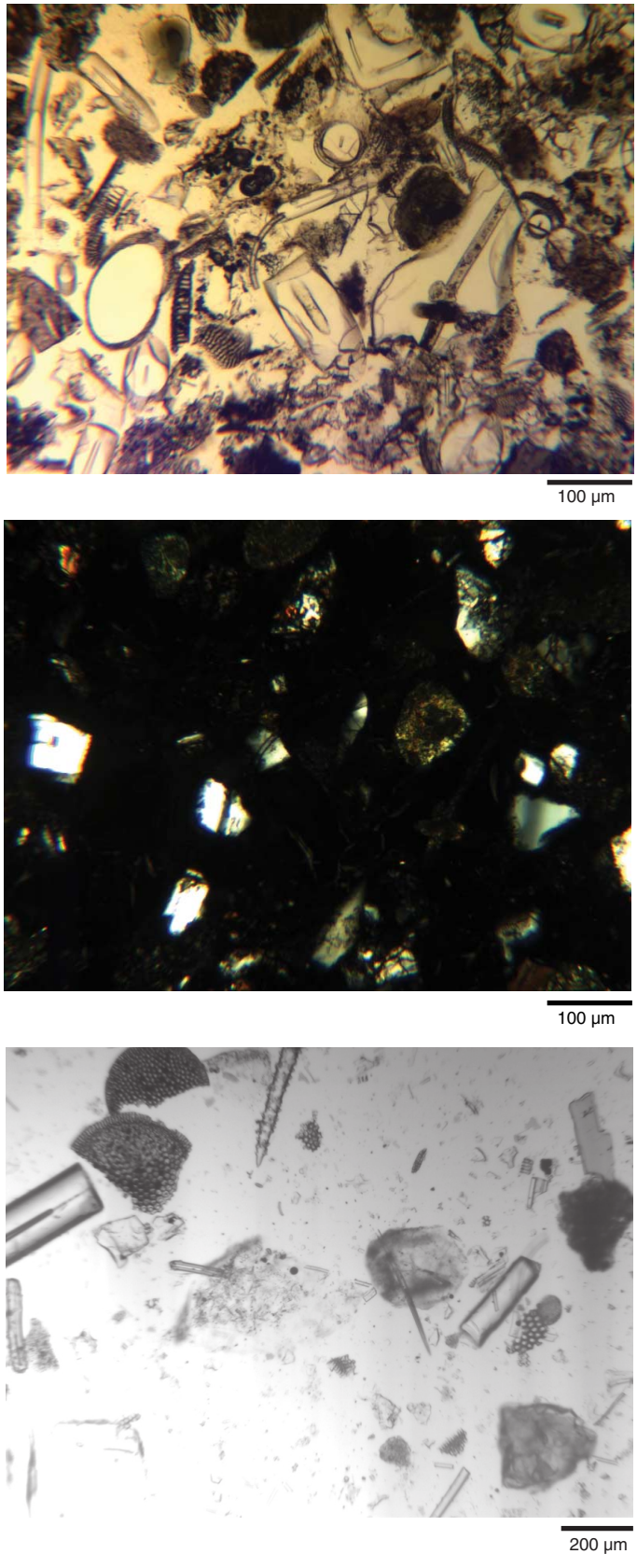

Figure F18. Photomicrograph of Subunit IIIB (sponge spicule–rich diatom ooze), Sample 323-U1340A-65H-7, 70 cm.

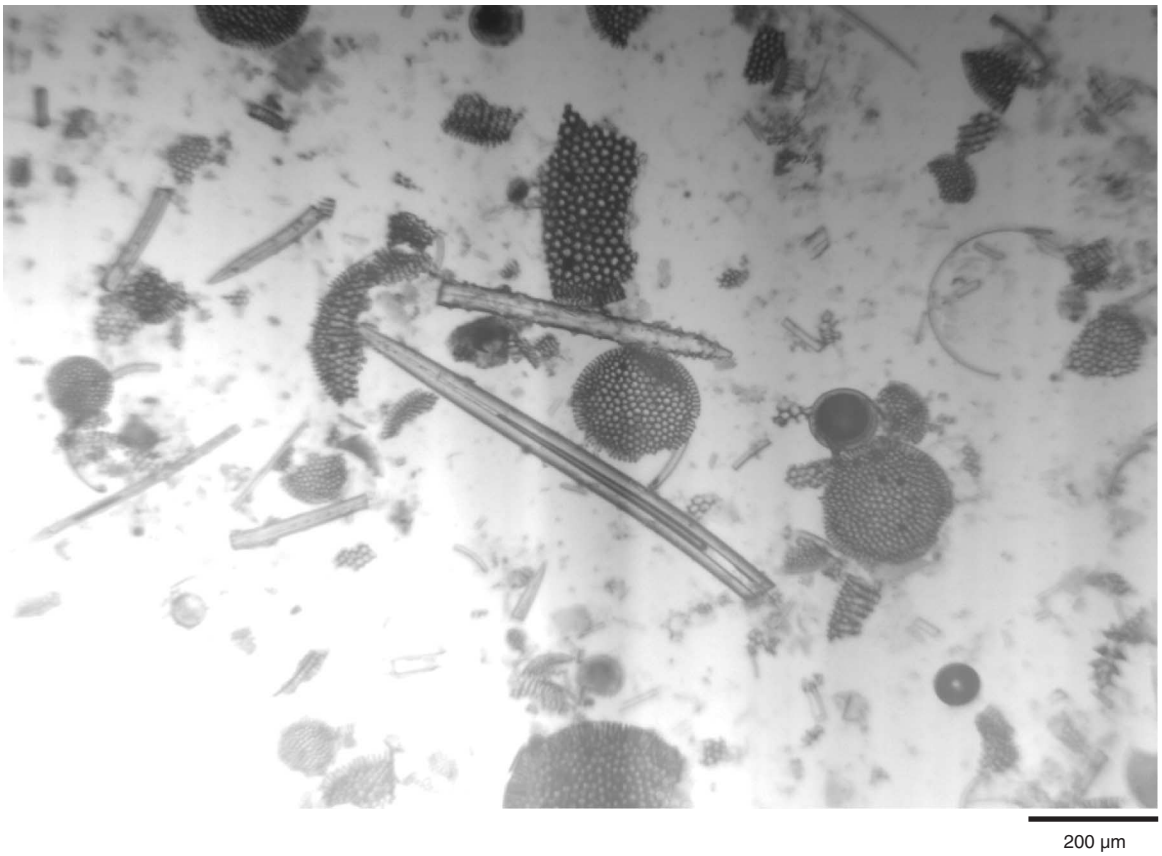

Figure F19. Age-depth plot for Hole U1340A showing biostratigraphic datums based on radiolarians, diatoms, calcareous nannofossils, and silicoflagellates. Paleomagnetic events are also shown.

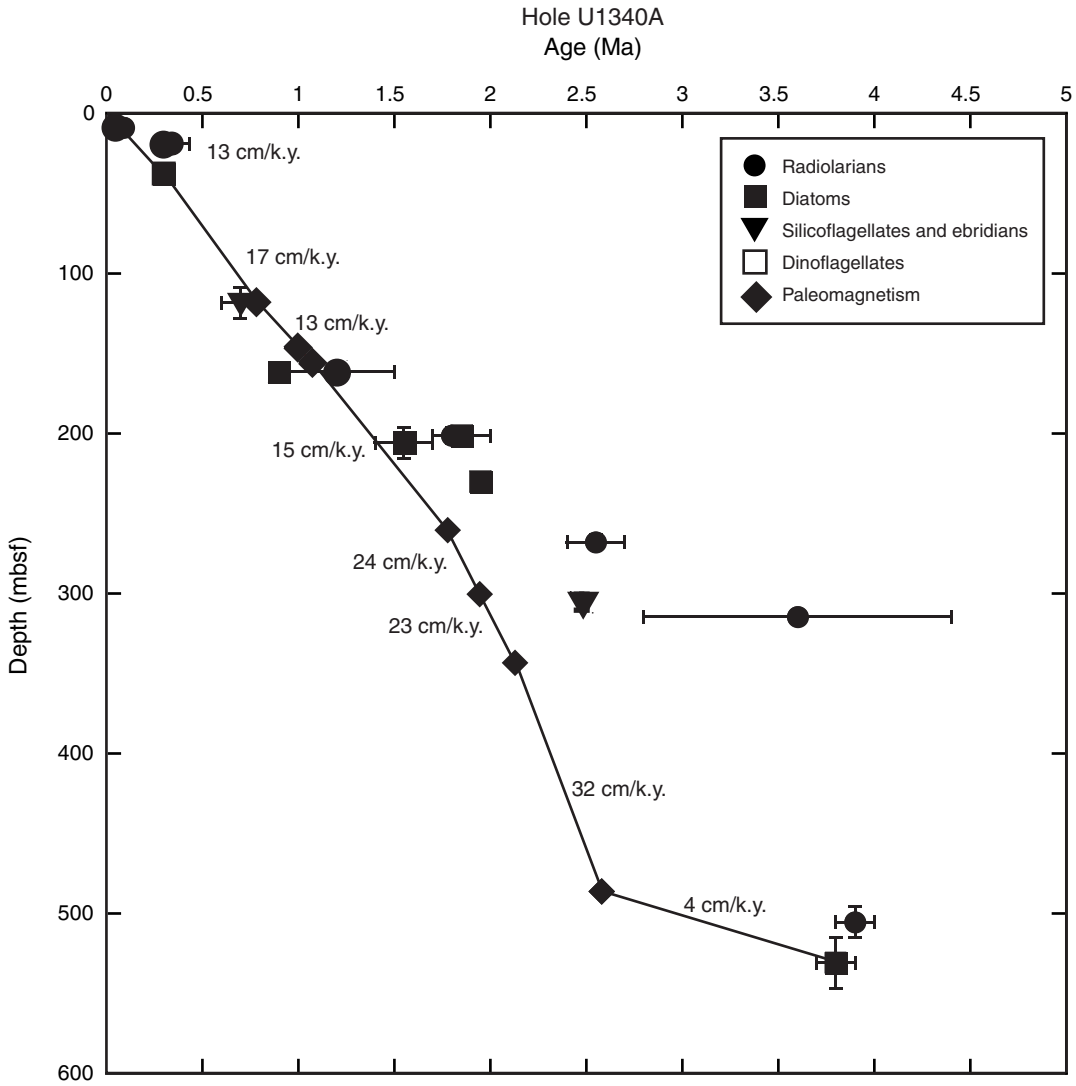

Figure F20. Comparison of biostratigraphic events in Holes U1340A and U1341B used for stratigraphic correlation between sites. The percentages of *Neodenticula seminae* and *Neodenticula kamtschatica* were used as the primary biostratigraphic events. Various other biostratigraphic and magnetostratigraphic events are also included. BM = Brunhes/Matuyama. T = top, B = bottom. FO = first occurrence, LO = last occurrence, RI = rapid increase. APC = advanced piston corer, XCB = extended core barrel.

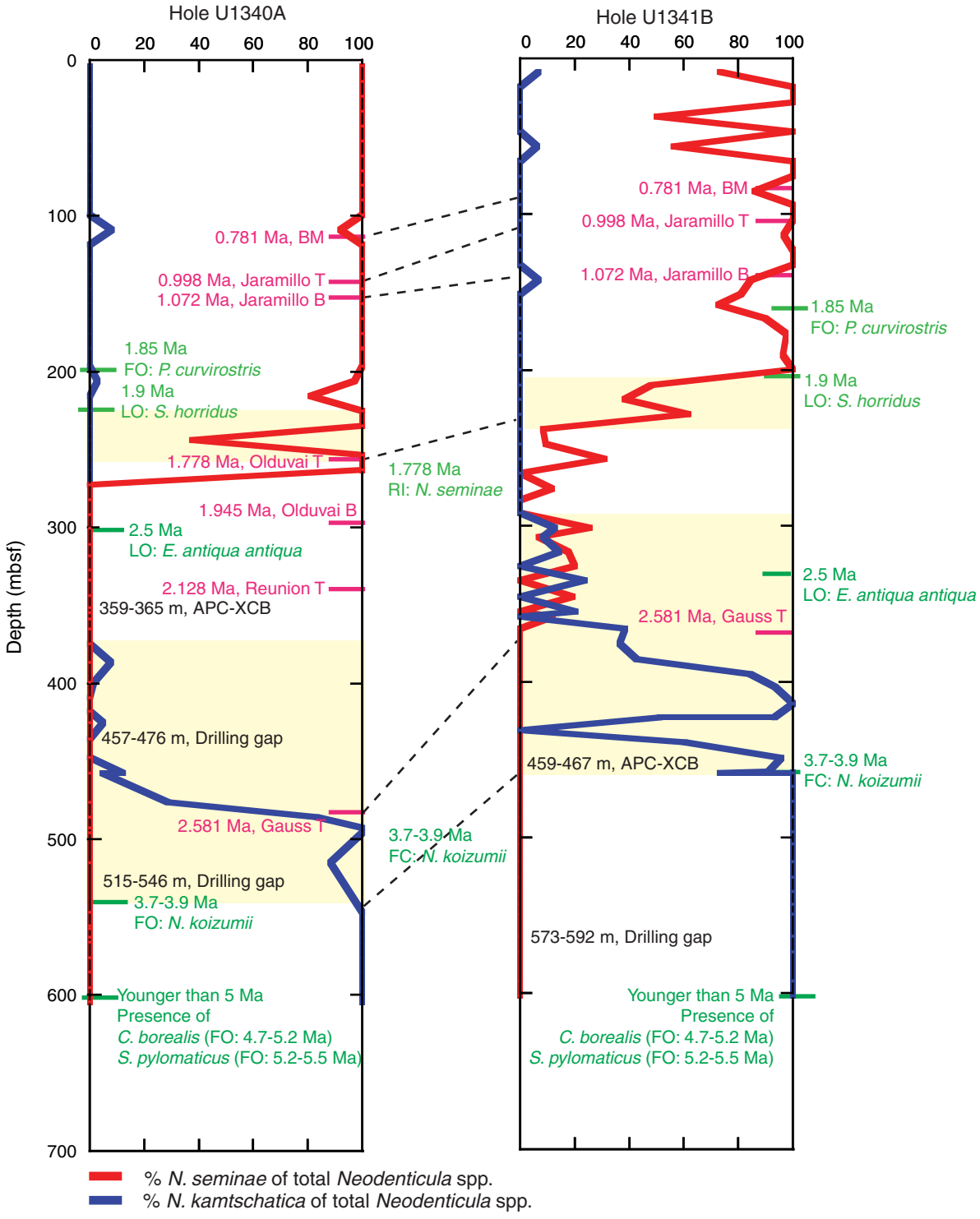

Figure F21. Abundances of various microfossil groups. Sea ice diatoms include *Thalassiosira antarctica* spores, *Bacteriosira fragilis, Porosira glacialis,* and *Fragilariopsis cylindrus*. Benthic foraminifer abundance calculations can be found in **"Biostratigraphy"** in the "Methods" chapter.

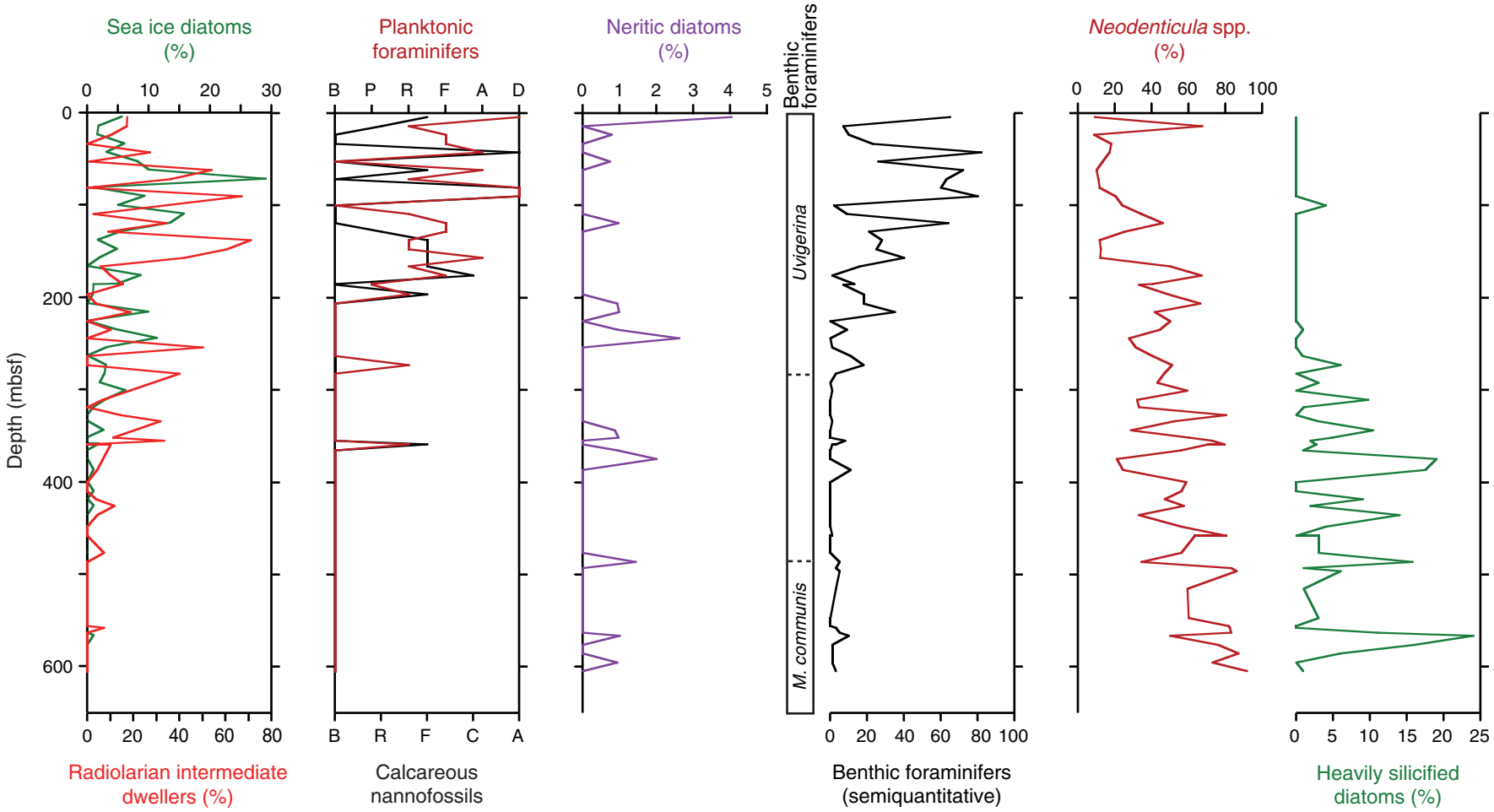

Figure F22. Inclination, declination, and intensity of remanent magnetization after 20 mT AF demagnetization ($Int_{20\ mT}$), Hole U1340A. Declination data (blue) have been corrected using FlexIt orientation tool data (black) in the uppermost 150 m.

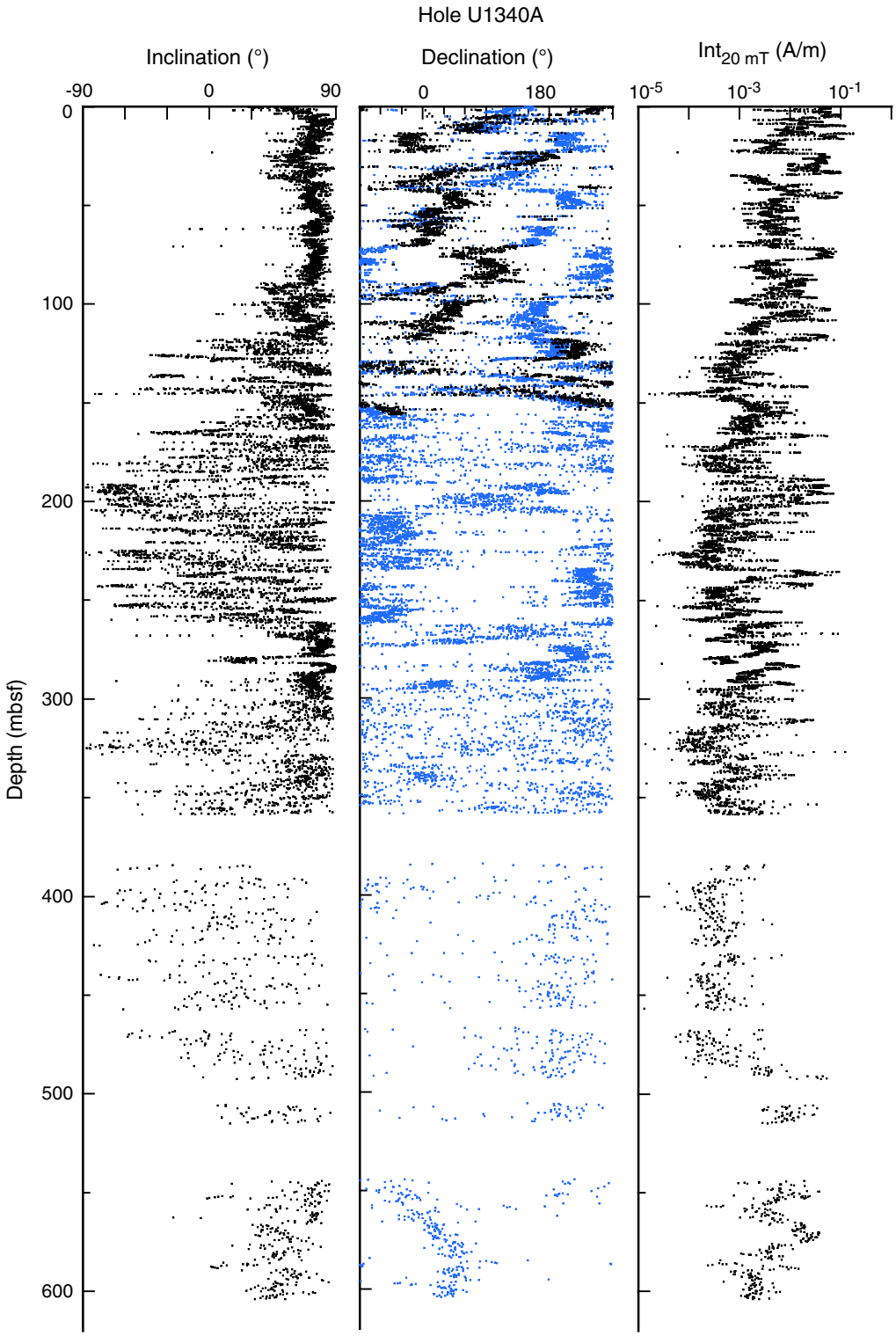

Figure F23. Inclination and intensity of remanent magnetization after 20 mT AF demagnetization ($Int_{20\ mT}$), Holes U1340B–U1340D.

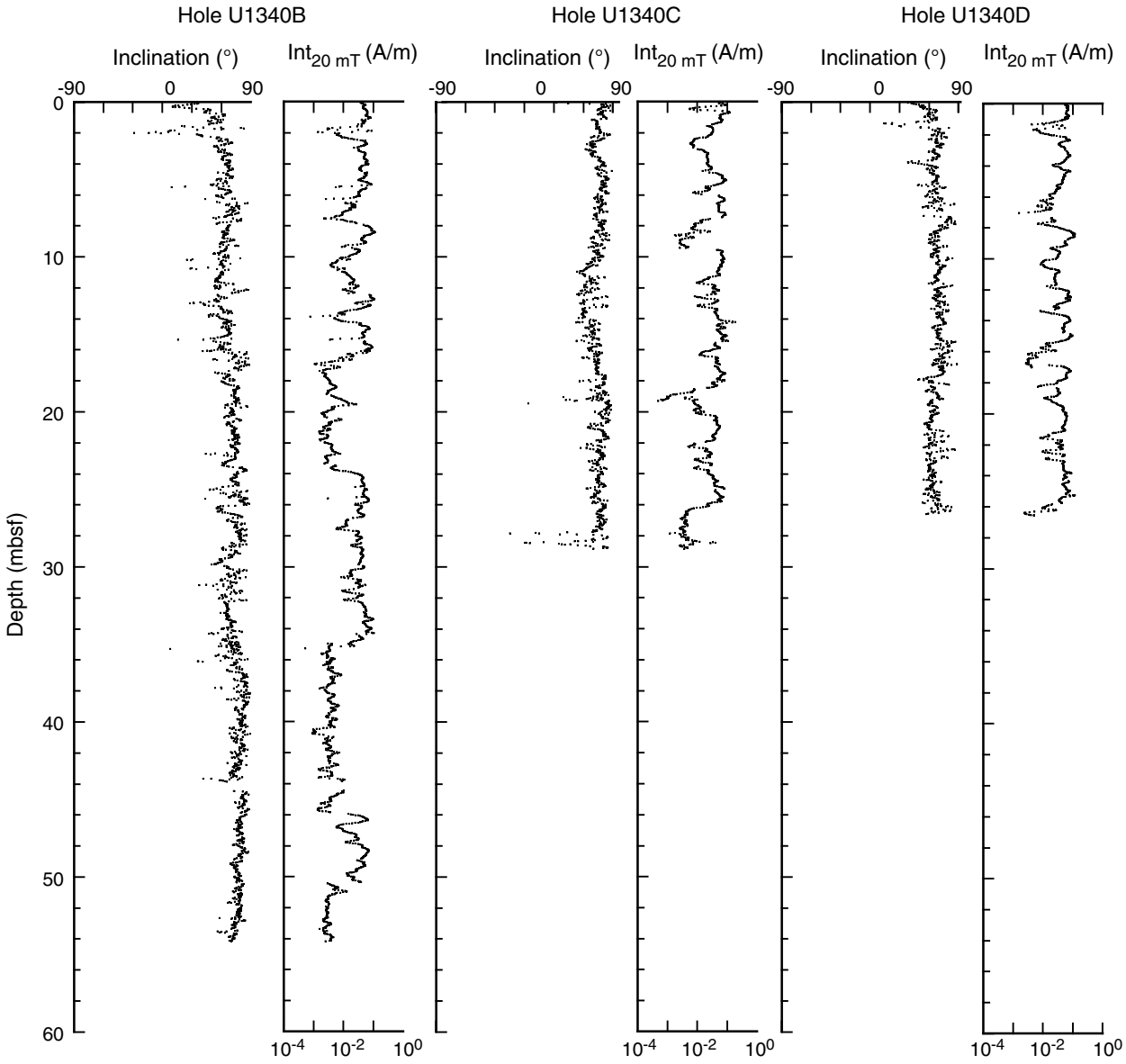

Figure F24. Inclination averages and tentative polarity zonation. Red = averaged inclination in each section, blue = averaged inclination in each core. Black = normal polarity, white = reversed polarity, gray = uncertain polarity.

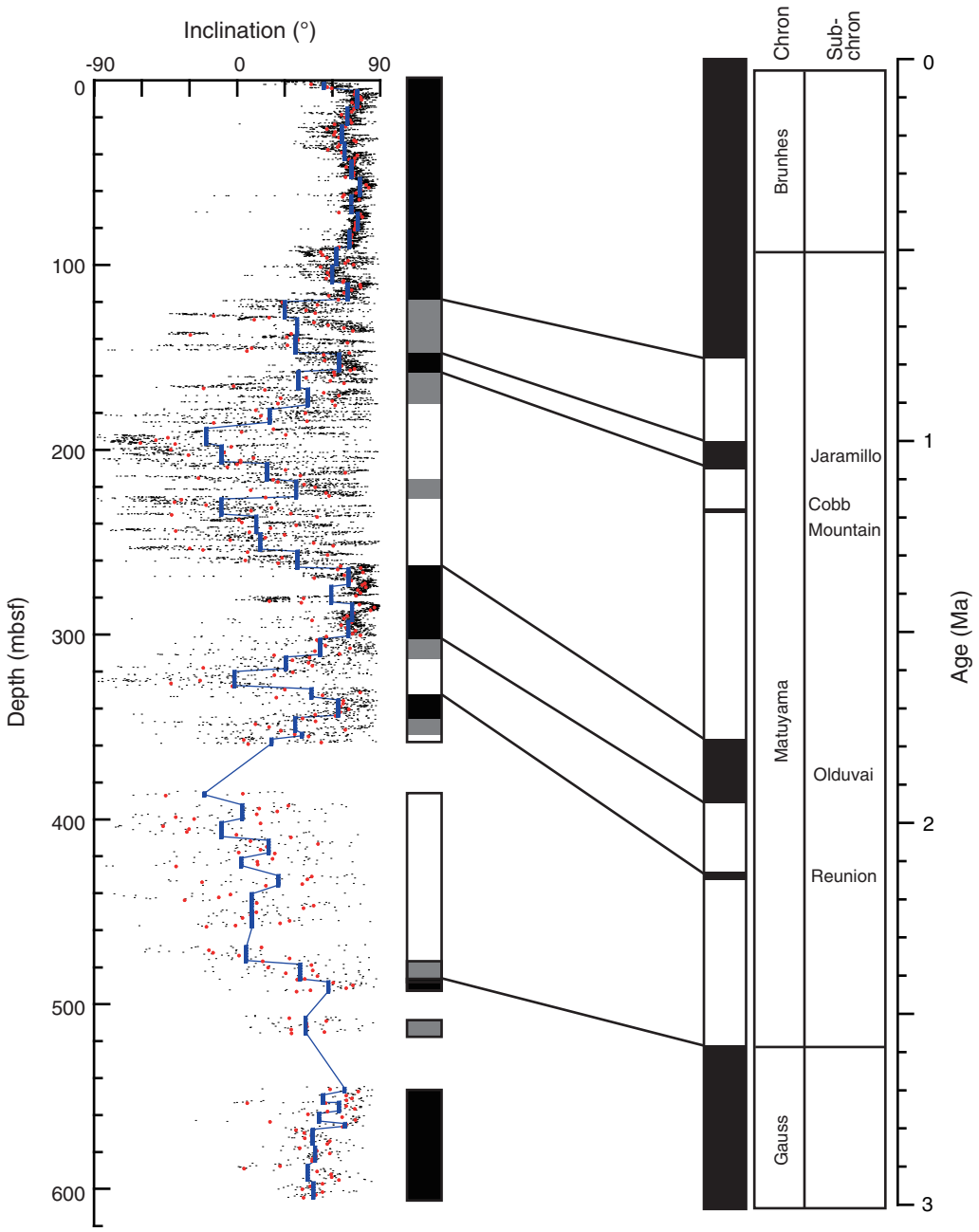

Figure F25. Magnetic susceptibility (MS) and intensity of remanent magnetization after 20 mT AF demagnetization ($Int_{20\ mT}$) normalized to MS, Hole U1340A.

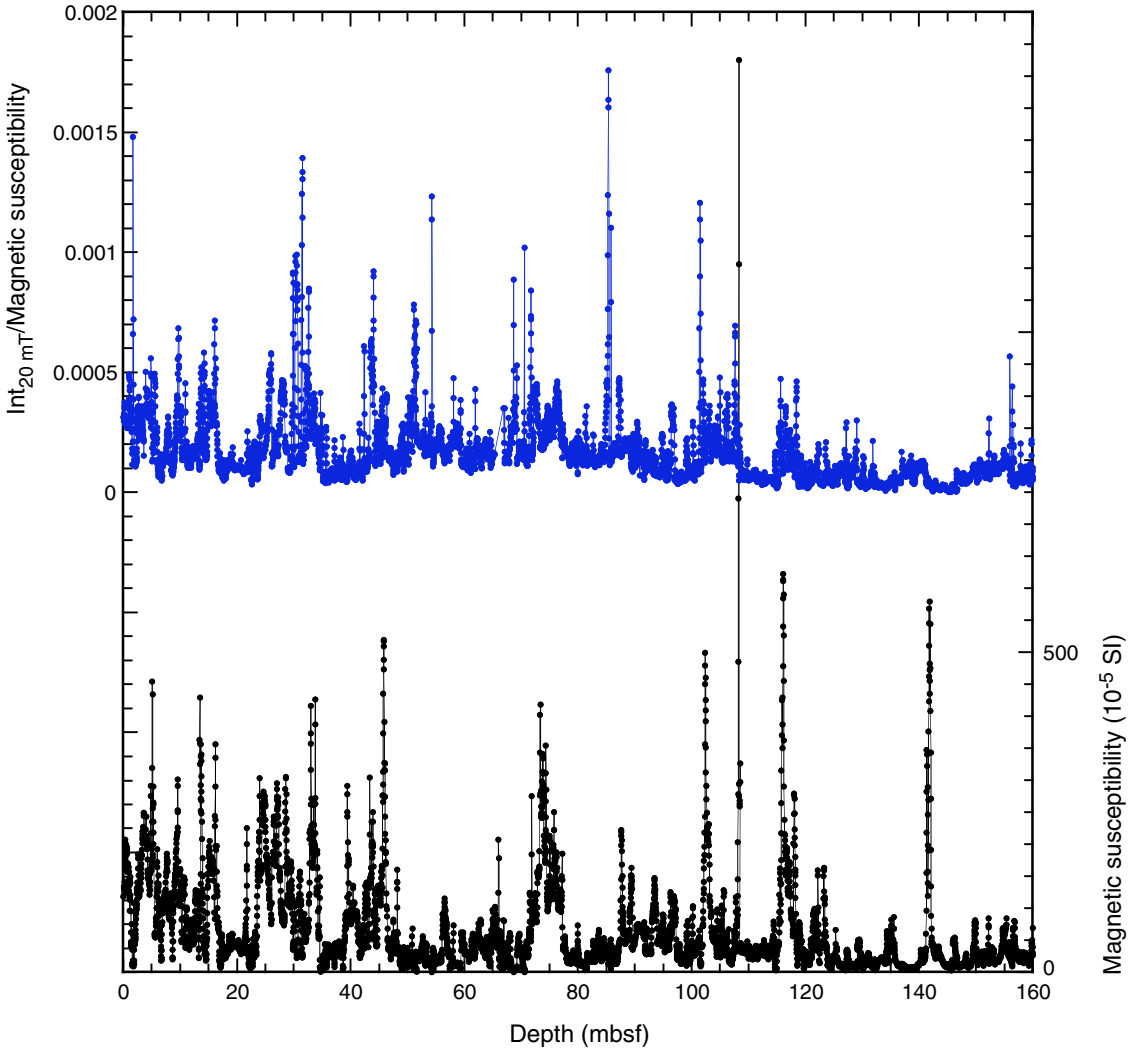

Figure F26. Dissolved chemical concentrations, Hole U1340B. **A.** Dissolved inorganic carbon (DIC). **B.** pH. **C.** Alkalinity. **D.** Total hydrogen sulfide ($\Sigma H_2S = H_2S + HS^-$). **E.** Sulfate. **F.** Methane (Holes U1340A and U1340B). **G.** Chloride. **H.** Salinity. **I.** Phosphate. **J.** Ammonium.

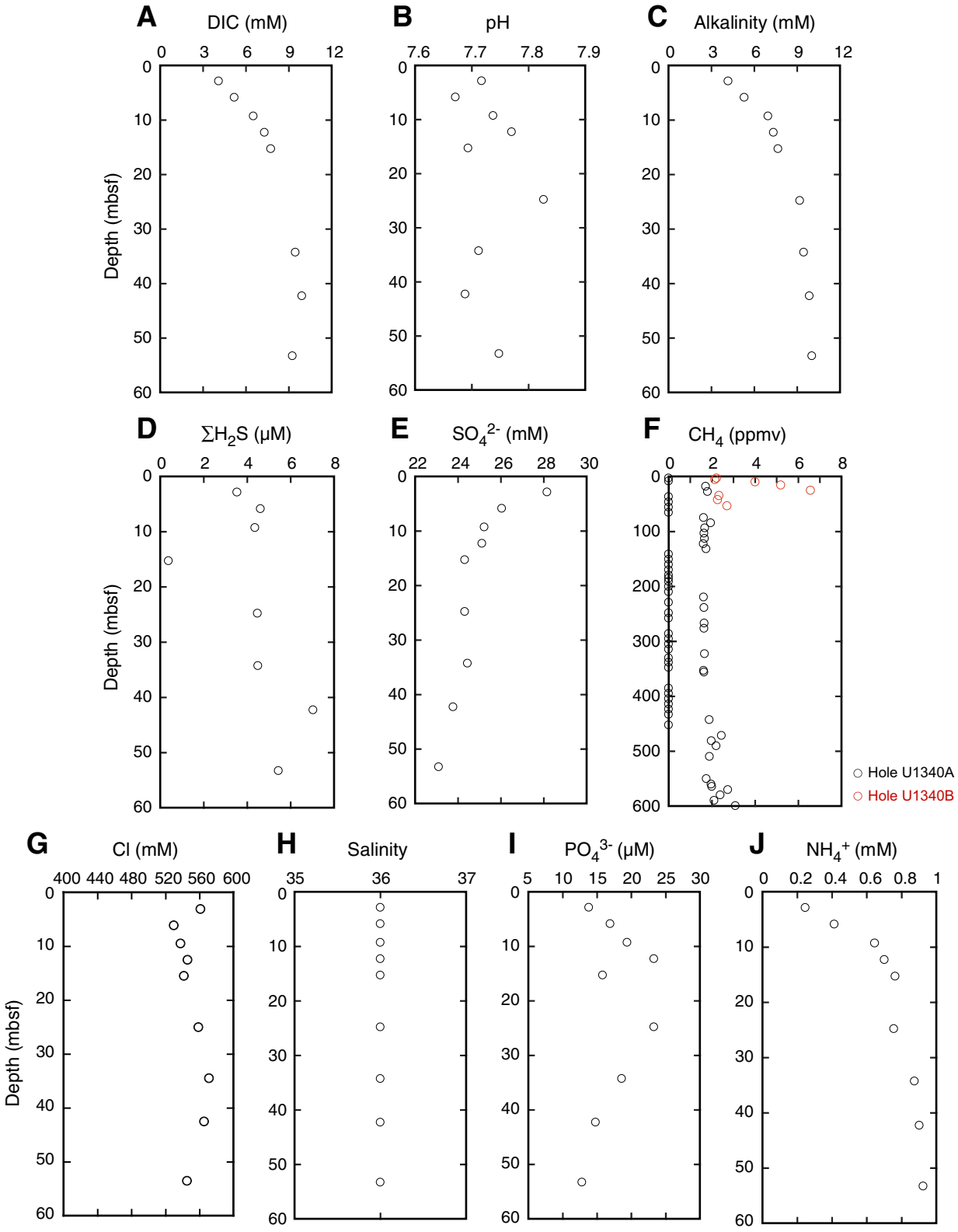

Figure F27. Dissolved chemical concentrations, Hole U1340B. **A.** Sodium. **B.** Magnesium. **C.** Potassium. **D.** Calcium. **E.** Strontium. **F.** Manganese. **G.** Boron. **H.** Lithium. **I.** Silica.

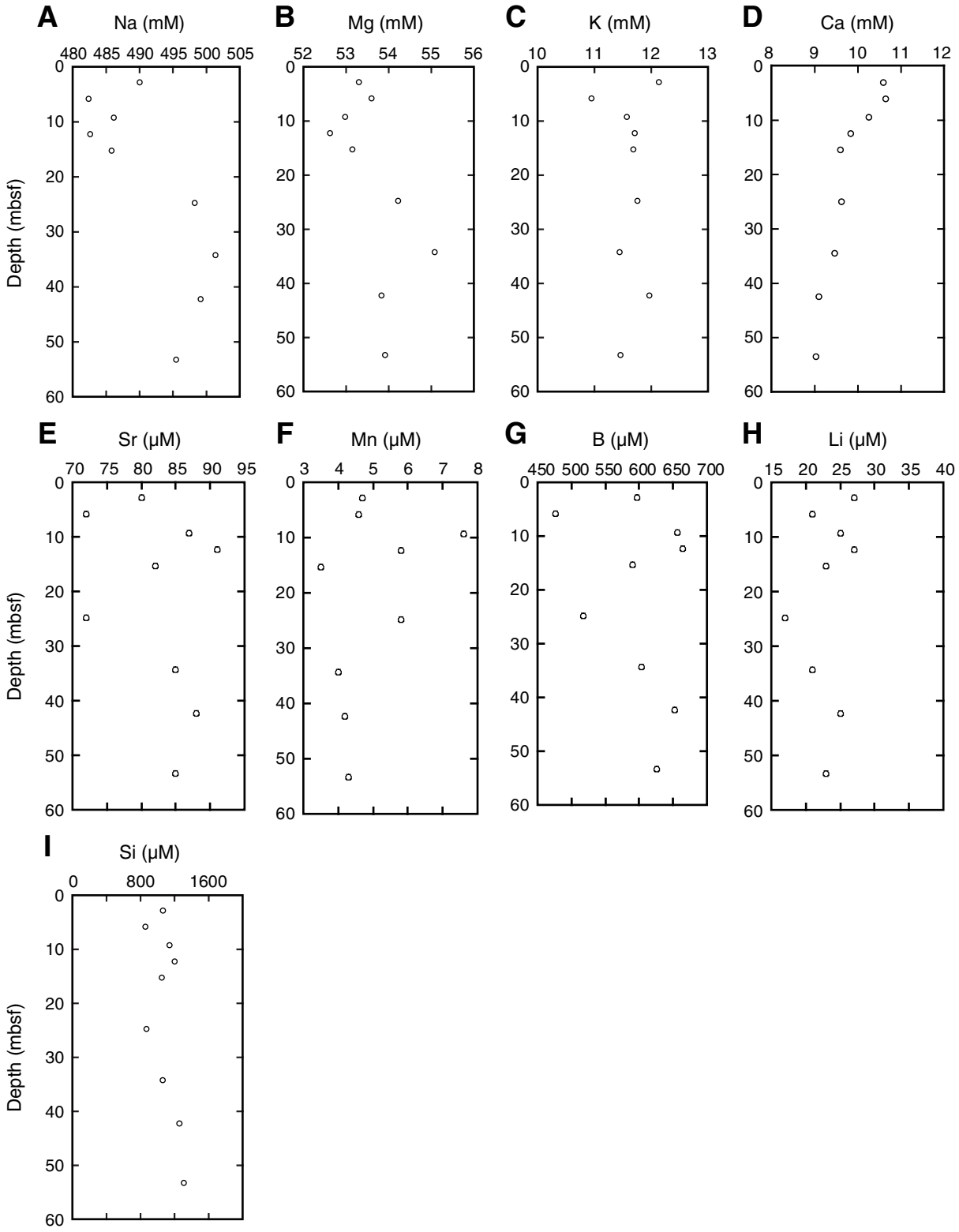

Figure F28. Solid-phase chemical concentrations, Hole U1340A. **A.** Calcium carbonate ($CaCO_3$). **B.** Total organic carbon (TOC). **C.** Total nitrogen (TN). **D.** Total sulfur (TS).

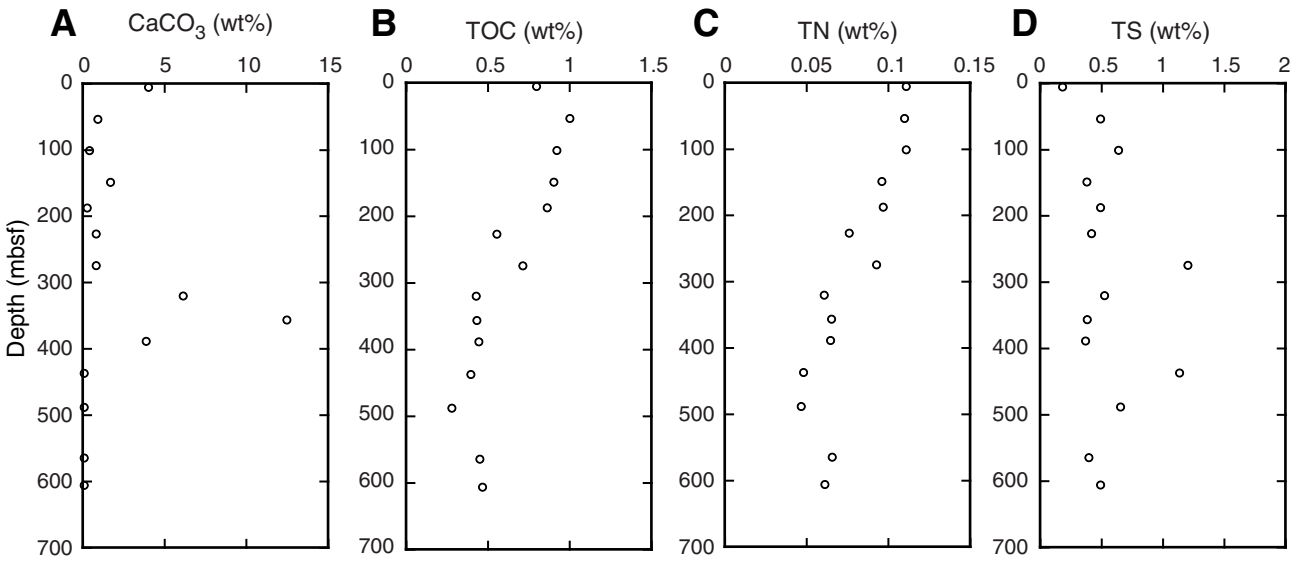

Figure F29. Downhole distribution of natural gamma ray (NGR), Hole U1340A.

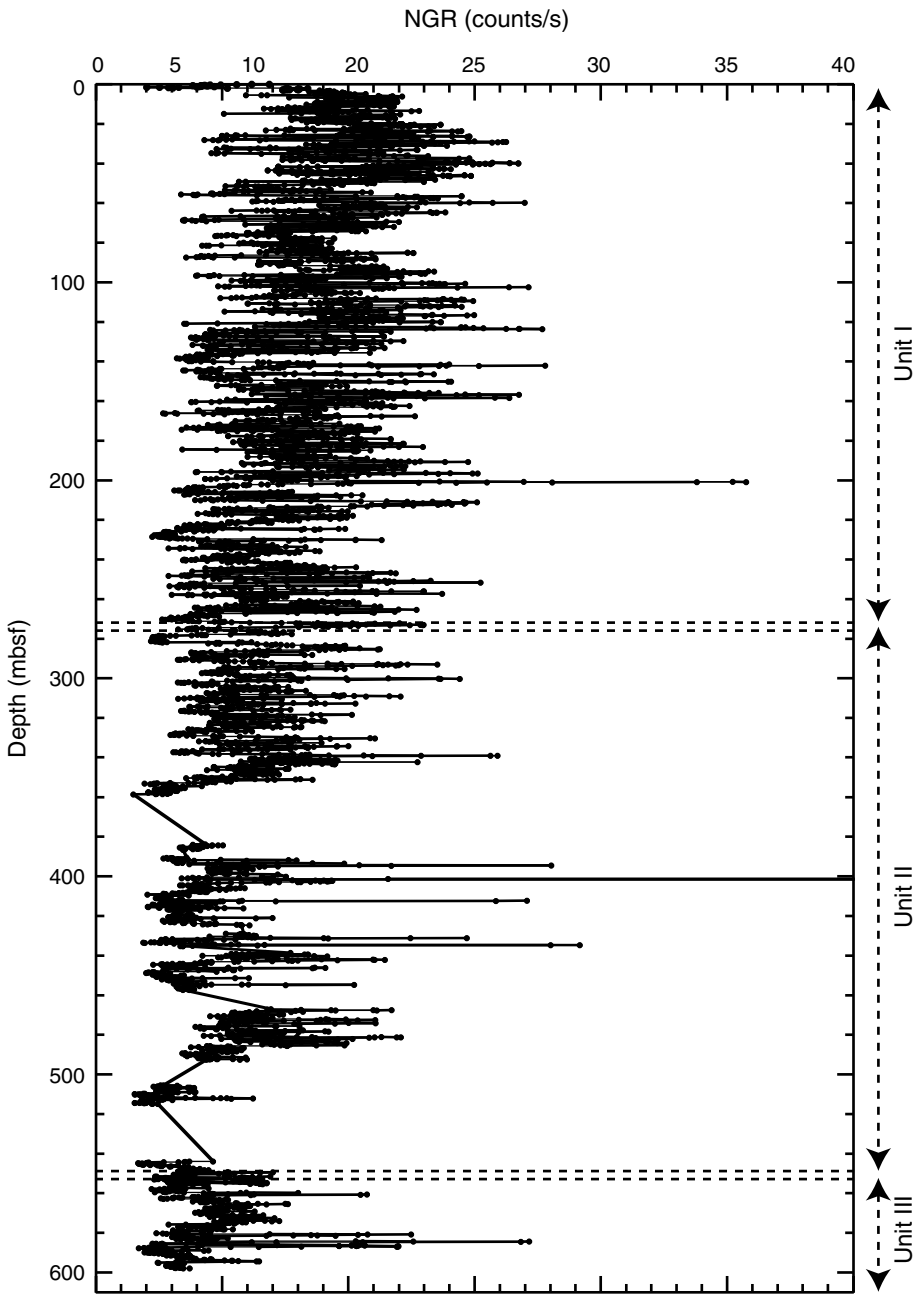

Figure F30. Downhole distribution of *P*-wave velocity recorded by the WRMSL, Hole U1340A.

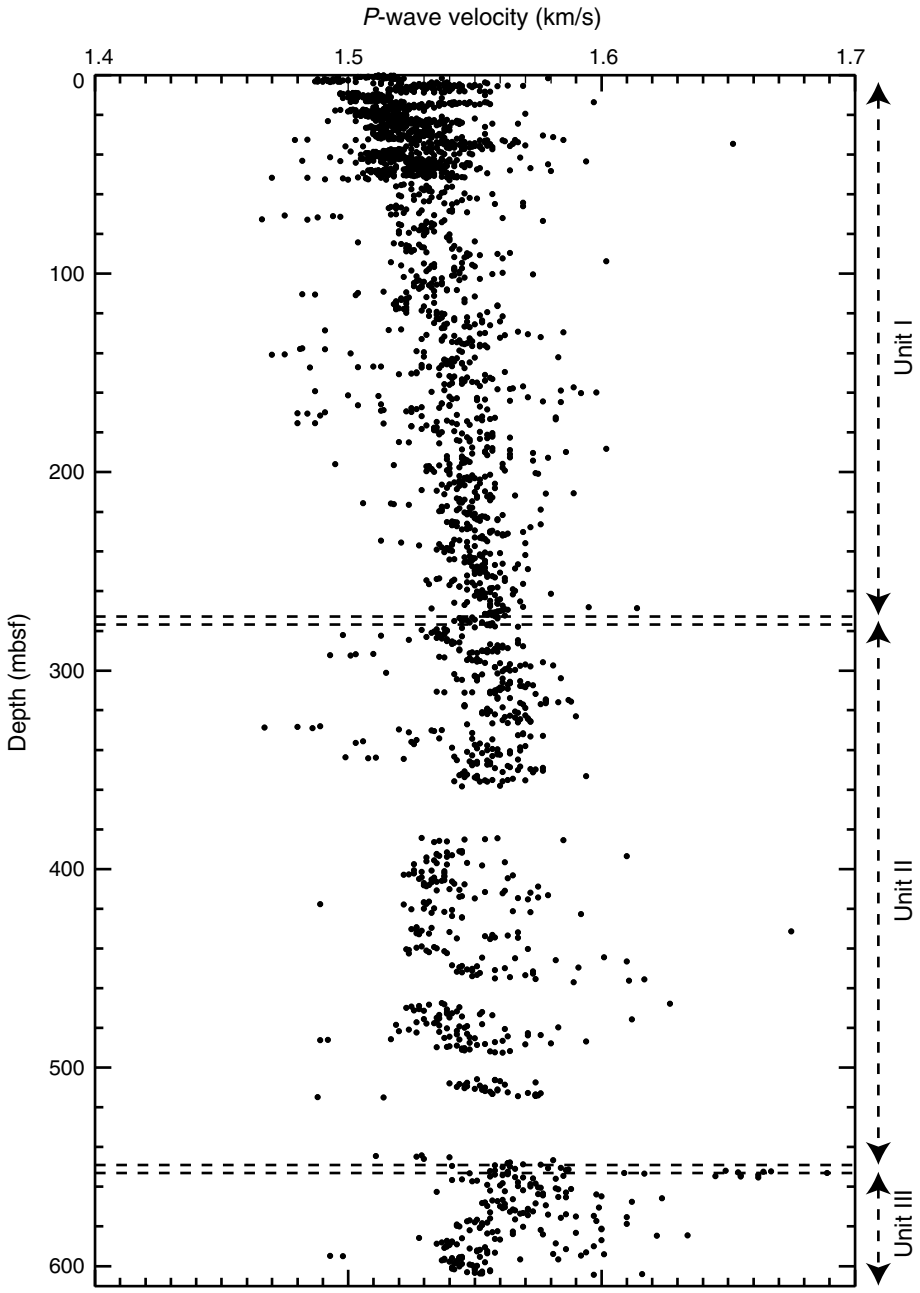

Figure F31. A. Downhole distribution of moisture and density (MAD) wet bulk density measurements on discrete samples of core sediment, Hole U1340A. (**Continued on next page.**)

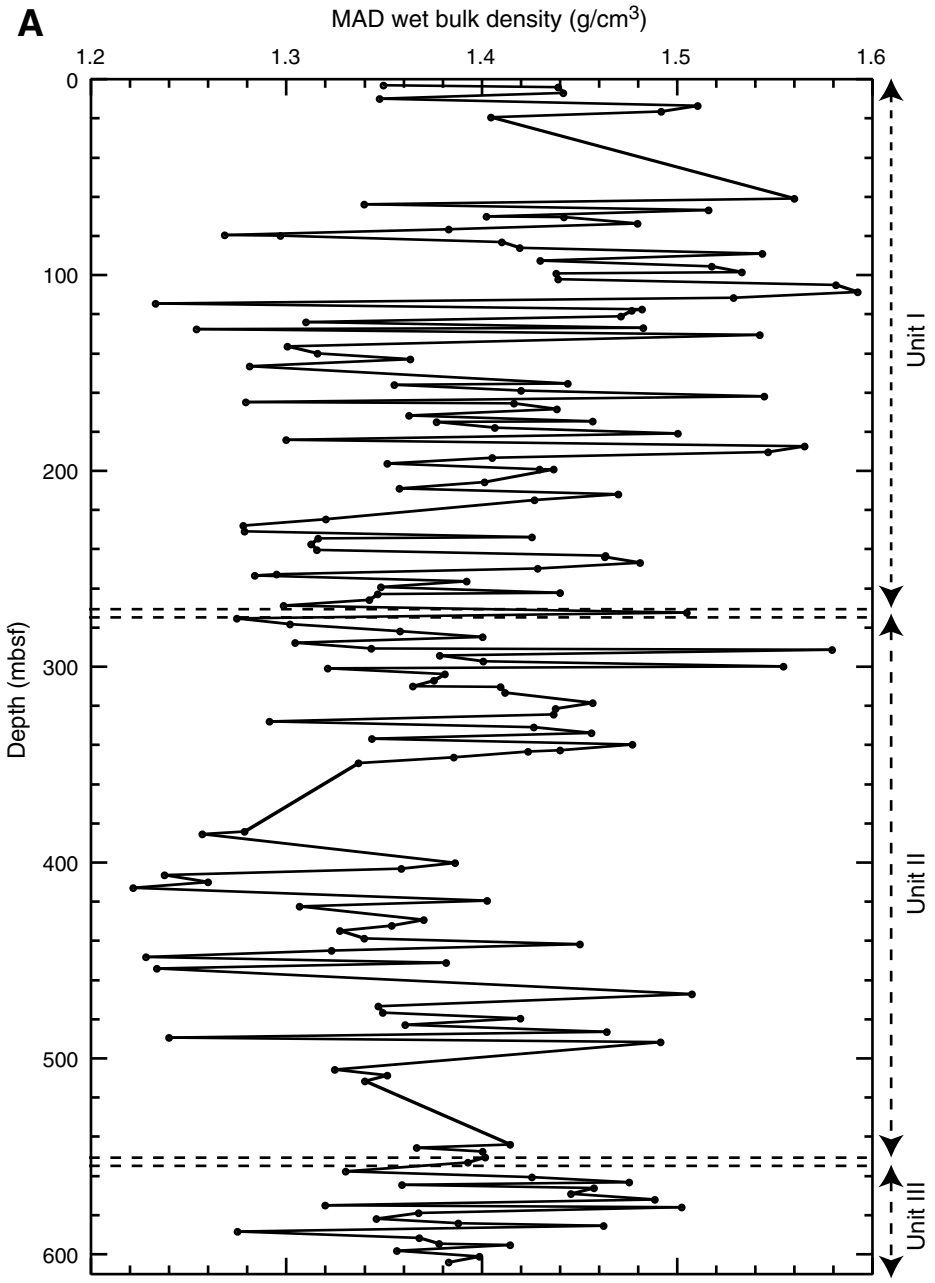

Figure F31 (continued). B. Downhole distribution of wet bulk density recorded by the WRMSL gamma ray attenuation (GRA) scanner, Hole U1340A.

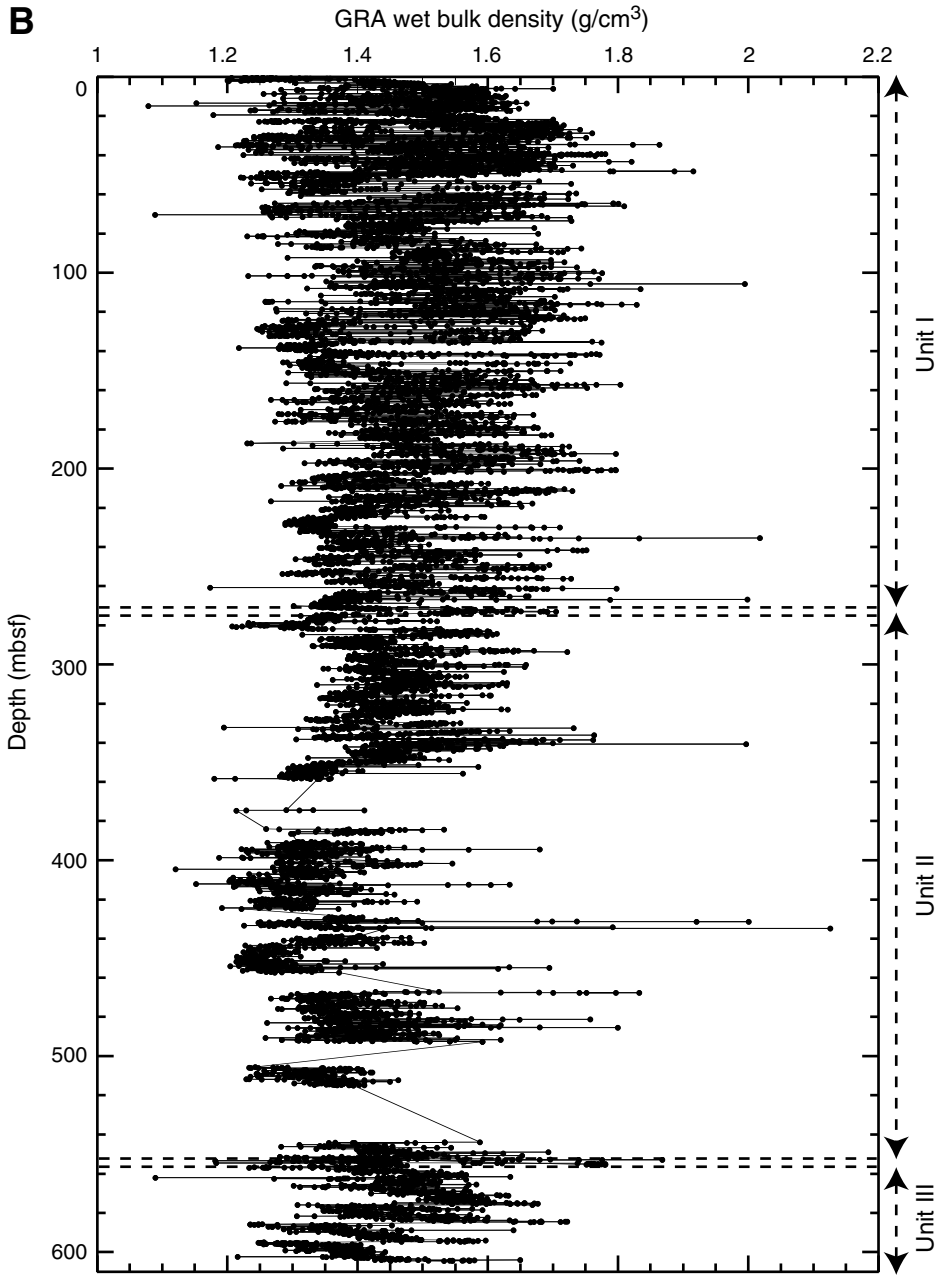

Figure F32. Downhole distribution of sediment water content (percent of total sediment weight) and sediment porosity, Hole U1340A.

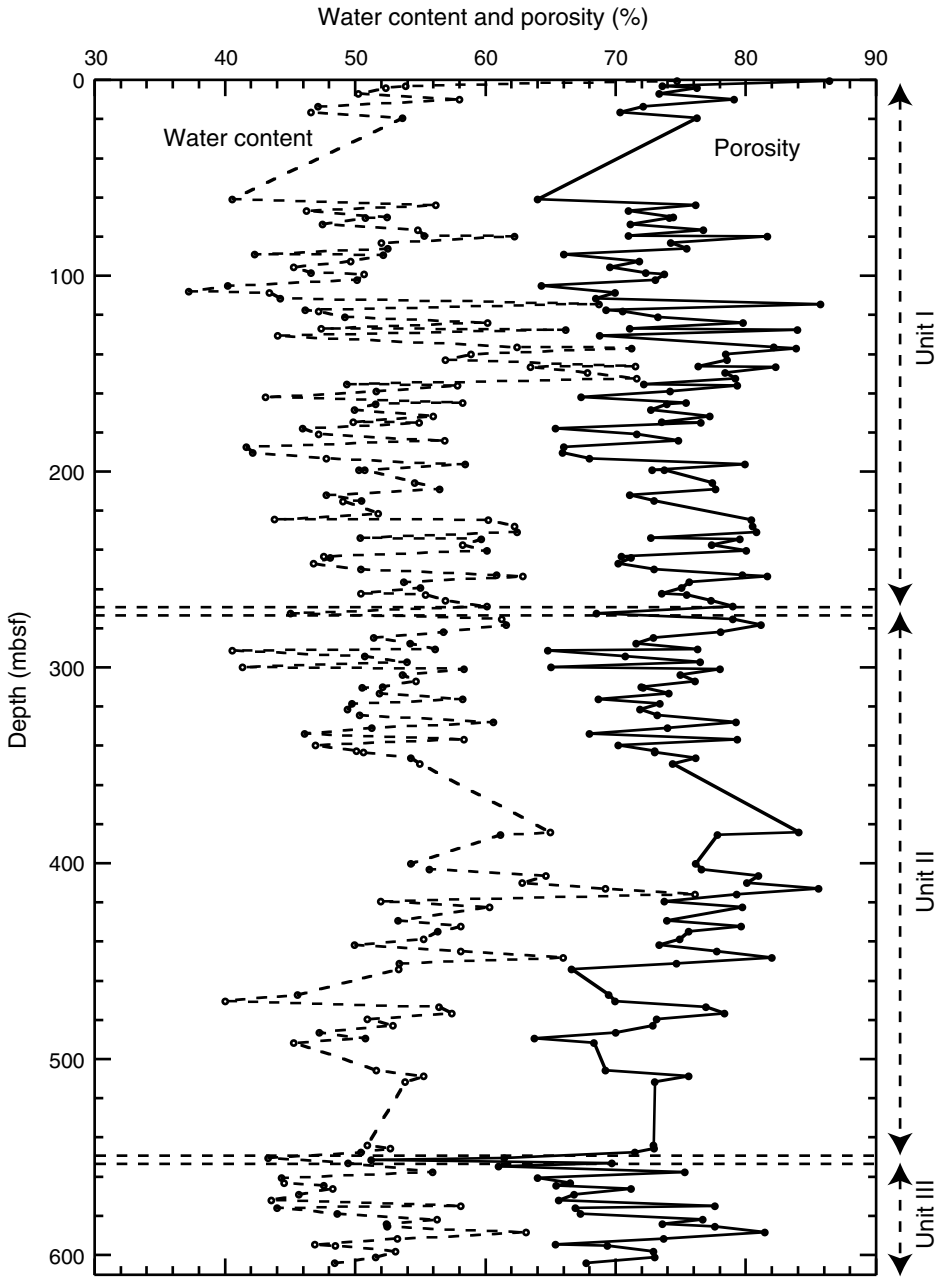

Figure F33. Downhole profile of dry grain density measured with the moisture and density system on discrete samples, Hole U1340A.

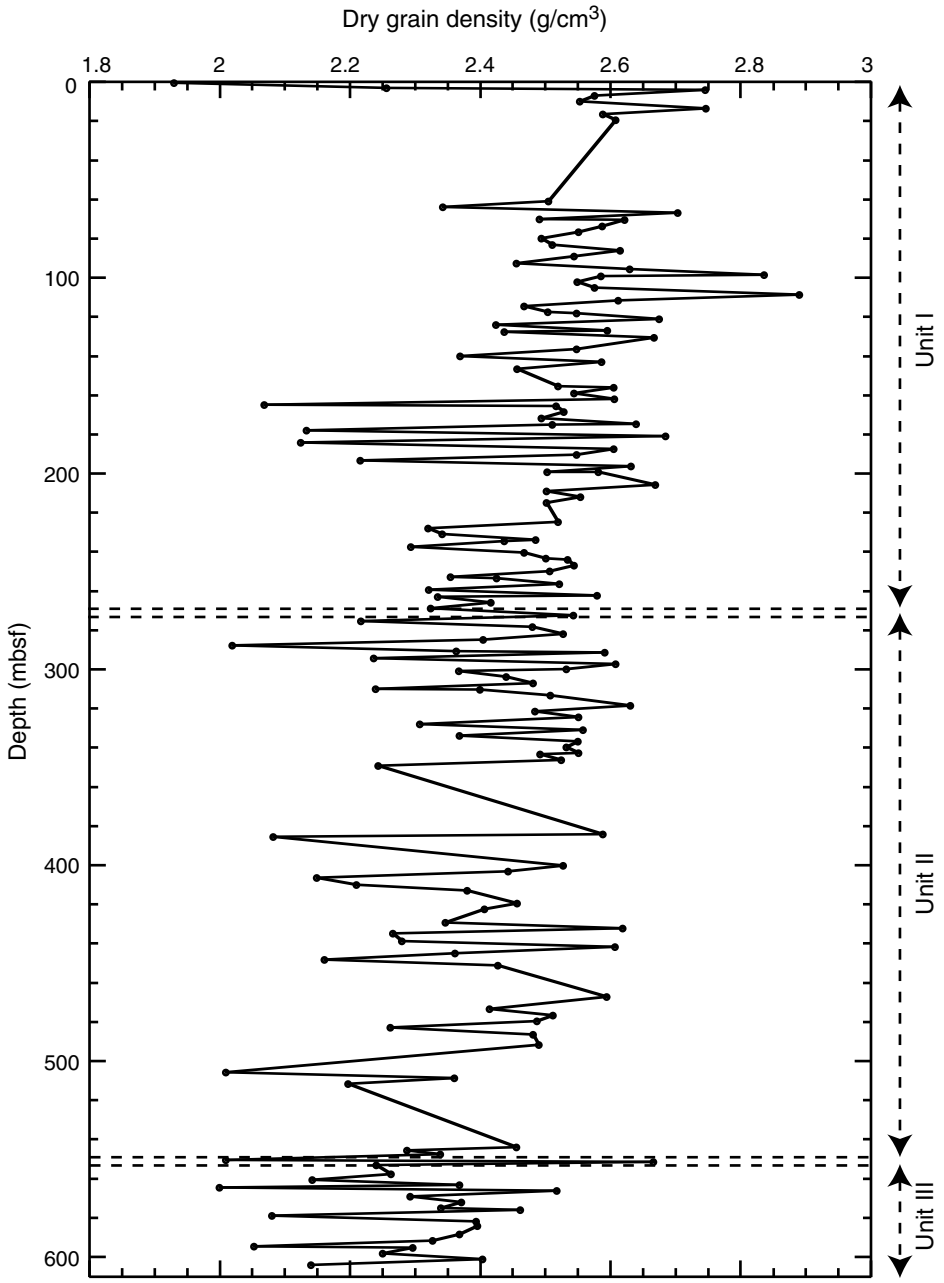

Figure F34. Downhole distribution of thermal conductivity, Hole U1340A.

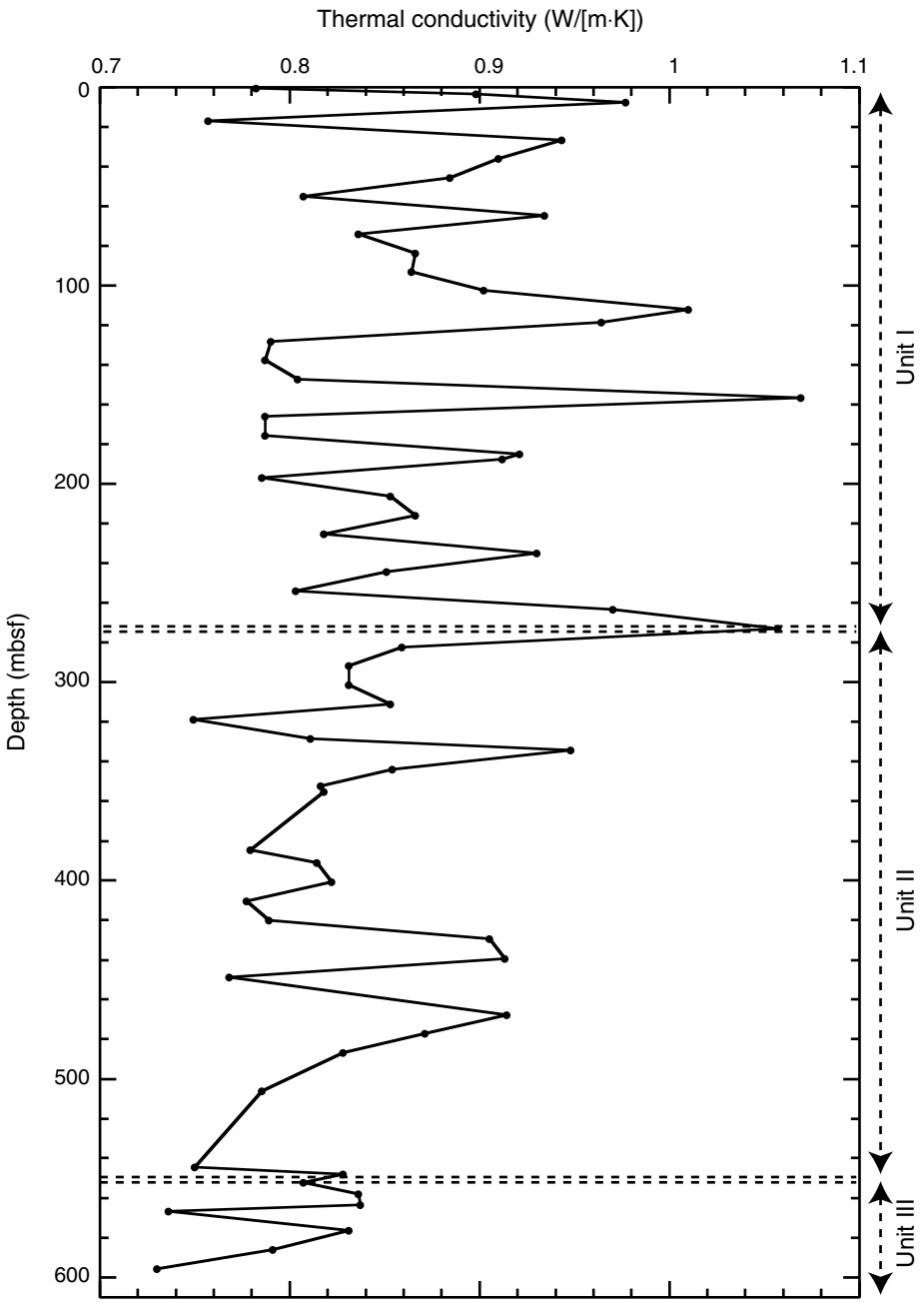

Figure F35. STMSL gamma ray attenuation (GRA) bulk density vs. composite depth, Site U1340.

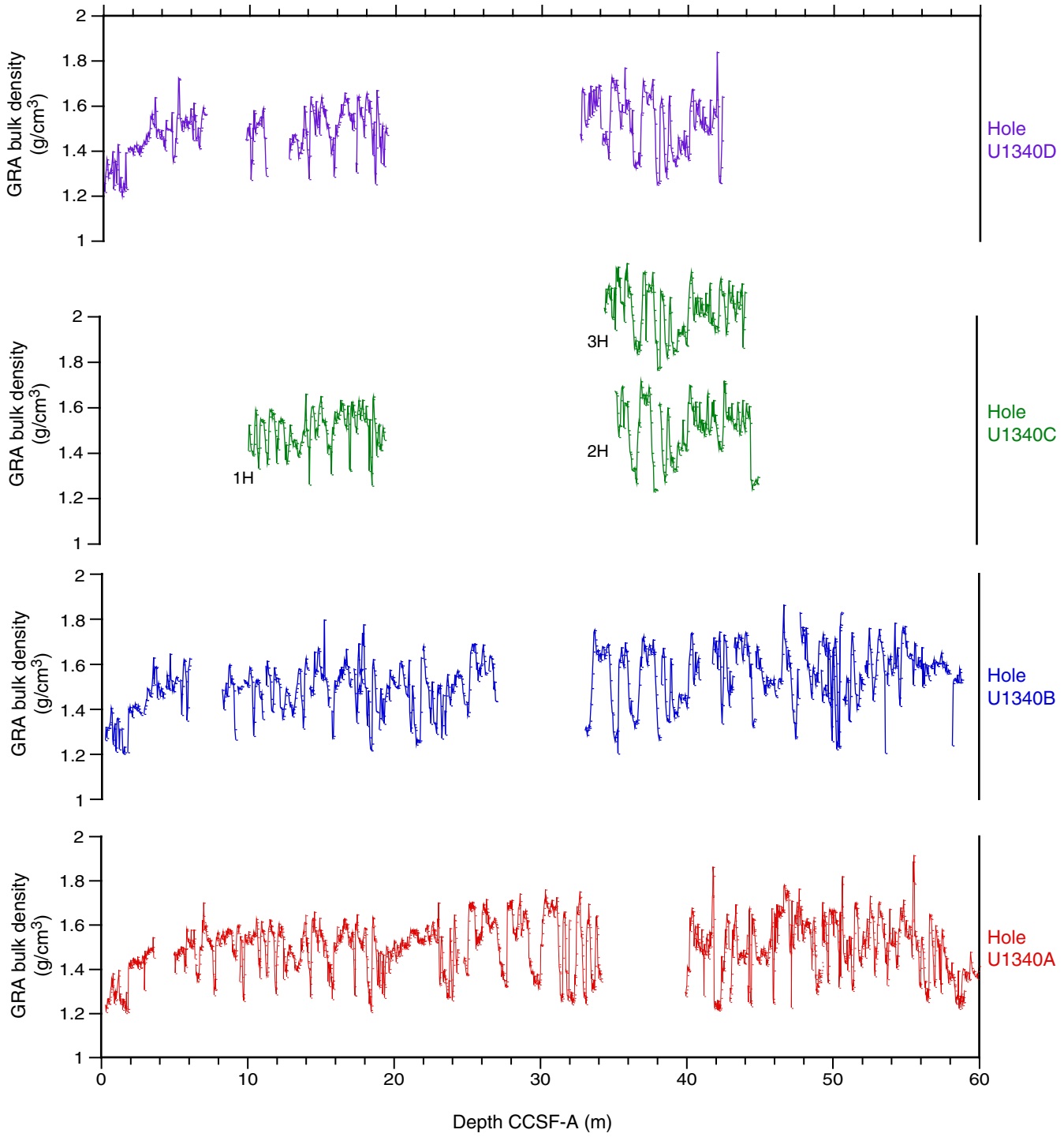

Figure F36. STMSL magnetic susceptibility vs. composite depth, Site U1340.

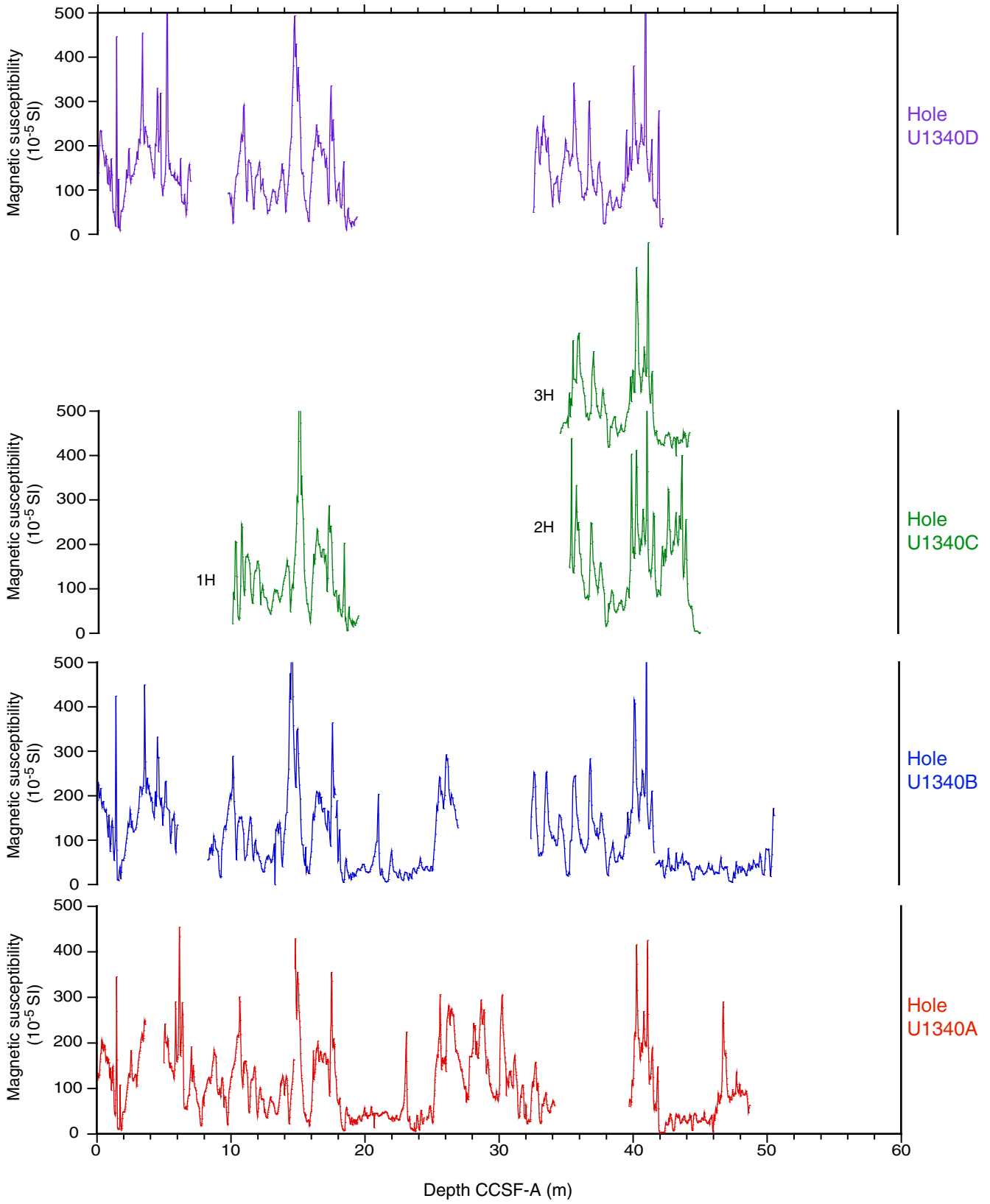

Figure F37. Color reflectance parameter b* vs. composite depth, Site U1340.

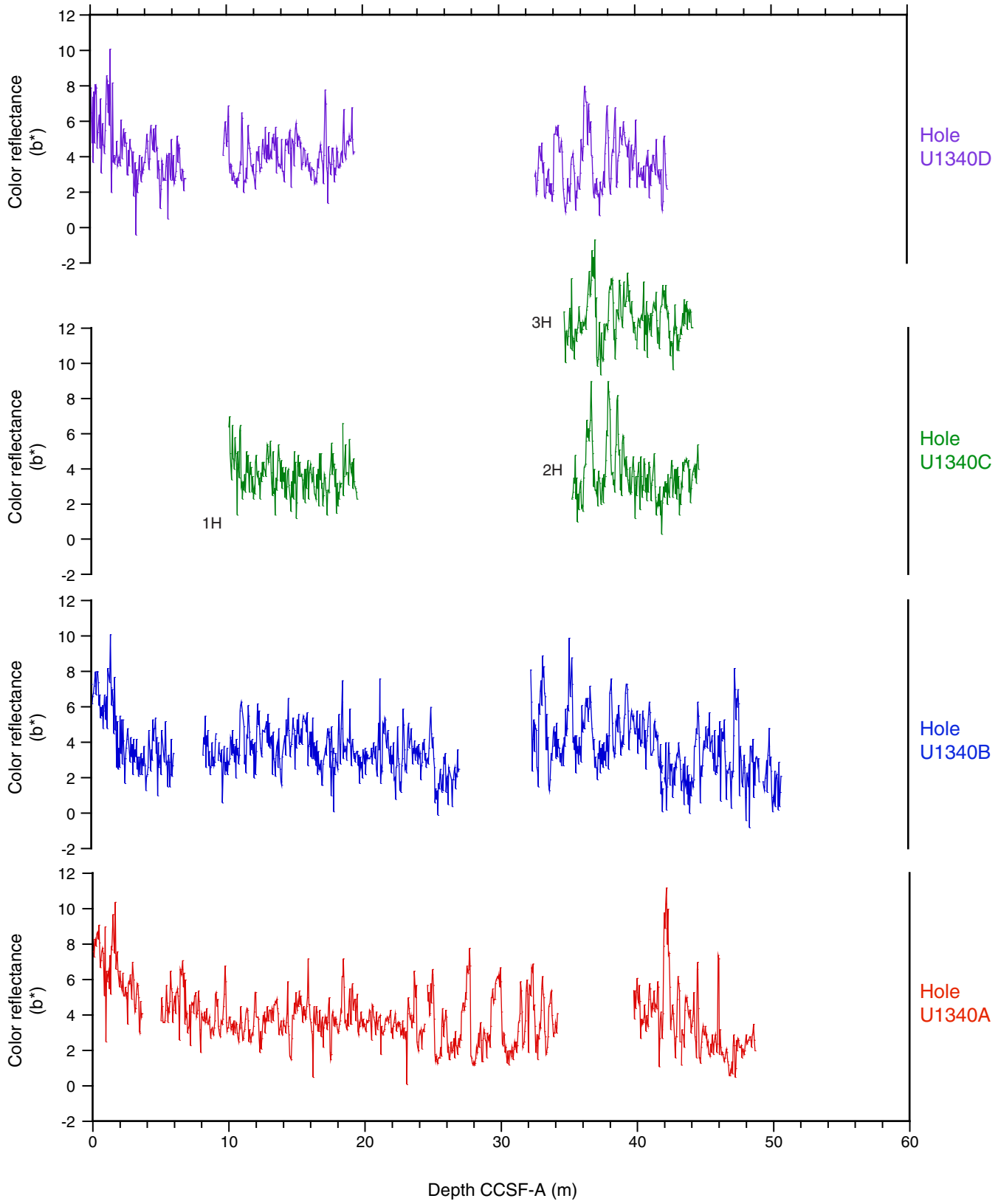

Figure F38. Digital line-scan images vs. composite depth, Site U1340. Note the pinkish ash marker beds in C in Sections 323-U1340A-5H-1, 323-U1340B-4H-3, 323-U1340C-2H-4 and 3H-4, and 323-U1340D-3H-6. Correlated features are visible throughout these cores. Offsets of a few centimeters are expected based on normal variations in sediment accumulation or minor drilling disturbance. **A.** 0–2 m CCSF-A. **B.** 36–38 m CCSF-A. (Continued on next page.)

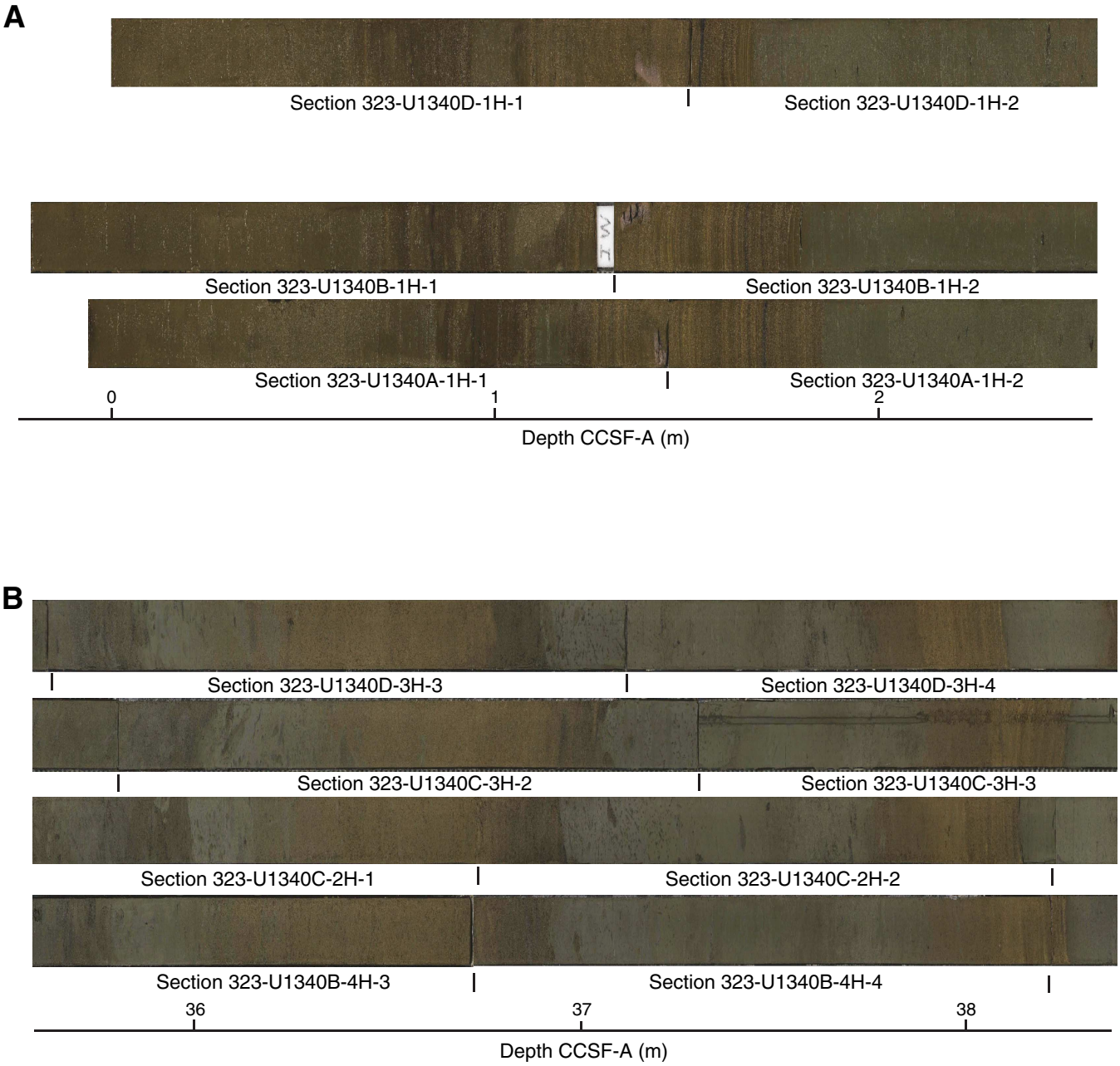

Figure F38 (continued). C. 39–41 m CCSF-A.

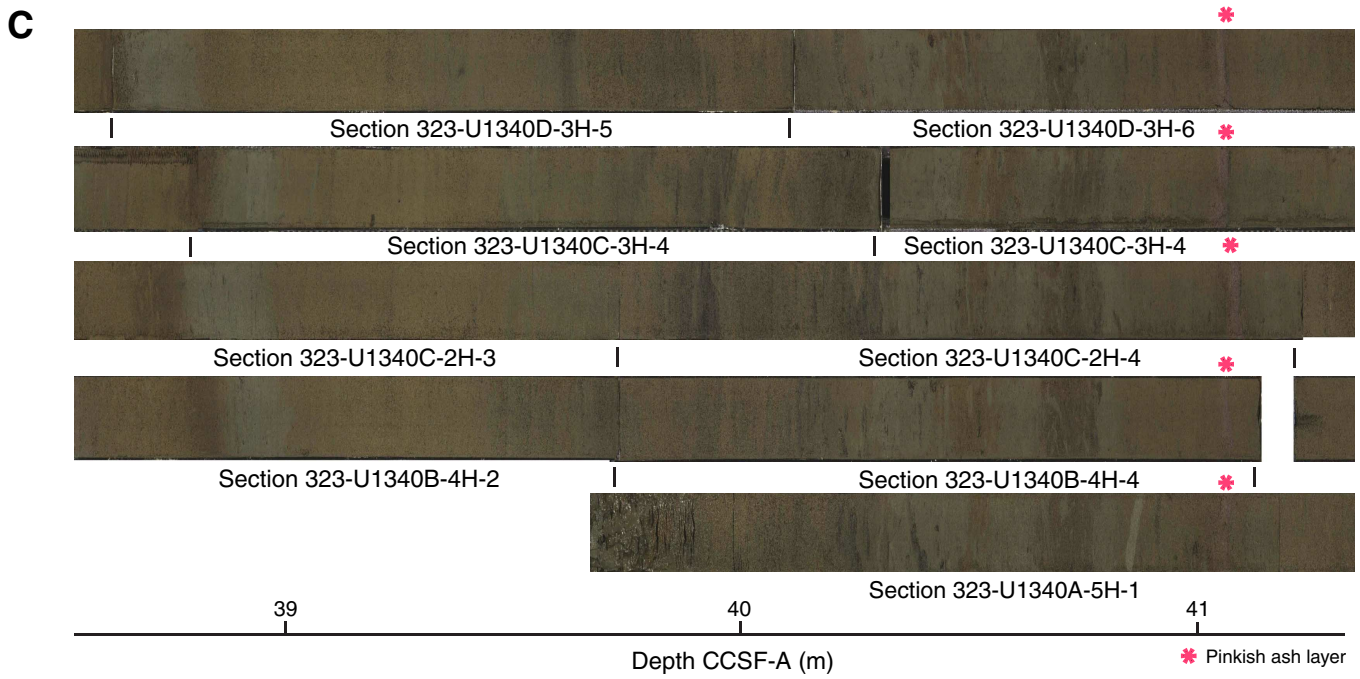

Figure F39. Spliced magnetic susceptibility, Site U1340, annotated to denote inferred intervals of soft-sediment deformation. Pink dots = locations of pinkish ash layers shown in Figure F38C. For the splice record (top panel), depth on the CCSF-D scale is equivalent to depth on the CCSF-A scale.

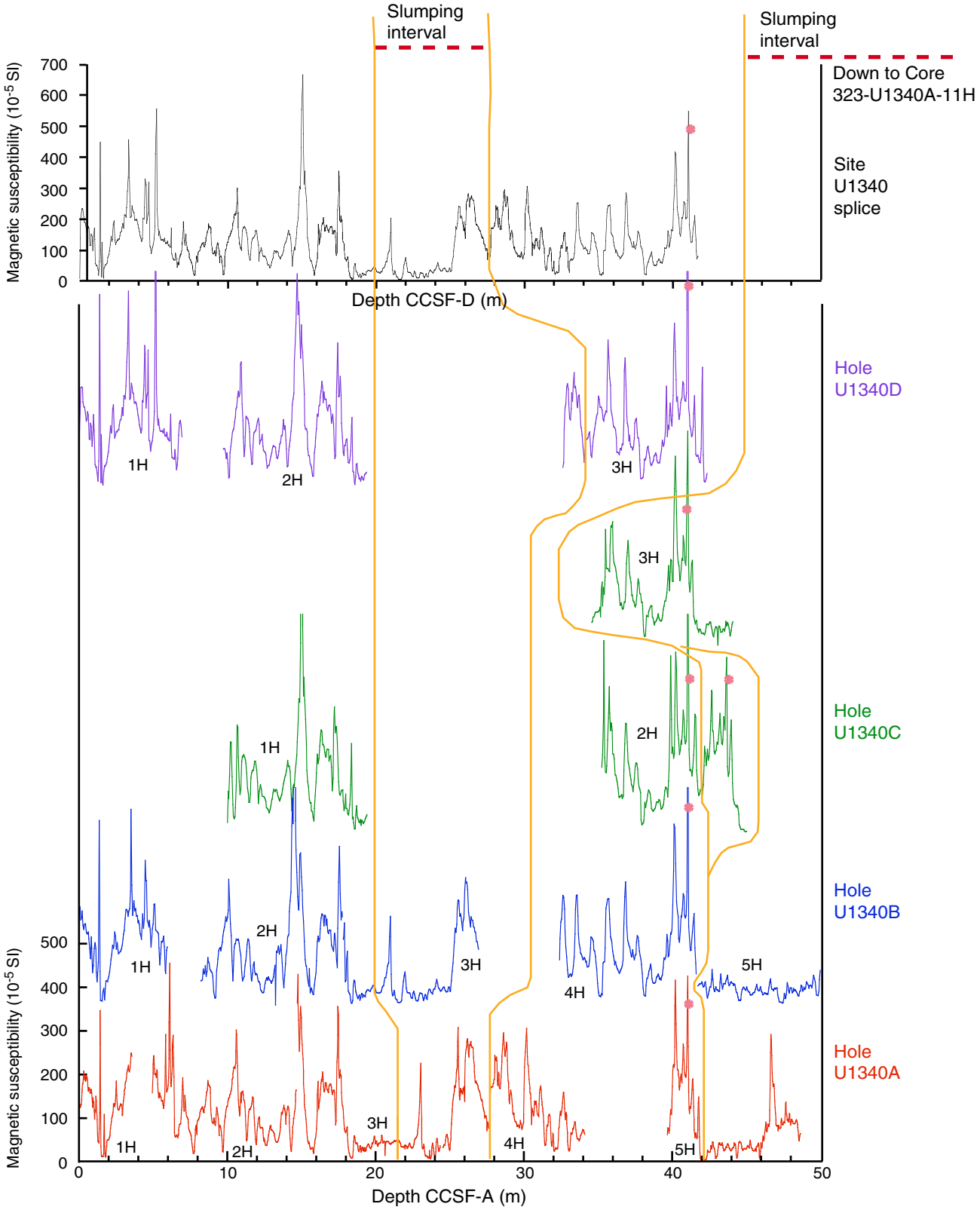

Figure F40. Spliced composite records of magnetic susceptibility, STMSL gamma ray attenuation (GRA) bulk density, and color reflectance parameter b* vs. splice composite depth, Site U1340. For the splice record (top panel), depth on the CCSF-D scale is equivalent to depth on the CCSF-A scale.

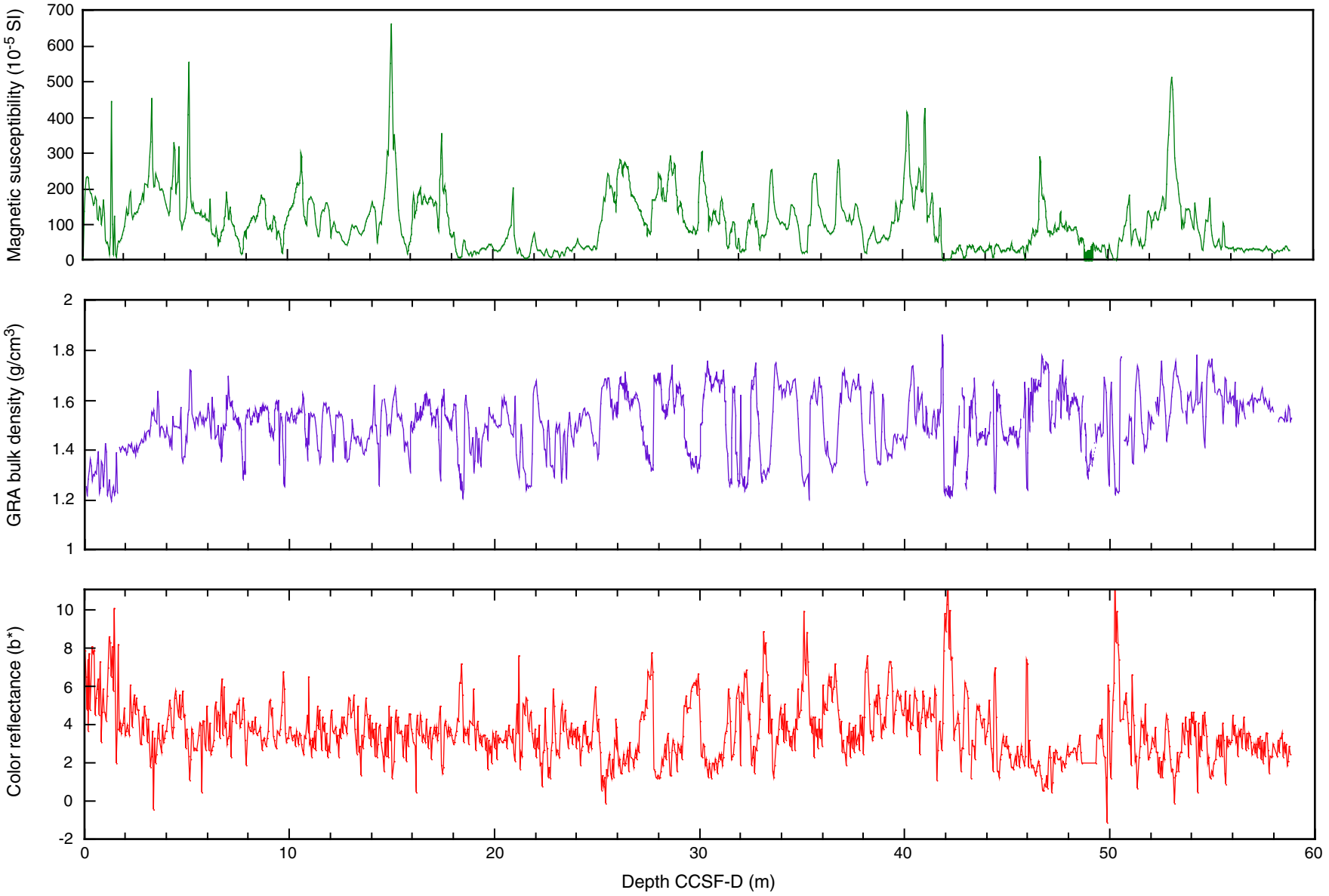

Figure F41. A. Mbsf vs. composite (CCSF-A) depth in the splice, Site U1340. A 1:1 line is shown for comparison. **B.** Growth of cumulative depth offset (m) vs. mbsf. Holes U1340A and U1340B in the spliced interval from 0.00 to 50 mbsf have affine growth factors of 1.14 and 1.18, respectively. Hole U1340C was started at 10.13 mbsf.

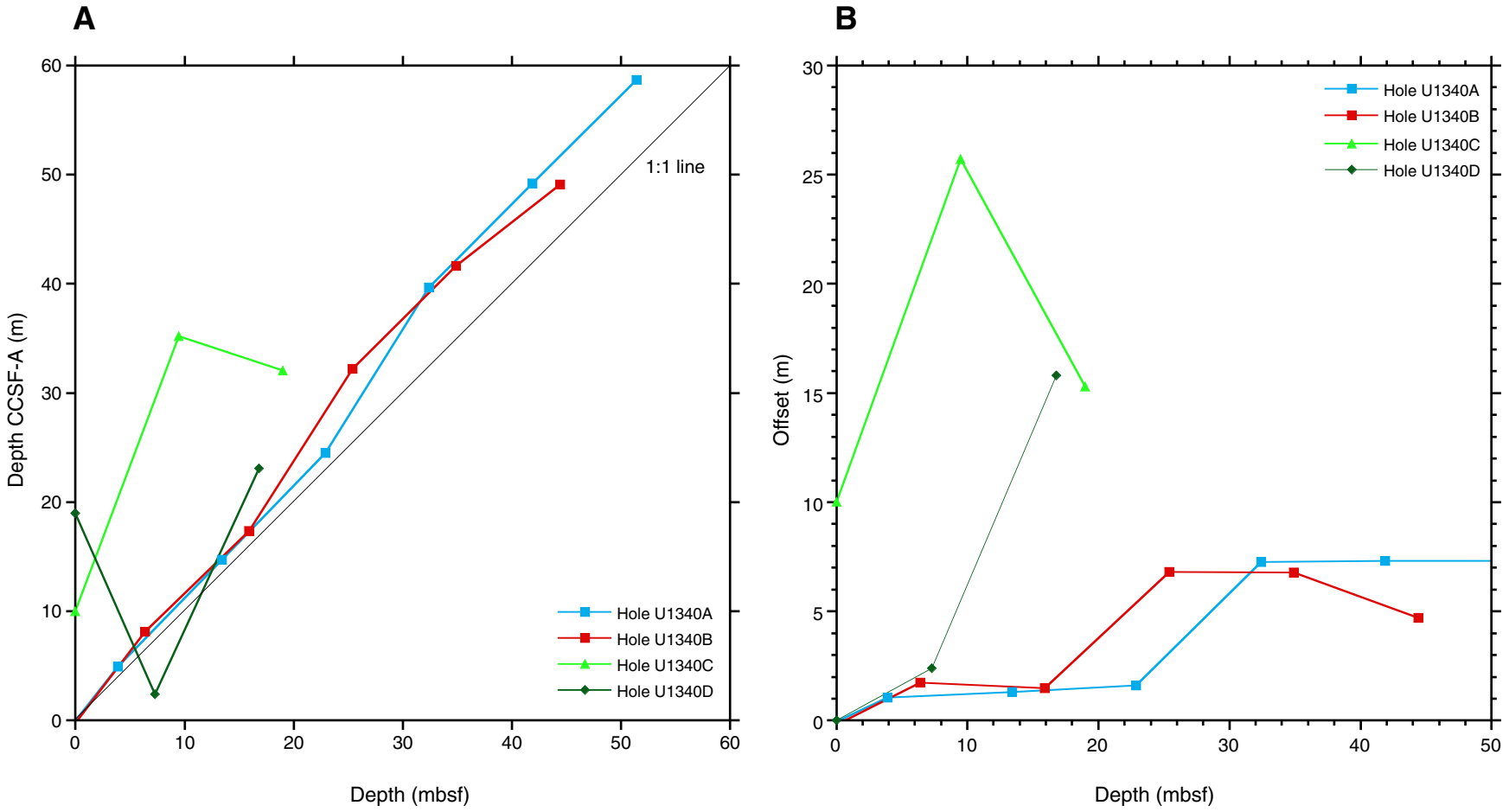

Figure F42. A. Records of APCT-3 penetrations and temperature decays, Site U1340. **B.** Summary of temperature measurements. The gradient was derived from a least square linear fit of the three successful records.

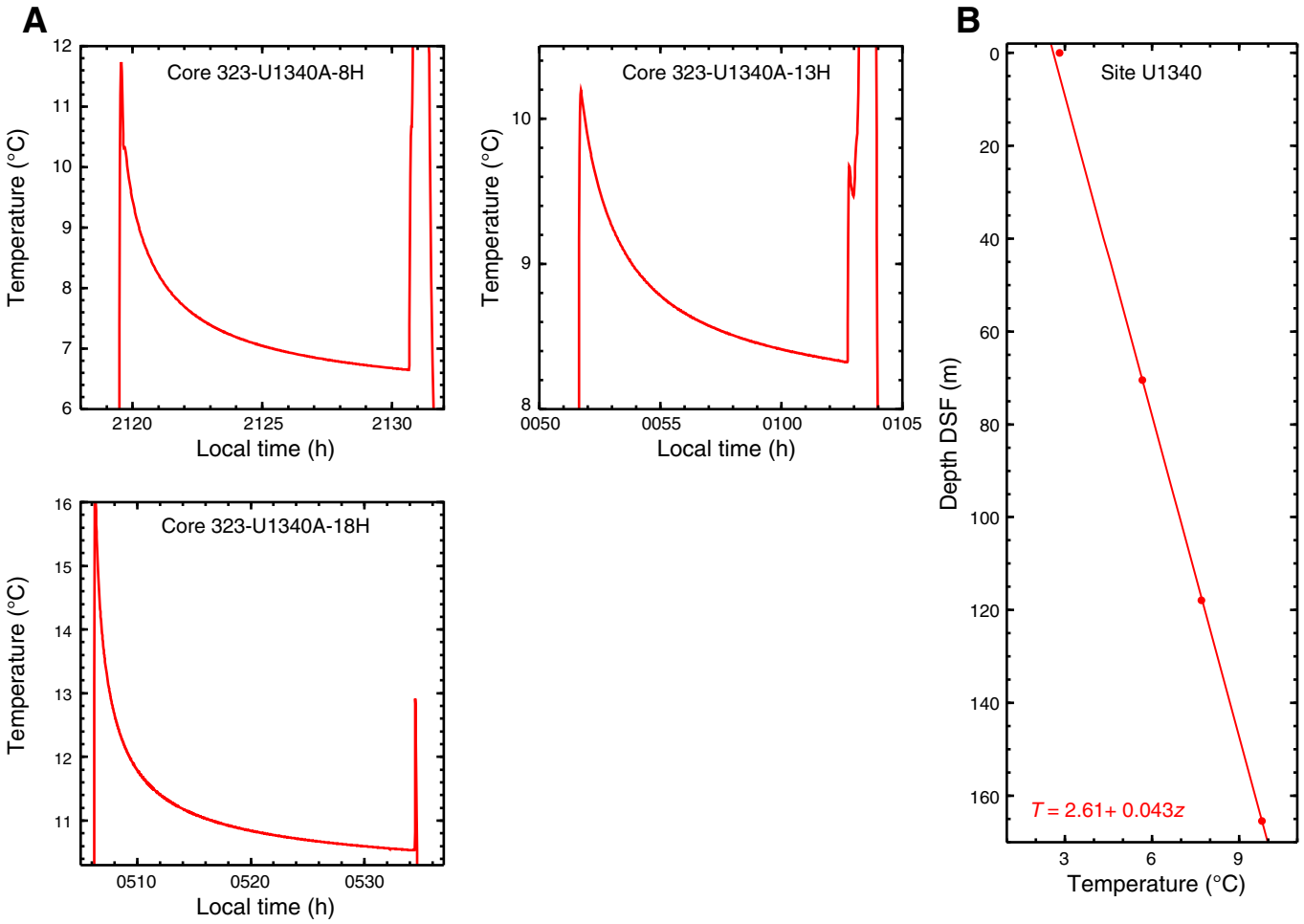

Table T1. Coring summary, Holes U1340A, U1340B, U1340C, and U1340D. (See table notes.) (Continued on next two pages.)

Hole U1340A
Latitude: 53°24.0008′N
Longitude: 179°31.2973′W
Time on hole (h): 69.8
Seafloor (drill pipe measurement from rig floor, m DRF): 1306.0
Distance between rig floor and sea level (m): 11.3
Water depth (drill pipe measurement from sea level, m): 1294.7
Total depth (drill pipe measurement from rig floor, m DRF): 1910.6
Total penetration (mbsf): 604.6
Total length of cored section (m): 604.6
Total core recovered (m): 535.91
Core recovery (%): 89
Total number of cores: 71

Hole U1340B
Latitude: 53°24.0002′N
Longitude: 179°30.9815′W
Time on hole (h): 6.95
Seafloor (drill pipe measurement from rig floor, m DRF): 1308.5
Distance between rig floor and sea level (m): 11.4
Water depth (drill pipe measurement from sea level, m): 1297.1
Total depth (drill pipe measurement from rig floor, m DRF): 1362.4
Total penetration (mbsf): 53.9
Total length of cored section (m): 53.9
Total core recovered (m): 55.53
Core recovery (%): 103
Total number of cores: 6

Hole U1340C
Latitude: 53°23.8113′N
Longitude: 179°31.2975′W
Time on hole (h): 4.58
Seafloor (drill pipe measurement from rig floor, m DRF): 1304.7
Distance between rig floor and sea level (m): 11.4
Water depth (drill pipe measurement from sea level, m): 1293.3
Total depth (drill pipe measurement from rig floor, m DRF): 1333.2
Total penetration (mbsf): 28.5
Total length of cored section (m): 28.5
Total core recovered (m): 30.00
Core recovery (%): 105
Total number of cores: 3

Hole U1340D
Latitude: 53°23.8004′N
Longitude: 179°31.2974′W
Time on hole (h): 6.98
Seafloor (drill pipe measurement from rig floor, m DRF): 1304.7
Distance between rig floor and sea level (m): 11.4
Water depth (drill pipe measurement from sea level, m): 1293.3
Total depth (drill pipe measurement from rig floor, m DRF): 1331.0
Total penetration (mbsf): 26.3
Total length of cored section (m): 26.3
Total core recovered (m): 27.23
Core recovery (%): 104
Total number of cores: 3

Core	Date (2009)	UTC (h)	Depth DSF (m) Top	Depth DSF (m) Bottom	Length (m) Cored	Length (m) Recovered	Recovery (%)	Comments
323-U1340A-								
1H	23 Jul	1630	0.0	3.9	3.9	3.90	100	Nonmagnetic barrel
2H	23 Jul	1725	3.9	13.4	9.5	10.02	105	Oriented nonmagnetic barrel
3H	23 Jul	1830	13.4	22.9	9.5	10.09	106	Oriented nonmagnetic barrel
4H	23 Jul	1900	22.9	32.4	9.5	9.95	105	Oriented nonmagnetic barrel
5H	23 Jul	1940	32.4	41.9	9.5	10.05	106	Oriented nonmagnetic barrel
6H	23 Jul	2015	41.9	51.4	9.5	10.12	107	Oriented nonmagnetic barrel
7H	23 Jul	2050	51.4	60.9	9.5	10.11	106	Oriented nonmagnetic barrel
8H	23 Jul	2140	60.9	70.4	9.5	10.18	107	Oriented nonmagnetic barrel
9H	23 Jul	2210	70.4	79.9	9.5	10.05	106	Oriented nonmagnetic barrel
10H	23 Jul	2255	79.9	89.4	9.5	10.03	106	Oriented nonmagnetic barrel
11H	23 Jul	2335	89.4	98.9	9.5	10.12	107	Oriented nonmagnetic barrel

Table T1 (continued). (Continued on next page.)

Core	Date (2009)	UTC (h)	Depth DSF (m) Top	Depth DSF (m) Bottom	Length (m) Cored	Length (m) Recovered	Recovery (%)	Comments
12H	24 Jul	0020	98.9	108.4	9.5	9.98	105	Oriented nonmagnetic barrel
13H	24 Jul	0115	108.4	117.9	9.5	10.23	108	Oriented nonmagnetic barrel
14H	24 Jul	0155	117.9	127.4	9.5	10.11	106	Oriented nonmagnetic barrel
15H	24 Jul	0235	127.4	136.9	9.5	9.82	103	Oriented nonmagnetic barrel
16H	24 Jul	0330	136.9	146.4	9.5	10.14	107	Oriented nonmagnetic barrel
17H	24 Jul	0440	146.4	155.9	9.5	10.18	107	Oriented nonmagnetic barrel
18H	24 Jul	0545	155.9	165.4	9.5	10.09	106	Steel barrel
19H	24 Jul	0640	165.4	174.9	9.5	10.15	107	Steel barrel
20H	24 Jul	0725	174.9	184.4	9.5	9.92	104	Steel barrel
21H	24 Jul	0805	184.4	185.7	1.3	1.31	101	Steel barrel
22D			***** Drilled from 185.7 to 186.7 m DSF*****					
23H	24 Jul	0900	186.7	196.2	9.5	9.74	103	Steel barrel
24H	24 Jul	1010	196.2	205.7	9.5	10.00	105	Steel barrel
25H	24 Jul	1125	205.7	215.2	9.5	10.00	105	Steel barrel
26H	24 Jul	1225	215.2	224.7	9.5	10.05	106	Steel barrel
27H	24 Jul	1325	224.7	234.2	9.5	10.02	105	Steel barrel
28H	24 Jul	1415	234.2	243.7	9.5	9.88	104	Steel barrel
29H	24 Jul	1505	243.7	253.2	9.5	9.91	104	Steel barrel
30H	24 Jul	1550	253.2	262.7	9.5	9.96	105	Steel barrel
31H	24 Jul	1645	262.7	272.2	9.5	9.97	105	Steel barrel
32H	24 Jul	1740	272.2	281.7	9.5	9.97	105	Steel barrel
33H	24 Jul	1830	281.7	291.2	9.5	10.06	106	Steel barrel
34H	24 Jul	1920	291.2	300.7	9.5	9.40	99	Steel barrel
35H	24 Jul	2000	300.7	310.2	9.5	9.98	105	Steel barrel
36H	24 Jul	2055	310.2	318.2	8.0	8.10	101	Steel barrel
37H	24 Jul	2135	318.2	327.7	9.5	9.16	96	Steel barrel
38H	24 Jul	2215	327.7	333.7	6.0	5.85	98	Steel barrel
39H	24 Jul	2345	333.7	343.2	9.5	9.95	105	Steel barrel
40H	25 Jul	0030	343.2	351.7	8.5	8.23	97	Steel barrel
41H	25 Jul	0115	351.7	354.7	3.0	3.03	101	Steel barrel
42H	25 Jul	0210	354.7	358.7	4.0	4.00	100	Steel barrel
43X	25 Jul	0330	358.7	364.7	6.0	0.07	1	Steel barrel
44X	25 Jul	0430	364.7	374.3	9.6	0.49	5	Steel barrel
45X	25 Jul	0555	374.3	383.9	9.6	0.45	5	Steel barrel
46X	25 Jul	0920	383.9	390.5	6.6	2.91	44	Steel barrel
47X	25 Jul	1000	390.5	400.1	9.6	9.01	94	Steel barrel
48X	25 Jul	1040	400.1	409.7	9.6	9.22	96	Steel barrel
49X	25 Jul	1120	409.7	419.3	9.6	8.36	87	Steel barrel
50X	25 Jul	1155	419.3	428.9	9.6	5.86	61	Steel barrel
51X	25 Jul	1230	428.9	438.6	9.7	6.71	69	Steel barrel
52X	25 Jul	1305	438.6	448.1	9.5	9.18	97	Steel barrel
53X	25 Jul	1335	448.1	457.4	9.3	9.62	103	Steel barrel
54X	25 Jul	1415	457.4	467.1	9.7	0.42	4	Steel barrel
55X	25 Jul	1440	467.1	476.6	9.5	9.23	97	Steel barrel
56X	25 Jul	1510	476.6	486.2	9.6	9.60	100	Steel barrel
57X	25 Jul	1615	486.2	495.8	9.7	6.72	69	Steel barrel
58X	25 Jul	1640	495.9	505.4	9.6	0.02	0	Steel barrel
59X	25 Jul	1720	505.5	515.0	9.6	9.70	101	Steel barrel
60X	25 Jul	1750	515.1	524.7	9.7	0.00	0	Steel barrel
61X	25 Jul	1820	524.8	534.3	9.6	0.00	0	Steel barrel
62X	25 Jul	1855	534.4	543.9	9.5	0.00	0	Steel barrel
63H	25 Jul	1955	543.9	547.5	3.5	2.87	82	Steel barrel, very sandy, "bounced" core liner to pack it full
64H	25 Jul	2100	547.4	551.5	4.0	8.26	206	Steel barrel
65H	25 Jul	2256	551.5	557.5	6.0	5.93	99	Steel barrel
66H	25 Jul	2355	557.5	563.0	5.5	5.47	99	Steel barrel
67H	26 Jul	0050	563.0	566.0	3.0	2.90	97	Steel barrel
68X	26 Jul	0155	566.0	575.7	9.7	9.99	103	Steel barrel
69X	26 Jul	0330	575.7	585.4	9.7	9.58	99	Steel barrel
70X	26 Jul	0405	585.4	595.0	9.6	9.92	103	Steel barrel
71X	26 Jul	0515	595.0	604.6	9.6	9.61	100	Steel barrel
				Cored totals:	604.5	535.91	89	
323-U1340B-								
1H	26 Jul	1050	0.0	6.4	6.4	6.43	100	Oriented nonmagnetic barrel
2H	26 Jul	1140	6.4	15.9	9.5	9.95	105	Oriented nonmagnetic barrel
3H	26 Jul	1220	15.9	25.4	9.5	9.89	104	Oriented nonmagnetic barrel
4H	26 Jul	1250	25.4	34.9	9.5	9.99	105	Oriented nonmagnetic barrel
5H	26 Jul	1330	34.9	44.4	9.5	9.24	97	Oriented nonmagnetic, shattered liner
6H	26 Jul	1415	44.4	53.9	9.5	10.03	106	Oriented nonmagnetic, liner cracked

Table T1 (continued).

Core	Date (2009)	UTC (h)	Depth DSF (m) Top	Depth DSF (m) Bottom	Length (m) Cored	Length (m) Recovered	Recovery (%)	Comments
				Cored totals:	53.9	55.53	103	Oriented nonmagnetic barrel
323-U1340C-								
1H	26 Jul	1730	0.0	9.5	9.5	9.85	104	Nonmagnetic barrel
2H	26 Jul	1820	9.5	19.0	9.5	10.07	106	Oriented nonmagnetic barrel
3H	26 Jul	1855	19.0	28.5	9.5	10.08	106	Oriented nonmagnetic barrel
				Cored totals:	28.5	30.00	105	
323-U1340D-								
1H	26 Jul	2015	0.0	7.3	7.3	7.29	100	Nonmagnetic barrel
2H	26 Jul	2050	7.3	16.8	9.5	9.91	104	Oriented nonmagnetic barrel
3H	26 Jul	2120	16.8	26.3	9.5	10.03	106	Oriented steel barrel
				Cored totals:	26.3	27.23	104	
				Site totals:	713.2	648.67	91	

Notes: DRF = drilling depth below rig floor, mbsf = meters below seafloor, DSF = drilling depth below seafloor. UTC = Universal Time Coordinated.

Table T2. Datum events of radiolarians, diatoms, silicoflagellates, ebridians, and dinoflagellates, Hole U1340A. (See table notes.)

Datum event	Taxon	Age (Ma)	Depth (mbsf)
LO *Lychnocanoma nipponica sakaii*	Radiolarian	0.05	8.9
LO *Amphimelissa setosa*	Radiolarian	0.08–1.0	8.9
LO *Spongodiscus* sp.	Radiolarian	0.28–0.32	18.7
LO *Axoprunum acquilonium*	Radiolarian	0.25–0.43	18.7
LO *Proboscia curvirostris*	Diatom	0.3	37.6
LO *Thalassiosira jouseae*	Diatom	0.3	37.6
LO *Proboscia barboi*	Diatom	0.3	37.6
LO *Dictyocha subarctios*	Silicoflagellate	0.6–0.8	118.4
LO *Actinocyclus oculatus*	Diatom	0.9	161.2
LO *Eucyrtidium matuyamai*	Radiolarian	0.9–1.5	161.2
LO *Filisphaera filifera*	Dinoflagellate	1.4–1.7	206.0
RI *Neodenticula seminae*	Diatom	1.778	260.7
FO *Eucyrtidium matuyamai*	Radiolarian	1.7–1.9	201.3
FCO *Proboscia curvirostris*	Diatom	1.7–2.0	201.2
LO *Stephanopyxis horridus*	Diatom	1.9–2.0	229.9
FCO *Neodenticula koizumii*	Diatom	2.1 ± 0.1	515.1
LO *Thecosphaera akitaensis*	Radiolarian	2.4–2.7	267.9
LO *Ebriopsis antiqua antiqua*	Ebridian	2.47–2.48	305.5
LCO *Neodenticula kamtschatica*	Diatom	2.7	486.2
LO *Phormostichoartus fistula*	Radiolarian	2.8–4.4	314.4
FO *Neodenticula koizumii*	Diatom	3.7–3.9	531.0
LO *Dictyophimus bullatus/Dictyophimus* sp. B	Radiolarian	3.8–4.0	531.0

Notes: For first occurrences (FO), the depth was estimated as the midpoint between the depth at which the species was first observed and the depth of the next sample below. For last occurrences (LO), the depth was estimated as the midpoint between the depth at which the species was last observed and the depth of the next sample above. FCO = first common occurrence, LCO = last common occurrence. RI = rapid increase.

Table T3. Calcareous nannofossil range chart, Holes U1340A, U1340B, and U1340D. (See table notes.) (Continued on next page.)

Core, section	Martini (1971) zone	Abundance	Preservation	*Coccolithus braarudii*	*Coccolithus miopelagicus*	*Coccolithus pelagicus*	*Cyclococcolithus leptoporus*	*Discoaster brouweri*	*Emiliania huxleyi*	*Gephyrocapsa* (small)	*Gephyrocapsa* (medium)	*Gephyrocapsa* (large)	*Pseudoemiliania lacunosa*	*Reticulofenestra minutula*	Other taxa	Comments
323-U1340A-																
1H-CC		F	M	R		D										Etching in *Coccolithus pelagicus*. *Thoracosphaera* spp.
2H-CC		R	M-G			R										
3H-CC		B														
4H-CC		B														
5H-CC		A	M-G	R	*	D		*		F	F					Reworked specimens of *Discoaster brouweri*, *Coccolithus miopelagicus*
6H-CC		B														Unknown reworked specimens
7H-CC		F	M-G			F				F	R		R			
8H-CC		B														
9H-CC		A	M-G			A				F	R			D	*Syracosphaera* spp.	Reworked specimens
10H-CC		A	G			A					R				*Syracosphaera* spp.	Reworked specimens of *Coccolithus* spp. and *Dictyococcites* spp. (Paleogene)
11H-CC		B														
12H-CC		B														
13H-CC		B														
14H-CC		R	M-G			R										Reworked specimens (Paleogene)
15H-CC		F	G			R				F			R			
16H-CC		F	M-G			F				R						
17H-CC		F	G			F					R		R			Reworked specimens (unknown)
18H-CC		F	M-G			F										Reworked specimens (unknown and *Coccolithus pelagicus*)
19H-CC		C	G			C	R			R			R			
20H-CC		B														
21H-CC	NN19	B														
22H-CC		—														Drilled interval
23H-CC		F	G		*	F							R			Reworked specimens (Paleogene: *Crucioplacolithus* spp. and *Reticulofenestra umbilica*; Miocene: *Coccolithus miopelagicus*)
24H-CC		B														
25H-CC		B														
26H-CC		B														
27H-CC		B														
28H-CC		B														
29H-CC		B														
30H-CC		B														
31H-CC		B														
32H-CC		B														
33H-CC		B														
34H-CC		B														
35H-CC		B														
36H-CC		B														
37H-CC		B														
38H-CC		B														
39H-CC		B														
40H-CC		B														
41H-CC		B														
42H-CC		F	M			F										Specimens show moderate to severe etching, all small size

Table T3 (continued).

Core, section	Martini (1971) zone	Abundance	Preservation	*Coccolithus braarudii*	*Coccolithus miopelagicus*	*Coccolithus pelagicus*	*Cyclococcolithus leptoporus*	*Discoaster brouweri*	*Emiliania huxleyi*	*Gephyrocapsa* (small)	*Gephyrocapsa* (medium)	*Gephyrocapsa* (large)	*Pseudoemiliania lacunosa*	*Reticulofenestra minutula*	Other taxa	Comments
43X-CC		F	M			F										Specimens show moderate to severe etching, all small size
44X-CC		B														
45X-CC		B														
46X-CC		B														
47X-CC		B														
48X-CC		B														
49X-CC		B														
50X-CC		B														
51X-CC		B														
52X-CC		B														
53X-CC		B														
54X-CC		B														
55X-CC		B														
56X-CC		B														
57X-CC	NN19	B														
58X-CC		B														
59H-CC		B														
60H-CC		—														No recovery
61H-CC		—														No recovery
62H-CC		—														No recovery
63H-CC		B														
64H-CC		B														
65H-CC		B														
66H-CC		B														
67H-CC		B														
68X-CC		B														
69X-CC		B														
70X-CC		B														
71X-CC		B														
323-U1340B-																
1H-CC		C	G			C			R	R	F					Reworked specimens of probable Paleogene age
2H-CC		A	G			A									*Syracosphaera* spp.	
3H-CC		R	M-G			R				D	A					
4H-CC		A	G			A			R							
5H-CC		B														
6H-CC	NN21	A	G			C				A	D					Medium and small gephyrocapsids mostly of the *Gephyrocapsa caribbeanica* type
323-U1340D-																
1H-CC		A	M-G			A			F						*Syracosphaera* spp.	Large (>4 µm) and small (<4 µm) specimens of *Emiliania huxleyi*
2H-CC		F	M-G			F										
3H-CC		A	G			A			F	D	A					More than 50 specimens/FOV

Notes: * = reworked. Abundance: D = dominant, A = abundant, C = common, F = few, R = rare, B = barren. Preservation: G = good, M = moderate, P = poor. FOV = field of view.

Table T4. Planktonic foraminifer range chart, Holes U1340A, U1340B, U1340C, and U1340D. (See table notes.) (Continued on next page.)

Core, section	Abundance	Preservation	*Globigerina bulloides*	*Globigerina umbilicata*	*Neogloboquadrina pachyderma* (dex)	*Neogloboquadrina pachyderma* (sin)	*Turborotalia quinqueloba*	Other observations
323-U1340A-								
Mudline	F	G	P			F		
1H-CC	D	VG	F			D	P	Dominant siliciclastics
2H-CC	R	G				R		Dominant siliciclastics and diatoms
3H-CC	F	P	P			A		
4H-CC	F	G	R			F		
5H-CC	A	G	F	P		D		
6H-CC	B							
7H-CC	A	G	R	F		D		
8H-CC	R	G				R		
9H-CC	D	VG	P	F		D		
10H-CC	D	G	P			D		
11H-CC	B							
12H-CC	R	G	P		P			
13H-CC	F	G	P			F		
14H-CC	F	G	P			F		Dominant siliciclastics and diatoms
15H-CC	R	G				R		Dominant diatoms, few siliciclastics
16H-CC	R	G	R			R		Dominant diatoms, few siliciclastics
17H-CC	A	G				D		Dominant siliciclastics, few sponge spicules
18H-CC	R	G				R		Dominant siliciclastics, few sponge spicules
19H-CC	F	M	R		F	R		Dominant siliciclastics, diatoms, and sponge spicules
20H-CC	P	M	P					Dominant siliciclastics, diatoms, and sponge spicules
21H-CC	P	M	P					Dominant siliciclastics, diatoms, and sponge spicules
22H-CC	NA							
23H-CC	R	M			R			Dominant siliciclastics, diatoms, and sponge spicules
24H-CC	B							Dominant siliciclastics, diatoms, and sponge spicules
25H-CC	B							Dominant diatoms, abundant siliciclastics, few sponge spicules
26H-CC	B							Dominant siliciclastics, few diatoms, rare sponge spicules
27H-CC	B							
28H-CC	B							
29H-CC	B							Dominant diatoms, few sponge spicules, few siliciclastics
30H-CC	B							
31H-CC	R	G	R	P	P			
32H-CC	B							
33H-CC	B							
34H-CC	B							Dominant siliciclastics (quartz), few sponge spicules, rare diatoms
35H-CC	B							Dominant siliciclastics (quartz), few sponge spicules, rare diatoms
36H-CC	B							Dominant siliciclastics (quartz), few sponge spicules, few diatoms
37H-CC	B							Dominant siliciclastics (quartz), few sponge spicules, few diatoms
38X-CC	B							
39X-CC	B							Dominant siliciclastics (quartz), few sponge spicules, rare diatoms
40X-CC	B							Dominant siliciclastics (quartz), few sponge spicules, rare diatoms
41X-CC	B							
42X-CC	R	M	R		R			Dominant diatoms, abundant sponge spicules, few siliciclastics
43X-CC	R	M	R		R			Dominant diatoms, abundant siliciclastics (>0.5 mm)
44X-CC	B							Dominant diatoms, abundant siliciclastics
45X-CC	B							Small clay aggregates
46X-CC	B							Dominant diatoms, abundant sponge spicules and siliciclastics (quartz)
47X-CC	B							Dominant siliciclastics (quartz), abundant diatoms, few sponge spicules, clay aggregates
48X-CC	B							Dominant siliciclastics (quartz), few sponge spicules, rare diatoms
49X-CC	B							Dominant diatoms, abundant sponge spicules and siliciclastics (quartz)
50X-CC	B							Dominant diatoms, abundant sponge spicules and siliciclastics (quartz)
51X-CC	B							Dominant siliciclastics (quartz), few sponge spicules, rare diatoms
52X-CC	B							Dominant diatoms, abundant sponge spicules, few siliciclastics
53X-CC	B							Dominant diatoms, abundant sponge spicules, few siliciclastics
54X-CC	B							Dominant diatoms, abundant sponge spicules, few siliciclastics
55X-CC	B							Dominant diatoms, abundant sponge spicules, few siliciclastics

Table T4 (continued).

Core, section	Abundance	Preservation	*Globigerina bulloides*	*Globigerina umbilicata*	*Neogloboquadrina pachyderma* (dex)	*Neogloboquadrina pachyderma* (sin)	*Turborotalia quinqueloba*	Other observations
56X-CC	B							Dominant diatoms, abundant sponge spicules, few siliciclastics
57X-CC	B							Dominant diatoms, abundant sponge spicules, few siliciclastics
58X-CC	B							Dominant diatoms, abundant sponge spicules, abundant siliciclastics
59X-CC	B							Dominant diatoms, abundant sponge spicules, abundant siliciclastics
60X-CC	NA							
61X-CC	NA							
62X-CC	NA							
63X-CC	B							Dominant diatoms, abundant sponge spicules, abundant siliciclastics
64X-CC	B							Dominant diatoms, abundant sponge spicules, few siliciclastics
65X-CC	B							Dominant diatoms, abundant sponge spicules
66X-CC	B							Dominant diatoms
67X-CC	B							Dominant diatoms, abundant sponge spicules
68X-CC	B							Dominant diatoms, abundant sponge spicules
69X-CC	B							Dominant diatoms, abundant sponge spicules
70X-CC	B							Dominant diatoms, abundant sponge spicules, few siliciclastics
71H-CC	B							Dominant diatoms, abundant sponge spicules, few siliciclastics
323-U1340B-								
1H-CC	A	G		R	P	A		Dominant siliciclastics (quartz), abundant diatoms, few sponge spicules
2H-CC	D	G	A		F	D		Dominant planktonic foraminifers, few sponge spicules, rare siliciclastics
3H-CC	A	G		R		A		Abundant diatoms, abundant siliciclastics, abundant sponge spicules
4H-CC	A	G	F			A		Abundant diatoms, abundant siliciclastics, abundant sponge spicules
5H-CC	P	G	P			P		Dominant siliciclastics (quartz), abundant diatoms, few sponge spicules
6H-CC	D	G	R		R	D		Dominant foraminifers, few sponge spicules, rare siliciclastics
323-U1340C-								
1H-CC	A	G	R	F		D		
2H-CC	R	G				R		
3H-CC	D	G	A	R	F	D		
323-U1340D-								
1H-CC	A	G				A		
2H-CC	F	G		P		F		
3H-CC	A	G		A		A		

Notes: Abundance: D = dominant, A = abundant, F = few, R = rare, P = present, B = barren, NA = not applicable. Preservation: VG = very good, G = good, M = moderate, P = poor. Dex = dextral, sin = sinistral.

Table T5. Benthic foraminifer range chart, Hole U1340A. This table is available in an **oversized format.**

Table T6. Benthic foraminifer range chart, Hole U1340B. (See table notes.)

Core, section	Abundance	Preservation	*Brizalina earlandi*	*Brizalina* sp.	*Bulimina* aff. *exilis*	*Elphidium* cf. *batialis*	*Epistominella pulchella*	*Globobulimina pacifica*	*Globocassidulina* sp.	*Gyroidinoides soldanii*	*Islandiella norcrossi*	*Melonis barleeanum*	*Nonionella labradorica*	*Nonionella turgida*	*Pullenia* sp.	*Stainforthia* aff. *fusiformis*	*Uvigerina auberiana*	*Uvigerina* cf. *peregrina*	Siliciclastics	Other observations
323-U1340B-																				
1H-CC	A	G			R		F	R	P		F			P			P	A	D	Quartz, few sponge spicules
2H-CC	A	G	R		F		F	P	F	F	P	P	P	R				A	R	Dominant planktonic foraminifers
3H-CC	A	G	P		A		P		R	P	F	P	P	P	P			R	A	Abundant sponge spicules
4H-CC	A	G	A		R		R		P							P			A	Abundant sponge spicules
5H-CC	F	G		P	F	P			R		F	P	R		P			R	A	Few sponge spicules
6H-CC		G	D		F				A		R		R			R		R	F	Few sponge spicules

Notes: Abundance: D = dominant, A = abundant, F = few, R = rare, P = present. Preservation: G = good.

Table T7. Benthic foraminifer range chart, Hole U1340C. (See table notes.)

Core, section	Abundance	Preservation	*Brizalina earlandi*	*Brizalina pygmaea*	*Bulimina* aff. *exilis*	*Bulimina* sp.	*Cancris* cf. *philippinensis*	*Cassidulina* sp.	*Elphidium* cf. *batialis*	*Globobulimina pacifica*	*Globocassidulina* sp.	*Gyroidinoides soldanii*	*Islandiella norcrossi*	*Melonis barleeanum*	*Nonionella labradorica*	*Nonionella turgida digitata*	*Uvigerina* cf. *peregrina*	*Valvulineria* sp.	Siliciclastics	Other observations
323-U1340C-																				
1H-CC	F	G	R			P	R					P	P		P		F	P	F	Quartz
2H-CC	A	G					F	F			A			F	F		D	R	R	Abundant sponge spicules
3H-CC	A	G	F	A	D		F		R			F			F	P		R	R	

Notes: Abundance: D = dominant, A = abundant, F = few, R = rare, P = present. Preservation: G = good.

Table T8. Benthic foraminifer range chart, Hole U1340D. (See table notes.)

Core, section	Abundance	Preservation	*Brizalina earlandi*	*Brizalina pygmaea*	*Bulimina* aff. *exilis*	*Cassidulina* sp.	*Cassidulinoides tenuis*	*Epistominella pulchella*	*Globobulimina pacifica*	*Islandiella norcrossi*	*Lenticulina* sp.	*Melonis barleeanum*	*Nonionella turgida digitata*	*Oridorsalis umbonatus*	*Procerolagena* cf. *gracillima*	*Pullenia* sp.	*Uvigerina* cf. *peregrina*	*Valvulineria* sp.	Siliciclastics	Other observations
323-U1340D-																				
1H-CC	A	G		R	F	F		F	F	P		R	F				D		F	Quartz
2H-CC	F	P					P		F	P							R		A	Quartz
3H-CC	A	G	R	F	A	F					P		R	R	P	R	A	F	F	Quartz, sponge spicules

Notes: Abundance: D = dominant, A = abundant, F = few, R = rare, P = present. Preservation: G = good, P = poor.

Table T9. Diatom range chart, Hole U1340A. This table is available in an oversized format.

Table T10. Silicoflagellate range chart, Hole U1340A. (See table notes.)

Core, section	Depth (mbsf) Top	Depth (mbsf) Bottom	Abundance	Preservation	Silicoflagellates: Aberrant silicoflagellate skeletons	*Dictyocha* cf. *mandrai*	*Dictyocha subarctios*	*Distephanus boliviensis*	*Distephanus jimlingii*	*Distephanus medianoctisol*	*Distephanus medianoctisol**	*Distephanus octangulatus*	*Distephanus octonarius*	*Distephanus quinquangellus*	*Distephanus speculum*	*Distephanus speculum**	Ebridians: *Ebriopsis antiqua antiqua*	Zone in Ling (1992)
323-U1340A-																		
1H-CC	3.69	3.90	T	M											T			
2H-CC	13.65	13.92	C	G	R						T		R		F	F		
3H-CC	23.12	23.49	R	G											T	R		
4H-CC	32.56	32.85	R	G							T					R		*Distephanus octangulatus*/*Distephanus octonarius*
5H-CC	42.13	42.45	F	G									F		T	R		
10H-CC	89.63	89.93	R	G											R			
11H-CC	99.17	99.52	C	G	T						R		T		F	C		
12H-CC	108.61	108.88	C	G						F	T		T	T	F	F	T	
13H-CC	118.06	118.63	C	G	R		R			F	F	R	T		R	R		
14H-CC	127.71	127.99	C	G			R				F		R			F		
15H-CC	137.00	137.22	C	G			F			T	F		T			C		
16H-CC	146.79	147.04	A	G	R	R	A			T					T	R		
17H-CC	156.21	156.58	C	G			F						T					
18H-CC	165.78	165.99	C	G						R	R		F			R		
19H-CC	175.28	175.55	F	M			R						R					
25H-CC	215.53	215.70	B															
26H-CC	225.04	225.25	R	M												R		
27H-CC	234.52	234.72	B															
28H-CC	243.81	244.08	A	G				R							F	A		
29H-CC	253.43	253.61	T	M												T		
30H-CC	262.96	263.16	F	G	T										R	F		
32H-CC	281.96	282.17	F	M						T					T	F		
33H-CC	291.44	291.76	C	G						T					R	C		
34H-CC	300.36	300.46	A	G	T		T				T		T		R	A		
35H-CC	310.39	310.68	A	G	T					R				T	F	A	T	
36H-CC	318.09	318.30	R	M												R	T	
40H-CC	351.33	351.43	B															
41H-CC	354.50	354.73	T	M												T		
42H-CC	358.58	358.70	R	M											T	T		
43X-CC	358.70	358.77	B															
44X-CC	364.70	365.19	R	M												R		
48X-CC	409.08	409.32	F	M	T				T						F	F		
70X-CC	594.92	595.32	B															

Notes: * = with short radial spines. Abundance: A = abundant, C = common, F = few, R = rare, T = trace, B = barren. Preservation: G = good, M = moderate.

Table T11. Radiolarian datum events, Holes U1340A, U1340B, U1340C, U1340D. (See table note.)

Zone	Marker species	Age (Ma)	Hole U1340A				Hole U1340B			
			Core, section		Depth (mbsf)		Core, section		Depth (mbsf)	
			Top	Bottom	Top	Bottom	Top	Bottom	Top	Bottom
Botryostrobus aquilonaris	T *Lychnocanoma nipponica sakaii*	0.05	1H-CC	2H-CC	3.9	13.9		1H-CC	0	6.3
	T *Amphimelissa setosa*	0.08–0.10	1H-CC	2H-CC	3.9	13.9	1H-CC	2H-CC	6.4	16.4
	T *Spongodiscus* sp.	0.28–0.32	2H-CC	3H-CC	13.9	23.5	5H-CC	6H-CC	44.1	54.4
	T *Axoprunum acquilonium*	0.25–0.43	2H-CC	3H-CC	13.9	23.5				
Stylatractus universus	T *Stylatractus universus*	0.41–0.51	Not found							
Eucyrtidium matuyamai	T *Eucyrtidium matuyamai*	0.9–1.4	17H-CC	18H-CC	156.2	166.0				
	B *Eucyrtidium matuyamai*	1.7–1.9	23H-CC	24H-CC	196.1	206.2				
Cycladophora sakaii	T *Thecosphaera akitaensis*	2.4–2.7	30H-CC	31H-CC	263.1	272.7				
	T *Phormostichoartus fistula*	2.8–4.4	35H-CC	36H-CC	300.6	318.3				
Dictyophimus bullatus	T *Dictyophimus bullatus*	3.8–4.0	58H-CC	59H-CC	495.9	515.2				
	B *Thecosphaera akitaensis*	3.8–4.0	71H-CC		604.6					

Note: T = top, B = bottom.

Table T11 (continued).

Zone	Marker species	Age (Ma)	Hole U1340C				Hole U1340D			
			Core, section		Depth (mbsf)		Core, section		Depth (mbsf)	
			Top	Bottom	Top	Bottom	Top	Bottom	Top	Bottom
Botryostrobus aquilonaris	T *Lychnocanoma nipponica sakaii*	0.05		1H-CC	0	9.75		1H-CC	0	7.19
	T *Amphimelissa setosa*	0.08–0.10	2H-CC	3H-CC	19.57	29.08				
	T *Spongodiscus* sp.	0.28–0.32		1H-CC	0	9.75				
	T *Axoprunum acquilonium*	0.25–0.43								
Stylatractus universus	T *Stylatractus universus*	0.41–0.51								
Eucyrtidium matuyamai	T *Eucyrtidium matuyamai*	0.9–1.4								
	B *Eucyrtidium matuyamai*	1.7–1.9								
Cycladophora sakaii	T *Thecosphaera akitaensis*	2.4–2.7								
	T *Phormostichoartus fistula*	2.8–4.4								
Dictyophimus bullatus	T *Dictyophimus bullatus*	3.8–4.0								
	B *Thecosphaera akitaensis*	3.8–4.0								

Table T12. Radiolarian range chart, Holes U1340A, U1340B, U1340C, and U1340D. (See table notes.) (Continued on next page.)

Core, section	Depth (mbsf) Top	Depth (mbsf) Bottom	Abundance	Preservation	*Actinomma boreale*	*Actinomma medianum*	*Amphimelissa setosa*	*Axoprunum acquilonium*	*Botryostrobus aquilonaris*	*Ceratospyris borealis*	*Collosphaera pyloma*	*Cycladophora cornutoides*	*Cycladophora cosma*	*Cycladophora davisiana*	*Cycladophora sakaii*	*Cyrtocapsella japonica*	*Dendrospyris sakaii*	*Dictyophimus bullatus*	*Dictyophimus hirundo*	*Eucyrtidium asanoi*	*Eucyrtidium inflatum*	*Eucyrtidium matuyamai*	*Lamprocyrtis heteroporos*	*Larcopyle butschlii*	*Lipmanella redondoensis*	*Lithelius barbatus*	*Lychnocanoma magnacornuta*	*Lychnocanoma nipponica sakaii*	*Lychnocanoma parallelipes*	*Phormostichoartus fistula*	*Porodiscus circularis*	*Sphaeropyle langii-robusta* group	*Spongodiscus* sp. (Ling, 1973)	*Spongopyle osculosa*	*Spongotrochus glacialis*	*Spongurus pylomaticus*	*Stichocorys delmontensis*	*Stichocorys peregrina*	*Stylatractus universus*	*Stylochlamydium venustum*	*Stylodictya validispina*	*Thecosphaera akitaensis*
323-U1340A-																																								
1H-CC	3.69	3.90	C	G	F				F	C				C																			F					F	F	
2H-CC	13.65	13.92	A	G	C		F		C	A				A									C				A						F					C	C	
3H-CC	23.12	23.49	A	G	C		F	F		C				C									C				C					F	F	F			C	C	
4H-CC	32.56	32.85	F	G			F			F																	F					F						F	
5H-CC	42.13	42.45	C	G	F					F				C													F											F	F	
6H-CC	51.68	52.02	C	M	F			F	F	F				F																		A						C		
7H-CC	61.20	61.51	C	G	F					C				A					F					F			F					C								
8H-CC	70.69	71.08	C	M	F			F		C				A					C													C						F		
9H-CC	80.11	80.45	F	G	F					F									F													F								
10H-CC	89.63	89.93	C	G						C				A																		F								
11H-CC	99.17	99.52	F	G										F																										
12H-CC	108.61	108.88	F	M						C				F																		F			F				F	F	
13H-CC	118.06	118.63	C	G						C				C					F													C	F		F				F	F	
14H-CC	127.71	127.99	F	G						F				F					F													F			F						
15H-CC	137.00	137.22	C	G						C				A					F													F			F						
16H-CC	146.79	147.04	C	G						C				A					F																F				F		
17H-CC	156.21	156.58	F	M						F				A					F													F			F						
18H-CC	165.78	165.99	C	M	F			F		C				F					F			F		F							F	F	F	F						
19H-CC	175.28	175.55	F	M	F					F				F					F			F												F						
20H-CC	184.65	184.82	F	G						F				F																			F	F						
21H-CC	185.52	185.71	F	M										F																										
23H-CC	196.25	196.44	F	M	F			F		F		F										F											F					F		
24H-CC	205.97	206.20	C	M	C			F	F	C				F								F												F						
25H-CC	215.53	215.70	F	M						F				F																										
26H-CC	225.04	225.25	F	P																																				
27H-CC	234.52	234.72	F	M										F																				F						
28H-CC	243.81	243.88	F	M						F																							F						F	
29H-CC	253.43	244.08	F	M										F																									F	
30H-CC	262.96	263.16	F	M				F		F																														
31H-CC	272.38	272.67	C	M				F																									F			F			F	F
32H-CC	281.96	282.17	F	M										F																										
33H-CC	291.44	291.76	F	M																																				
34H-CC	300.36	300.46	F	M						F				F																						F				
35H-CC	310.39	310.68	F	M				F		F				F																				F		F			F	F
36H-CC	318.09	318.30	F	M			F																							F									F
37H-CC	327.17	327.36	F	M										F																						F			F	
38H-CC	333.36	333.55	F	M						F		F		C																						F			F	
39H-CC	343.39	343.65	F	M						F				F																						F				
40H-CC	351.33	351.43	F	M										F																				F	F	F				F
41H-CC	354.50	354.73	F	M						F				F	F																									
42H-CC	358.58	358.70	F	M																																F				
43H-CC	358.70	358.77	F	M						F				F																										

Table T12 (continued).

Core, section	Depth (mbsf) Top	Depth (mbsf) Bottom	Abundance	Preservation	*Actinomma boreale*	*Actinomma medianum*	*Amphimelissa setosa*	*Axoprunum acquilonium*	*Botryostrobus aquilonaris*	*Ceratospyris borealis*	*Collosphaera pyloma*	*Cycladophora cornutoides*	*Cycladophora cosma*	*Cycladophora davisiana*	*Cycladophora sakaii*	*Cyrtocapsella japonica*	*Dendrospyris sakaii*	*Dictyophimus bullatus*	*Dictyophimus hirundo*	*Eucyrtidium asanoi*	*Eucyrtidium inflatum*	*Eucyrtidium matuyamai*	*Lamprocyrtis heteroporos*	*Larcopyle butschlii*	*Lipmanella redondoensis*	*Lithelius barbatus*	*Lychnocanoma magnacornuta*	*Lychnocanoma nipponica sakaii*	*Lychnocanoma parallelipes*	*Phormostichoartus fistula*	*Porodiscus circularis*	*Sphaeropyle langii-robusta* group	*Spongodiscus* sp. (Ling, 1973)	*Spongopyle osculosa*	*Spongotrochus glacialis*	*Spongurus pylomaticus*	*Stichocorys delmontensis*	*Stichocorys peregrina*	*Stylatractus universus*	*Stylochlamydium venustum*	*Stylodictya validispina*	*Thecosphaera akitaensis*
44X-CC	364.70	365.19	F	M						F				F																								F		
45X-CC	374.64	374.75	F	P										F																										
46X-CC	386.55	386.81	F	M				F		F				F																				F						F
47X-CC	399.05	399.51	F	P						F																														
48X-CC	409.08	409.32	F	M						F																								F	F					F
49X-CC	417.77	418.06	F	M	F			F		F		F		F																			F	F						
50X-CC	424.85	425.16	F	M	F					C				F																								F		
51X-CC	435.32	435.61	F	M	F					F				F																		F		F						
52X-CC	447.48	447.78	F	G				F																								F					F	F	F
53X-CC	457.40	457.72	F	G						F																												F		
54X-CC	457.42	457.82	F	M						F																						F					F	F	F
55X-CC	476.03	476.33	F	M						F				F																										
56X-CC	486.08	486.20	F	M				F																											F					F
57X-CC	492.56	492.92	F	P																														F					F	
58X-CC	495.90	495.92	F	M						F																						F								
59X-CC	514.97	515.21	F	M														F																	F				F	F
63H-CC	546.74	546.77	F	M														F																					F	
64H-CC	555.44	555.66	F	M						F																													F	F
65H-CC	557.37	557.43	F	M						F				F				F																						F
66H-CC	562.87	562.97	F	M														F																F					F		
67H-CC	565.80	565.90	F	M														F						F														F		
68H-CC	575.59	575.99	F	P																				F															F	
69H-CC	584.79	585.28	F	P																				F																
70X-CC	594.92	595.32	F	P																																			F	
71X-CC	604.51	604.61	F	M				F																F														F		F
323-U1340B-																																								
1H-CC	6.29	6.43	F	G						F				F														F										F		
2H-CC	16.10	16.35	C	G	F		F			F				C					F									F										F		
3H-CC	25.54	25.79	F	G			F			F				F														F										F	F	
4H-CC	35.15	35.39	C	M	F		C			C				F														F										F	C	
5H-CC	43.90	44.12	F	P																																			F	
6H-CC	54.15	54.43	F	G	F		C		C	F																							F						F	
323-U1340C-																																								
1H-CC	9.47	9.85	A	G	F					C				A					C									C					F					C	C	
2H-CC	19.31	19.57	C	G						C				F					F					F				C						F				F	F	
3H-CC	28.83	29.08	C	G	F		F			C																		F						F				F	F	
323-U1340D-																																								
1H-CC	7.03	7.29	C	G	F					F				C														C										F	C	
2H-CC	17.02	17.21	C	G	F					C				C										F				F						F				F	C	
3H-CC	26.59	26.83	C	G						F				C																				F				F	F	

Notes: Abundance: D = dominant, A = abundant, C = common, F = few, R = rare. Preservation: G = good, M = moderate, P = poor.

Table T13. Dinoflagellate cyst, pollen, and palynomorph range chart, Hole U1340A. (See table notes.)

Core, section	Depth (mbsf) Top	Depth (mbsf) Bottom	Preservation	Marine: Dinoflagellate cysts	Marine: Organic lining of foraminifers	Pollen and spores: *Pediastrum* + *Botryococcus*	Pollen and spores: Pollen (herbs)	Pollen and spores: Pollen (shrubs)	Pollen and spores: Pollen (trees)	Pollen and spores: Spores of pteridophytes	Reworked palynomorphs	Dinoflagellate cyst assemblages: *Brigantedinium cariacoense*	*Brigantedinium simplex*	*Brigantedinium* spp.	*Filisphaera filifera*	*Impagidinium pallidum*	*Impagidinium aculeatum*	*Impagidinium japonicum*	*Islandinium imnutum*	*Impagidinium* spp.	*Operculodinium centrocarpum*	*Operculodinium centrocarpum* var. short processes	*Polykrikos* - Arctic morphotype	*Protoperidinium americanum*	*Quinquecuspis concreta*	*Selenopemphix nephroides*	*Spiniferites belerius*
323-U1340A-																											
1H-CC	3.80	3.90	M	A	C				F	R	F	R	A	D					A		D	R	R	R			
3H-CC	23.39	23.49	M	A	C				C	F	C	F	A	D							F	R	R	R			
5H-CC	42.35	42.45	M	A	C	F		F	C	F	F	F	A	D					R		R			R		R	
7H-CC	61.41	61.51	G	A	C		F		C	F	F	F	A	D					R	R	F						
9H-CC	80.35	80.45	M	C	A	F		R	F	R	F		F	D										R	R		
11H-CC	99.42	99.52	M	C	C	R		F	C	F	C		A	D													
13H-CC	118.53	118.63	M	A	C	F			C		C	F	A	D					R								
15H-CC	137.12	137.22	P	C	C	R		F	F	R	C		F	D					F		F	R					
17H-CC	156.48	156.58	M	A	F			F	C	C	C		F	D					R								
19H-CC	175.45	175.55	P	C	C				F		C		F	D													
21H-CC	185.61	185.71	P	C	C	F		C	F	C	C			P													
23HC-C	196.34	196.44	P	C	C			F			C		R	D													
25H-CC	215.60	215.70	G	C	C				F	F	F	R	A	D	F				R							R	
27H-CC	234.62	234.72	M	C	C		C	F	F	C	C			P	P												
29H-CC	243.98	244.08	G	C	C			F	F		F	F	A	A	D												
31H-CC	272.57	272.67	M	C	C						C			P	P												
33H-CC	291.66	291.76	M	C	F		F				C	R	F	D													
35H-CC	310.58	310.68	M	C	C				F	F	C		F	D			R	R									
37H-CC	327.26	327.36	M	C	F				F	F	F		F	D													
39H-CC	343.55	343.65	M	C	F				C		C		R	D	R												
41H-CC	354.63	354.73	G	A	C						F		A	D													
42H-CC	358.58	358.70	G	C	C			F			C		F	D	R			R			R						
43H-CC	358.70	358.77	M	C	F						F		R	F	D												
44X-CC	365.09	365.19	P	F	C			F	F	F	C			P													
47X-CC	399.41	399.51	P	C	C				C	C	C		P	P													
49X-CC	417.96	418.06	M	C	C			F		F	C		F	D	A												
51H-CC	435.51	435.61	P	F					C	F	C			P													
53X-CC	457.62	457.72	M	C	C						C		P	P	P												
55X-CC	476.23	476.33	G	C	C				C	F	F	R	F	D													
57X-CC	492.82	492.92	P	F	F						R			P													
59X-CC	515.11	515.21	M	C	C			F	F		F			P	P	P											
63H-CC	546.74	546.77	M	F	R			R	F		F			P	P				P		P						
65H-CC	557.37	557.43	P	C	C						F			P													
67H-CC	565.80	565.90	G	C	C			F			F		F	D													P
69H-CC	585.18	585.28	M	C						F				P													
71X-CC	604.51	604.61	M	C	C				F	R			R	D													

Notes: Absolute abundance: A = abundant (>2000/cm^3), C = common (>200/cm^3), F = few (>100/cm^3), R = rare (<100/cm^3). Relative abundance of dinoflagellate cysts: D = dominant (>30%), A = abundant (>10%), F = few (>5%), R = rare (<5%), P = occurrence (when counts are <20). Preservation: G = good, M = moderate, P = poor.

Table T14. Chron ages and preliminary depths, Hole U1340A. (See table note.)

Event	Age (ka)	Core, section	Depth (mbsf)
		323-U1340A-	
B Brunhes	781	13H (B)	117.9
T Jaramillo	998	17H (T)	146.4
B Jaramillo	1072	17H (B)	155.9
T Olduvai	1778	30H-6	260.7
B Olduvai	1945	34H (B)	300.7
T Reunion	2128	40H (T)	343.2
T Gauss	2581	57X (T)	486.2

Note: T = top, B = bottom.

Table T15. Moisture and density, Hole U1340A. (See table note.) (Continued on next two pages.)

Core, section, interval (cm)	Depth (mbsf)	Density (g/cm^3)			Void ratio	Water content (%)	Porosity (%)
		Dry grain	Wet bulk	Dry bulk			
323-U1340A-							
1H-1, 59–61	0.6	1.93	1.14	0.29	6.36	74.7	86.4
1H-3, 29–31	3.3	2.26	1.35	0.62	2.79	53.9	73.6
2H-1, 29–31	4.2	2.74	1.44	0.69	3.21	52.4	76.2
2H-3, 29–31	7.2	2.58	1.44	0.72	2.75	50.3	73.3
2H-5, 29–31	10.2	2.55	1.35	0.57	3.79	58.0	79.1
3H-1, 29–31	13.7	2.75	1.51	0.80	2.58	47.2	72.1
3H-3, 29–31	16.7	2.59	1.49	0.80	2.37	46.6	70.4
3H-5, 29–31	19.7	2.61	1.40	0.65	3.21	53.6	76.3
8H-1, 29–31	61.2	2.50	1.56	0.93	1.78	40.5	64.0
8H-3, 29–31	64.2	2.34	1.34	0.59	3.19	56.2	76.2
8H-5, 29–31	67.2	2.70	1.52	0.81	2.45	46.3	71.0
8H-7, 29–31	70.2	2.49	1.40	0.67	2.91	52.4	74.4
9H-1, 29–31	70.7	2.62	1.44	0.71	2.87	50.8	74.1
9H-3, 29–31	73.7	2.59	1.48	0.78	2.46	47.5	71.1
9H-5, 29–31	76.7	2.55	1.38	0.62	3.30	54.8	76.7
9H-7, 29–31	79.7	1.88	1.27	0.57	2.45	55.3	71.0
10H-1, 29–31	80.2	2.49	1.30	0.49	4.46	62.2	81.7
10H-3, 29–31	83.2	2.51	1.41	0.68	2.88	52.0	74.2
10H-5, 29–31	86.2	2.61	1.42	0.67	3.07	52.5	75.4
10H-7, 29–31	89.2	2.54	1.54	0.89	1.94	42.3	66.0
11H-3, 29–31	92.7	2.46	1.43	0.72	2.55	49.6	71.8
11H-5, 29–31	95.7	2.63	1.52	0.83	2.28	45.3	69.5
11H-7, 29–31	98.7	2.84	1.53	0.82	2.61	46.6	72.3
12H-1, 29–31	99.2	2.59	1.44	0.71	2.81	50.7	73.7
12H-3, 29–31	102.2	2.55	1.44	0.72	2.71	50.1	73.0
12H-5, 29–31	105.2	2.58	1.58	0.95	1.80	40.2	64.3
13H-1, 29–31	108.7	2.89	1.59	0.90	2.33	43.4	69.9
13H-3, 29–31	111.7	2.61	1.53	0.85	2.17	44.3	68.5
13H-5, 29–31	114.7	2.47	1.23	0.39	6.02	68.7	85.7
13H-7, 29–31	117.7	2.50	1.48	0.80	2.25	46.2	69.2
14H-1, 29–31	118.2	2.55	1.48	0.78	2.40	47.2	70.5
14H-3, 29–31	121.2	2.68	1.47	0.75	2.74	49.2	73.2
14H-5, 29–31	124.2	2.42	1.31	0.52	3.94	60.2	79.8
14H-7, 29–31	127.2	2.60	1.48	0.78	2.46	47.4	71.1
15H-1, 29–31	127.7	2.44	1.25	0.42	5.23	66.1	83.9
15H-3, 29–31	130.7	2.67	1.54	0.86	2.20	44.1	68.8
15H-7, 29–31	136.7	2.55	1.30	0.49	4.60	62.4	82.1
16H-1, 29–31	137.2	1.92	1.16	0.34	5.20	71.2	83.9
16H-3, 29–31	140.2	2.37	1.32	0.54	3.64	58.9	78.4
16H-5, 29–31	143.2	2.59	1.36	0.59	3.67	56.9	78.6
17H-1, 29–31	146.7	2.46	1.28	NM	NM	63.5	82.3
17H-7, 29–31	155.7	2.52	1.44	0.73	2.59	49.4	72.1
18H-1, 29–31	156.2	2.60	1.36	0.57	3.84	57.9	79.4
18H-2, 29–31	159.2	2.54	1.42	0.69	2.87	51.6	74.2
18H-3, 29–31	162.2	2.61	1.54	0.88	2.06	43.1	67.4
18H-4, 29–31	165.2	2.07	1.28	0.53	3.06	58.2	75.4
19H-1, 29–31	165.7	2.52	1.42	0.69	2.84	51.6	73.9

Table T15 (continued). (Continued on next page.)

Core, section, interval (cm)	Depth (mbsf)	Density (g/cm^3)			Void ratio	Water content (%)	Porosity (%)
		Dry grain	Wet bulk	Dry bulk			
19H-3, 29–31	168.7	2.53	1.44	0.72	2.66	49.9	72.7
19H-5, 29–31	171.7	2.49	1.36	0.60	3.38	56.0	77.2
19H-7, 29–31	174.7	2.64	1.46	0.73	2.78	49.9	73.5
20H-1, 29–31	175.2	2.51	1.38	0.62	3.26	54.9	76.5
20H-3, 29–31	178.2	2.13	1.41	0.76	1.89	45.9	65.4
20H-5, 29–31	181.2	2.68	1.50	0.79	2.53	47.2	71.6
20H-7, 29–31	184.2	2.12	1.30	0.56	2.97	56.9	74.8
23H-1, 79–80	187.5	2.60	1.57	0.91	1.94	41.7	66.0
23H-3, 79–80	190.5	2.55	1.55	0.90	1.94	42.1	65.9
23H-5, 79–80	193.5	2.22	1.41	0.73	2.12	47.8	68.0
24H-1, 29–31	196.5	2.63	1.35	0.56	3.99	58.4	79.9
24H-3, 29–31	199.5	2.50	1.43	0.71	2.67	50.3	72.8
24H-5, 29–31	199.5	2.58	1.44	0.71	2.81	50.7	73.8
25H-1, 29–31	206.0	2.67	1.40	0.64	3.42	54.6	77.4
25H-3, 29–31	209.0	2.50	1.36	0.59	3.47	56.5	77.6
25H-5, 29–31	212.0	2.55	1.47	0.77	2.46	47.8	71.1
25H-7, 29–31	215.0	2.50	1.43	0.71	2.70	50.5	72.9
27H-1, 29–31	225.0	2.52	1.32	0.53	4.11	60.2	80.4
27H-3, 29–31	228.0	2.32	1.28	0.48	4.13	62.3	80.5
27H-5, 29–31	231.0	2.34	1.28	0.48	4.20	62.4	80.8
27H-7, 29–31	234.0	2.48	1.43	0.71	2.67	50.4	72.7
28H-1, 29–31	234.5	2.44	1.32	0.53	3.88	59.7	79.5
28H-3, 29–31	237.5	2.29	1.31	0.55	3.41	58.2	77.3
28H-5, 29–31	240.5	2.47	1.32	0.52	4.01	60.1	80.0
28H-7, 29–31	243.5	2.50	1.46	0.77	2.38	47.6	70.5
29H-1, 29–31	244.0	2.53	1.46	0.76	2.47	48.1	71.2
29H-3, 29–31	247.0	2.54	1.48	0.79	2.35	46.8	70.2
29H-5, 29–31	250.0	2.51	1.43	0.71	2.69	50.4	72.9
29H-7, 29–31	253.0	2.35	1.30	0.51	3.94	60.9	79.8
30H-1, 29–31	253.5	2.43	1.28	0.48	4.45	62.8	81.7
30H-3, 29–31	256.5	2.52	1.39	0.64	3.11	53.7	75.7
30H-5, 29–31	259.5	2.32	1.35	0.61	3.01	55.0	75.1
30H-7, 29–31	262.5	2.58	1.44	0.71	2.78	50.4	73.5
31H-1, 29–31	263.0	2.33	1.35	0.60	3.08	55.4	75.5
31H-3, 29–31	266.0	2.42	1.34	0.58	3.41	56.9	77.3
31H-5, 29–31	269.0	2.32	1.30	0.52	3.76	60.1	79.0
32H-1, 29–31	272.5	2.54	1.51	0.83	2.18	45.0	68.6
32H-3, 29–31	275.5	2.22	1.27	0.49	3.76	61.2	79.0
32H-5, 29–31	278.5	2.48	1.30	0.50	4.30	61.6	81.1
33H-1, 29–31	282.0	2.53	1.36	0.59	3.55	56.8	78.0
33H-3, 29–31	285.0	2.40	1.40	0.68	2.69	51.4	72.9
33H-5, 29–31	288.0	2.02	1.30	0.60	2.52	54.2	71.6
33H-7, 29–31	291.0	2.36	1.34	0.59	3.22	56.1	76.3
34H-1, 29–31	291.5	2.59	1.58	0.94	1.84	40.5	64.8
34H-3, 29–31	294.5	2.24	1.38	0.68	2.42	50.7	70.8
34H-5, 29–31	297.5	2.61	1.40	0.64	3.26	54.0	76.5
34H-7, 29–31	300.0	2.53	1.55	0.91	1.86	41.3	65.0
35H-1, 29–31	301.0	2.37	1.32	0.55	3.55	58.3	78.0
35H-3, 29–31	304.0	2.44	1.38	0.64	2.99	53.6	75.0
35H-5, 29–31	307.0	2.48	1.38	0.62	3.18	54.7	76.1
35H-7, 29–31	310.0	2.24	1.36	0.65	2.57	52.1	72.0
36H-1, 29–31	310.5	2.40	1.41	0.70	2.58	50.5	72.1
36H-3, 29–31	313.5	2.51	1.41	0.68	2.86	51.9	74.1
36H-5, 29–31	316.5	NM	1.17	0.49	2.19	58.3	68.7
37H-1, 29–31	318.5	2.63	1.46	0.73	2.75	49.8	73.4
37H-3, 29–31	321.5	2.48	1.44	0.73	2.55	49.4	71.9
37H-5, 29–31	324.5	2.55	1.44	0.71	2.73	50.3	73.2
38H-1, 29–31	328.0	2.31	1.29	0.51	3.82	60.6	79.2
38H-3, 29–31	331.0	2.56	1.43	0.70	2.85	51.3	74.0
39H-1, 29–31	334.0	2.37	1.46	0.78	2.12	46.1	68.0
39H-3, 29–31	337.0	2.55	1.34	0.56	3.84	58.3	79.3
39H-5, 29–31	340.0	2.53	1.48	0.78	2.35	47.0	70.2
39H-7, 29–31	343.0	2.55	1.44	0.72	2.70	50.1	73.0
40H-1, 29–31	343.5	2.49	1.42	0.70	2.70	50.7	73.0
40H-3, 29–31	346.5	2.52	1.39	0.63	3.19	54.3	76.1
40H-5, 29–31	349.5	2.24	1.34	0.60	2.90	55.0	74.4
46X-1, 29–31	384.2	2.59	1.28	0.45	5.27	65.0	84.1
46X-2, 29–31	385.7	2.08	1.26	0.49	3.51	61.2	77.8

Table T15 (continued).

Core, section, interval (cm)	Depth (mbsf)	Density (g/cm^3)			Void ratio	Water content (%)	Porosity (%)
		Dry grain	Wet bulk	Dry bulk			
48X-1, 29–31	400.4	2.53	1.39	0.63	3.19	54.3	76.2
48X-3, 29–31	403.4	2.44	1.36	0.60	3.27	55.7	76.6
48X-5, 29–31	406.4	2.15	1.24	0.44	4.25	64.6	80.9
49X-1, 29–31	410.0	2.21	1.26	0.47	4.02	62.8	80.1
49X-3, 29–31	413.0	2.38	1.22	0.38	5.93	69.2	85.6
50X-1, 29–31	419.6	2.46	1.40	0.67	2.81	51.9	73.7
50X-3, 29–31	422.6	2.41	1.31	0.52	3.93	60.3	79.7
51X-1, 49–51	429.4	2.35	1.37	0.64	2.83	53.3	73.9
51X-3, 49–51	432.4	2.62	1.35	0.57	3.91	58.1	79.6
51X-5, 49–51	434.9	2.27	1.33	0.58	3.10	56.3	75.6
52X-1, 29–31	438.9	2.28	1.34	0.60	2.98	55.2	74.9
52X-3, 29–31	441.9	2.61	1.45	0.73	2.75	50.0	73.4
52X-5, 29–31	444.9	2.36	1.32	0.55	3.50	58.1	77.8
53X-1, 29–31	448.4	2.16	1.23	0.42	4.55	66.0	82.0
53X-3, 29–31	451.4	2.43	1.38	0.64	2.95	53.4	74.7
53X-5, 29–31	454.4	1.67	1.23	0.58	1.99	53.3	66.6
55X-1, 29–31	467.4	2.59	1.51	0.82	2.28	45.5	69.5
55X-3, 29–31	470.4	3.32	1.73	1.04	2.33	40.0	70.0
55X-5, 29–31	473.4	2.41	1.35	0.59	3.33	56.4	76.9
56X-1, 29–31	476.9	2.51	1.35	0.57	3.63	57.4	78.4
56X-3, 29–31	479.9	2.49	1.42	0.70	2.73	50.9	73.2
56X-5, 29–31	482.9	2.26	1.36	0.64	2.68	52.9	72.8
57X-1, 29–31	486.5	2.48	1.46	0.77	2.33	47.2	70.0
57X-3, 29–31	489.5	1.64	1.24	0.61	1.76	50.8	63.7
57X-5, 29–31	492.0	2.49	1.49	0.82	2.16	45.3	68.3
59X-1, 29–31	505.8	2.01	1.32	0.64	2.25	51.6	69.2
59X-3, 29–31	508.8	2.36	1.35	0.60	3.10	55.3	75.6
59X-5, 29–31	511.8	2.20	1.34	0.62	2.71	53.8	73.0
63X-1, 29–31	544.2	2.46	1.41	0.69	2.69	50.9	72.9
63X-2, 29–31	545.7	2.29	1.37	0.65	2.69	52.7	72.9
64X-1, 29–31	547.7	2.34	1.40	0.69	2.51	50.4	71.5
64X-3, 29–31	550.7	2.01	1.40	0.79	1.59	43.3	61.4
65X-1, 29–31	553.2	2.24	1.39	0.70	2.30	49.4	0.7
65X-3, 29–31	554.8	3.20	1.88	1.28	1.57	32.0	0.6
66X-1, 29–31	557.8	2.26	1.33	0.59	3.05	56.0	0.8
66X-3, 29–31	560.8	2.14	1.43	0.79	1.78	44.3	0.6
67X-1, 29–31	563.3	2.37	1.48	0.82	1.99	44.5	0.7
67X-2, 29–31	564.8	2.00	1.36	0.71	1.89	47.6	0.7
68X-1, 29–31	566.3	2.52	1.46	0.75	2.47	48.3	0.7
68X-3, 29–31	569.3	2.29	1.45	0.79	2.01	45.7	0.7
68X-5, 29–31	572.3	2.37	1.49	0.84	1.91	43.6	0.7
68X-7, 29–31	575.3	2.34	1.32	0.55	3.47	58.1	0.8
69X-1, 29–31	576.0	2.46	1.50	0.84	2.02	44.0	0.7
69X-3, 29–31	579.0	2.08	1.37	0.70	2.06	48.6	0.7
69X-5, 29–31	582.0	2.39	1.35	0.59	3.28	56.3	0.8
69X-7, 29–31	584.5	2.40	1.39	0.66	2.79	52.4	0.7
70X-1, 29–31	585.7	2.94	1.46	0.70	3.47	52.4	0.8
70X-3, 29–31	588.7	2.37	1.28	0.47	4.39	63.1	0.8
70X-5, 29–31	591.7	2.33	1.37	0.64	2.80	53.2	0.7
70X-7, 29–31	594.7	2.05	1.38	0.73	1.89	46.9	0.7
71X-1, 29–31	595.3	2.30	1.41	0.73	2.26	48.5	0.7
71X-3, 29–31	598.3	2.25	1.36	0.64	2.69	53.1	0.7
71X-5, 29–31	601.3	2.40	1.40	0.68	2.70	51.6	0.7
71X-7, 29–31	604.3	2.14	1.38	0.71	2.10	48.4	0.7

Note: NM = not measured.

Table T16. Affine table indicating the amount that each core in each hole needs to be offset in order to construct a continuous record, Site U1340. (**Continued on next page.**)

Core	Depth (mbsf) Top	Depth (mbsf) Bottom	Offset (m)	Depth CCSF-A (m) Top	Depth CCSF-A (m) Bottom	Recovered (m)	Recovery (%)
323-U1340A-							
1H	0.00	3.90	–0.06	–0.06	3.84	3.90	100
2H	3.90	13.92	1.05	4.95	14.97	10.02	105
3H	13.40	23.49	1.30	14.70	24.79	10.09	106
4H	22.90	32.85	1.61	24.51	34.46	9.95	105
5H	32.40	42.45	7.27	39.67	49.72	9.73	102
6H	41.90	52.02	7.31	49.21	59.33	9.78	103
7H	51.40	61.51	7.31	58.71	68.82	9.80	103
8H	60.90	71.08	7.31	68.21	78.39	9.79	103
9H	70.40	80.45	7.31	77.71	87.76	9.71	102
10H	79.90	89.93	7.31	87.21	97.24	9.73	102
11H	89.40	99.52	7.31	96.71	106.83	10.12	107
12H	98.90	108.88	7.31	106.21	116.19	9.98	105
13H	108.40	118.63	7.31	115.71	125.94	10.23	108
14H	117.90	128.01	7.31	125.21	135.32	10.09	106
15H	127.40	137.22	7.31	134.71	144.53	9.82	103
16H	136.90	147.04	7.31	144.21	154.35	10.14	107
17H	146.40	156.58	7.31	153.71	163.89	10.18	107
18H	155.90	165.99	7.31	163.21	173.30	10.09	106
19H	165.40	175.55	7.31	172.71	182.86	10.15	107
20H	174.90	184.82	7.31	182.21	192.13	9.92	104
21H	184.40	185.71	7.31	191.71	193.02	1.31	101
22D	185.70	185.70	7.31	193.01	193.01	0.00	0
23H	186.70	196.44	7.31	194.01	203.75	9.74	103
24H	196.20	206.20	7.31	203.51	213.51	10.00	105
25H	205.70	215.70	7.31	213.01	223.01	10.00	105
26H	215.20	225.25	7.31	222.51	232.56	10.05	106
27H	224.70	234.72	7.31	232.01	242.03	10.02	105
28H	234.20	244.08	7.31	241.51	251.39	9.88	104
29H	243.70	253.61	7.31	251.01	260.92	9.90	104
30H	253.20	263.16	7.31	260.51	270.47	9.96	105
31H	262.70	272.67	7.31	270.01	279.98	9.97	105
32H	272.20	282.17	7.31	279.51	289.48	9.76	103
33H	281.70	291.76	7.31	289.01	299.07	9.74	103
34H	291.20	300.60	7.31	298.51	307.91	9.40	99
35H	300.70	310.68	7.31	308.01	317.99	9.98	105
36H	310.20	318.30	7.31	317.51	325.61	7.89	99
37H	318.20	327.36	7.31	325.51	334.67	8.97	94
38H	327.70	333.55	7.31	335.01	340.86	5.66	94
39H	333.70	343.65	7.31	341.01	350.96	9.95	105
40H	343.20	351.43	7.31	350.51	358.74	8.23	97
41H	351.70	354.73	7.31	359.01	362.04	3.03	101
42H	354.70	358.70	7.31	362.01	366.01	4.00	100
43X	358.70	358.77	7.31	366.01	366.08	0.07	1
44X	364.70	365.19	7.31	372.01	372.50	0.49	5
45X	374.30	374.75	7.31	381.61	382.06	0.45	5
46X	383.90	386.81	7.31	391.21	394.12	2.91	44
47X	390.50	399.51	7.31	397.81	406.82	9.01	94
48X	400.10	409.32	7.31	407.41	416.63	8.98	94
49X	409.70	418.06	7.31	417.01	425.37	8.07	84
50X	419.30	425.16	7.31	426.61	432.47	5.55	58
51X	428.90	435.61	7.31	436.21	442.92	6.42	66
52X	438.60	447.78	7.31	445.91	455.09	8.88	93
53X	448.10	457.72	7.31	455.41	465.03	9.32	100
54X	457.40	457.82	7.31	464.71	465.13	0.42	4
55X	467.10	476.33	7.31	474.41	483.64	9.23	97
56X	476.60	486.20	7.31	483.91	493.51	9.60	100
57X	486.20	492.92	7.31	493.51	500.23	6.72	69
58X	495.90	495.92	7.31	503.21	503.23	0.02	0
59X	505.50	515.20	7.31	512.81	522.51	9.48	99
60X	515.10	515.10	7.31	522.41	522.41	0.00	0
61X	524.80	524.80	7.31	532.11	532.11	0.00	0
62X	534.40	534.40	7.31	541.71	541.71	0.00	0
63H	543.90	546.77	7.31	551.21	554.08	2.87	82
64H	547.40	555.66	7.31	554.71	562.97	8.26	206
65H	551.50	557.43	7.31	558.81	564.74	5.93	99
66H	557.50	562.97	7.31	564.81	570.28	5.47	99

Table T16 (continued).

Core	Depth (mbsf) Top	Depth (mbsf) Bottom	Offset (m)	Depth CCSF-A (m) Top	Depth CCSF-A (m) Bottom	Recovered (m)	Recovery (%)
67H	563.00	565.90	7.31	570.31	573.21	2.90	97
68X	566.00	575.99	7.31	573.31	583.30	9.99	103
69X	575.70	585.28	7.31	583.01	592.59	9.58	99
70X	585.40	595.32	7.31	592.71	602.63	9.92	103
71X	595.00	604.61	7.31	602.31	611.92	9.61	100
323-U1340B-							
1H	0.00	6.43	–0.21	–0.21	6.22	6.43	100
2H	6.40	16.35	1.74	8.14	18.09	9.95	105
3H	15.90	25.79	1.48	17.38	27.27	9.89	104
4H	25.40	35.39	6.81	32.21	42.20	9.99	105
5H	34.90	44.14	6.77	41.67	50.91	9.24	97
6H	44.40	54.43	4.71	49.11	59.14	10.03	106
323-U1340C-							
1H	0.00	9.85	10.03	10.03	19.88	9.85	104
2H	9.50	19.31	25.72	35.22	45.03	9.81	103
3H	19.00	28.83	15.29	34.29	44.12	9.83	103
323-U1340D-							
1H	0.00	7.29	0.00	0.00	7.29	7.29	100
2H	7.30	17.02	2.41	9.71	19.43	9.72	102
3H	16.80	26.83	15.80	32.60	42.63	10.03	106

Table T17. Splice table indicating tie points between holes, Site U1340. Sampling along the splice should be used to construct a continuous record.

Hole, core, section, interval (cm)	Depth mbsf	Depth CCSF-D (m)		Hole, core, section, interval (cm)	Depth mbsf	Depth CCSF-D (m)
323-				323-		
U1340D-1H-5, 59.5	6.59	6.59	Tie to	U1340A-2H-2, 14.5	5.55	6.59
U1340A-2H-4, 140.9	9.81	10.86	Tie to	U1340C-1H-1, 83.0	0.83	10.86
U1340C-1H-4, 125.0	5.75	15.78	Tie to	U1340A-3H-1, 107.7	14.48	15.78
U1340A-3H-3, 77.8	17.13	18.43	Tie to	U1340B-3H-1, 105.5	16.95	18.43
U1340B-3H-6, 101.6	24.42	25.89	Tie to	U1340A-4H-1, 137.7	24.28	25.89
U1340A-4H-6, 100.7	31.41	33.02	Tie to	U1340B-4H-1, 81.1	26.21	33.02
U1340B-4H-6, 116.0	34.06	40.87	Tie to	U1340A-5H-1, 120.2	33.60	40.87
U1340A-5H-7, 61.9	42.02	49.29	Tie to	U1340B-6H-1, 17.7	44.58	49.29
U1340B-6H-7, 71.9	54.12	58.83	Append to	U1340A-7H-1, 12.0	51.52	58.83
U1340A-71X-7, 51.0	604.51	611.82				

Table T18. Temperature data, Site U1340. (**See table note.**)

Core	Depth (mbsf)	Thermal resistance (m^2K/W)	T (°C)	T_s (°C)	Remarks
323-U1340A-					
3H	22.9	26.77	NA		Unusable
8H	70.4	80.70	5.67	2.83	Calm sea
13H	117.9	133.07	7.70	2.83	Calm sea
18H	165.4	189.76	9.79	2.80	Calm sea

Note: T = formation temperature, T_s = seafloor temperature, NA = not applicable.